Manifestation of Entanglement in Quantum Foundation & Quantum Thermodynamics

by

Arpan Das

PHYS07201304001

Institute of Physics, Bhubaneswar

A thesis submitted to the
Board of Studies in Physical Sciences
In partial fulfillment of requirements
for the Degree of

DOCTOR OF PHILOSOPHY
of
HOMI BHABHA NATIONAL INSTITUTE

July, 2019

Homi Bhabha National Institute

Recommendations of the Viva Voce Committee

As members of the Viva Voce Committee, we certify that we have read the dissertation prepared by *Arpan Das* entitled "*Manifestation of Entanglement in Quantum Foundation & Quantum Thermodynamics*", and recommend that it may be accepted as fulfilling the dissertation requirement for the Degree of Doctor of Philosophy.

Am Jayannavar

Chairman - ***Prof. Arun M. Jayannavar*** Date: 10/01/2020

Pankaj Agrawal

Guide - ***Prof. Pankaj Agrawal*** Date: 10/01/2020

Co-guide (if any) Date:

Examiner - ***Prof. A. R. Usha Devi*** Date: 10/01/2020

Ajit M. Srivastava

Member 1 - ***Prof. Ajit M. Srivastava*** Date: 10/01/2020

Member 2 - ***Prof. Suresh K. Patra*** Date: 10/01/2020

Final approval and acceptance of this thesis is contingent upon the candidate's submission of the final copies of the dissertation to HBNI.

I hereby certify that I have read this thesis prepared under my direction and recommend that it may be accepted as fulfilling the thesis requirement.

Date: 10-1-20

Place: BHUBANESWAR

Pankaj Agrawal

Guide

STATEMENT BY AUTHOR

This dissertation has been submitted in partial fulfillment of requirements for an advanced degree at Homi Bhabha National Institute (HBNI) and is deposited in the Library to be made available to borrowers under rules of the HBNI.

Brief quotations from this dissertation are allowable without special permission, provided that accurate acknowledgement of source is made. Requests for permission for extended quotation from or reproduction of this manuscript in whole or in part may be granted by the Competent Authority of HBNI when in his or her judgment the proposed use of the material is in the interests of scholarship. In all other instances, however, permission must be obtained from the author.

Arpan Das

DECLARATION

I, hereby declare that the investigation presented in the thesis has been carried out by me. The work is original and has not been submitted earlier as a whole or in part for a degree / diploma at this or any other Institution / University.

Arpan Das

List of Publications arising from the thesis

Journal

- New Bell inequalities for three-qubit pure states, A. Das, C. Datta and P. Agrawal, *Phys. Lett. A* **381**, 3928 (2017).
- Measurement based quantum heat engine with coupled working medium, A. Das and S. Ghosh, *Entropy* **21 (11)**, 1131 (2019).

Communicated

- Resource state structure for cooperative quantum key distribution, A. Das, S. Nandi, S. Sazim, and P. Agrawal, arXiv: 1903.10163 (2019).
- New facet Bell inequalities for multi-qubit states, A. Das, C. Datta and P. Agrawal, arXiv: 1809.05727 (2018).

Conferences

- "New Bell inequalities for three-qubit pure states" (presented a talk), Young Quantum (Feb, 2017), Harish-Chandra Research Institute (HRI), Allahabad.
- "New Bell inequalities for three-qubit pure states" (presented a talk), Advanced School and Workshop on Quantum Science and Quantum Technologies (Sep, 2017), ICTP, Trieste, Italy.
- "Minimal scenario facet Bell inequalities for multi-qubit states" (presented a poster), International Conference for Young Quantum Information Scientists and Summer School of the Vienna Doctoral Program on Complex Quantum Systems (Sep, 2018), University of Vienna, Austria.

Arpan Das

Dedicated to my parents

ACKNOWLEDGEMENTS

This thesis is a culmination of sincere supports from a lot of people. First of all, I want to thank my supervisor Prof. Pankaj Agrawal for his guidance and support throughout my PhD career. Besides, he gave me immense independence to choose my research interests and always encouraged me to do good research. Next, I want to thank my collaborators, Prof. Sibasish Ghosh, Prof. C. M. Chandrashekar, Dr. Satyabrata Adhikari, Sk Sazim, Sumit Nandi, Chandan Datta, Sagnik Chakraborty and Arindam Mallick for their co-operation.

I would like to thank my family for always being there in my good and bad times. Especially, I am grateful to my parents, grand parents, brother and my fiancée Monalisa for their constant support and love.

Lastly, a big thanks for all of my friends, seniors and juniors from IOP and outside for making my life more enjoyable.

Contents

SUMMARY

Quantum Entanglement, first perceived as a spooky action at a distance by Einstein, Rosen and Podolosky (EPR) is an important resource in modern day Quantum Information Processing (QIP) tasks. Arising form the Hilbert space structure of Quantum mechanics (QM), entanglement is important not only for its practical relevance in present quantum technologies but for its mathematical structure in complex scenarios and significance from foundational perspective. Phenomena like Bell nonlocality and Steering are due to the presence of entangled states. In the age of miniaturization of technologies, it is highly desirable to understand the energetics of microscopic systems in quantum regime, where quantum correlations like entanglement inevitably comes into the picture. Whether these quantum effects limit our capability in controlling the system or they are actually advantageous in different protocols is the question at stake. There are many examples, where quantum correlation is exploited for better performance of a quantum thermodynamic protocol. This thesis aims to discuss about these different uses of quantum entanglement in Bell nonlocality, in a QIP task and in Quantum Thermodynamics.

In Bell Nonlocality, we are mainly interested in multipartite scenario involving three or more parties. The area we investigated is based on a particular shortcoming of some well known Bell inequalities for a class of entangled states. MABK inequalities were first constructed looking at the structure of the GHZ state. Surprisingly, generalized GHZ states do not violate these inequalities for a certain parameter range. Not only that no correlation Bell inequality with two dichotomic measurement settings per party is violated by the generalized GHZ states for odd number of qubits. There are correlation Bell inequalities with more than two measurement settings per party that show violation for the entire parameter range of generalized GHZ states. we have constructed a set of six Bell inequalities in the minimal measurement scenario, such that they are violated by all three-qubit generalized GHZ states. Moreover, the more entangled a generalized GHZ state is, the more will be the violation. We also provide numerical evidence that at least one of these Bell inequalities is violated by a pure three-qubit genuinely entangled state. These Bell inequalities can distinguish between separable, bi-separable and genuinely entangled pure three-qubit states. We also generalize this set of inequalities to n-qubit systems. One important fact of those inequalities was the scenario we considered, i.e three parties,

two dichotomic measurement settings for two parties and one dichotomic measurement for the remaining.

But our inequalities are not facet inequalities for the particular scenario we considered. So, the next question we ask that what about the facet inequalities in this special scenario? We first explicitly construct the facets of the local polytope for three qubits. We find only one nontrivial facet inequality upto the relabeling of indices. With permutation of qubits, the number is three. Interestingly, this facet inequality is equivalent to the lifted version of Bell-CHSH inequality for more parties. We then showed that the facet inequalities are also violated by all generalized GHZ states and order them according to their entanglement. We generalize the inequalities for n qubits and in each case there is only one non-trivial facet inequality.

Next we introduce a new QIP task called Co-operative Quantum Key Distribution (CoQKD), where secret key is established between two parties with the involvement of other parties. The other parties act as the controller and supervisor of the whole procedure of key making between two parties such that there is no possibility of cheating. We find the necessary multipartite resource state structure for this new scheme. Along with GHZ states, we find some other states which are suitable for the scheme. Three-qubit case is completely worked out and for more parties we also discuss the structure of the states. After developing the CoQKD protocol with three qubit resource states, we show that these states are also useful in the conference key distribution. Lastly, we discuss the usefulness of entanglement in quantum thermodynamic scenario.

Role of entanglement is yet to be fully understood in Quantum Thermodynamics. We take the scenario of quantum heat engines to shed some light in that direction. We consider the role of entanglement for a single temperature quantum heat engine without feedback control, introduced recently by Talkner and Kim [Phys. Rev. E 96, 022108 (2017)]. We take the working medium of the engine to be a 1-dim Heisenberg model of two spins. We calculate the efficiency of the engine undergoing a cyclic process at a single temperature and show that for a coupled working medium the efficiency can be higher than that of an uncoupled one. By establishing a connection between the coupling and the entanglement we show that entanglement indeed helps us to achieve the efficiency beyond the classical limit.

List of Figures

List of Tables

CHAPTER 1

Introduction

Despite being invented more than a century, quantum mechanics still does not cease to surprise the scientific community. Till date there is no experimental evidence which questions its validity and yet from the foundational perspective there is a lot to understand. The mathematical formalism of quantum mechanics is based on the abstract notion of Hilbert space, which opens up many plausible ways to reconcile it with the physical reality, giving rise to intense debates and different interpretations of quantum mechanics. In 1935, based on local causality, Einstein, Podolosky and Rosen (EPR) argued that [1] quantum mechanics is not a complete theory to describe the laws of nature. According to their viewpoint, statistical nature of quantum mechanics is due to the lack of our knowledge about the concerned system. They introduced the concept of hidden variables, knowledge about which can restore the realism and determinism in the theory. But, in 1964, in a seminal paper [2], John. S. Bell showed that quantum mechanics is not compatible with any local hidden variable (LHV) theories. Due to this work, largely ignored philosophical aspects of quantum mechanics got firmly rooted in mathematical notions and a vast research field known as Bell nonlocality [3] was born. Recent loophole free tests [4] of Bell inequalities have firmly established the fact that certain correlations of quantum states cannot be explained by a LHV model. In the same year of EPR, Schrödinger elaborated on the proposal of EPR and pioneered the idea of quantum Steering (a weaker notion of Bell nonlocality), which is recently formalized [5] and investigated [6]. The phenomena of Bell Nonlocality and Steering are due to the existence of entangled states in quantum mechanics. Entanglement [7] is a particular form of correlations present in a composite quantum system. On one hand entanglement is necessary for the revelation of the nonlocal correlations in quantum states, on the other hand entanglement can be used as a useful resource in the field of quantum information [8], which started in 1970s and 1980s. Manipulation, quantification and application of the properties of quantum states comprise the area of quantum information. Study of quantum correlation [9, 10] is one of the potential areas to investigate in QI theory. From the operational point of view, entanglement [7, 11] can be posed as a Quantum Resource theory [12], where separable states are the free states, Local operation and classical communication (LOCC) is the free operation and Entangled state is a resource state. Resource theoretic structure of entanglement enables one to quantify and manipulate entanglement in an organized manner and develop new protocols. Entanglement can be used as a resource for different quantum information processing tasks like teleportation [13], Quantum Key Distribution (QKD) [14], Secret sharing [15] etc. Entanglement and nonlocality are two very different resources, though intimately connected. Entanglement in a state does not always guarantee nonlocality. Werner state [16] is a very well known example for this kind of situation. For certain parameter range, the state is entangled but LHV model can be constructed for both projective measurements and POVM [17], implying that the state is Bell local in that specified parameter range. If one goes beyond the normal Bell scenario consisting of non-sequential measurements [18, 19, 20, 21] and a single copy of the state [22, 23], nonlocality can be revealed for some states which allowed LHV model before. This phenomena is termed as "Hidden Nonlocality". Till now it is an open question in which framework (if there is any) entanglement and nonlocality can be regarded as equivalent resources.

Other than in nonlocality and different information processing tasks, quantum correlation plays an important role in Quantum Thermodynamics [24]. Thermodynamics is one of the oldest fields of Physics, which has been profoundly successful. Laws of Thermodynamics were mainly empirical and constructed for macroscopic systems. In present day, with the miniaturization of technology, applicability of the thermodynamics to microscopic systems is a challenge both from theoretical and practical viewpoint. Modifications and emergence of thermodynamics laws in the regime, where dynamics is governed by quantum mechanics is the premise of Quantum Thermodynamics. Peculiarity in the energetics of small systems due to the quantum effects is manifold. How the quantum resources can be used for the betterment of the performance of different thermodynamics protocols is yet to be fully understood. There are many instances, where quantum correlations can be used in an advantageous way. Still, to understand fully the role of quantum effects in Quantum Thermodynamics requires further studies.

This thesis is organized as follows. In this chapter, next few sections will be devoted to cover some basics needed for the subsequent discussion. Specifically, in the next section, I discuss the basic mathematical formalism of quantum mechanics. In section 1.2, different aspects of entanglement are discussed. Section 1.3 gives an outline of Bell nonlocality. In the last section, I review some results about the role of quantum correlations in Quantum Thermodynamics. After the preliminaries the works are described in the next few chapters.

1.1 Basic formalism of Quantum Mechanics

Mathematical formalism of quantum mechanics is well established [25]. Basically it is a statistical theory, whose predictions are probabilistic. But to interpret these probabilities and their connection to the real world is still a debatable topic giving rise to the notorious questions, like the "Measurement problem" [26], different interpretations of quantum mechanics, etc. I am not going into these philosophical issues but rather briefly recapitulate the mathematical structure of quantum mechanics. It is based on some postulates,

1. *Preparation :* In a physical experiment, the system under study is prepared in a quantum state ρ. Mathematically, it is a positive (and trace-class) unit trace linear operator in a Hilbert space $\mathcal{H}$, $\rho : \mathcal{H} \rightarrow \mathcal{H}\{\rho \geq 0, Tr[\rho] = 1\}$, and known as density matrix. In this thesis, we are dealing with finite dimensional Hilbert space (let's say of dimension d), which is isomorphic to a Complex Euclidean space $\mathbb{C}^d$. The dimension d of this Euclidean space is determined by the system under study. For example, if the system is a spin-$1/2$ operator, the dimension is 2. We denote the set of density matrices by $\mathcal{P}^d$, s.t the state of the studied system $\rho \in \mathcal{P}^d$. This set is convex and compact, with the extreme points known as pure state. A state ρ is called a pure state if $\rho = |\psi\rangle \langle\psi|$, for some vector $|\psi\rangle \in \mathcal{H}$.

2. *Measurement :* The most general measurement in QM is described by a set of positive operators $\{E_\alpha\}$, satisfying, $0 \leq E_\alpha \leq \mathbb{1}$ and $\sum_\alpha E_\alpha = \mathbb{1}$. This set is known as Positive Operator Valued Measure (POVM) and E_α's are known as Effect operators. When, in addition $E_\alpha E_\beta = \delta_{\alpha\beta}$,

they are the usual orthogonal projectors. For a given state ρ and a POVM $\{E_\alpha\}$, if the measurement outcomes are denoted by $a_\alpha \in \mathcal{A}$ (a nonempty and finite set), then the probability for getting an outcome a_α is calculated as, $p_\alpha = Tr[\rho E_\alpha]$. Equivalently, a measurement can be completely described by a set of measurement operators $\{M_\alpha\}$, with $M_\alpha^\dagger M_\alpha = E_\alpha$. It is important to note that coresponding to a particular POVM, there exists infinite set of measurement operators, each connected by a unitary. For example, $M'_\alpha = U_\alpha M_\alpha$, satisfying ${M'}^\dagger_\alpha M'_\alpha = E_\alpha$, where U_α is a unitary operator. Now, given a set of measurement operators $\{M_\alpha\}$, if the state of the system before the measurement is $|\phi\rangle$, then corresponding to the outcome a_α, the state of the system after measurement is, $\frac{M_\alpha|\phi\rangle}{\sqrt{p_\alpha}}$ or $\frac{M_\alpha \rho_\phi M_\alpha^\dagger}{p_\alpha}$, where $\rho_\phi = |\phi\rangle\langle\phi|$ and $p_\alpha = Tr[\rho_\phi M_\alpha^\dagger M_\alpha] = \langle\phi| M_\alpha^\dagger M_\alpha |\phi\rangle$ is the probability for getting the outcome a_α. When E_α's are orthogonal projectors, from spectral decomposition theorem, one can associate a Hermitian operator $\hat{O} = \sum_\alpha a_\alpha E_\alpha$, commonly known as an observable, with a_α's now to be the eigenvalues of $\hat{O}$. The expectation value of the observable $\hat{O}$ is given by, $\langle\hat{O}\rangle = \sum_\alpha a_\alpha p_\alpha$. Now, the next question is, which decides that the probability structure in QM arises from the above rule, known as the Born's rule [27] and what guarantees that it is the unique way. Gleason's theorem [28] answers this question. It states that for a given Effect operator E_α, there is some density matrix ρ, such that there is only one probability measure, which is given by the Born's rule as $p_\alpha = Tr[\rho E_\alpha]$. This result was first given by Gleason for projective measurements, valid for dimension three or more. Later, it was generalized [29] for POVM without any constraints in dimension of the Hilbert space.

3. *Dynamics :* Time evolution of a closed quantum system ρ is described by a Unitary dynamics, specifically by the Liouville-Von Neumann equation : $i\hbar\dot{\rho}(t) = [H, \rho]$, where H is the Hamiltonian of the system. This is equivalent to the Schrödinger equation written for pure states. The formal solution of this equation is, $\rho(t_2) = U(t_2, t_1)\rho(t_1)U^\dagger(t_2, t_1)$, where, $U^\dagger(t_2, t_1)U(t_2, t_1) = \mathbb{1}$. The unitary U is given by the solution of the equation, $i\hbar\frac{dU}{dt} = HU$.

4. *Composite system :* The Hilbert space of a composite quantum system $\mathcal{H}$ is obtained from the tensor product of the Hilbert spaces of constituent systems as $\mathcal{H} = \mathcal{H}_1 \otimes \mathcal{H}_2 \otimes ... \otimes \mathcal{H}_n$.

This completes the building blocks of the mathematical formalism. Next, we discuss the entanglement in a composite quantum system, which arises due to the last postulate mentioned above.

1.2 Quantum Entanglement

The concept of quantum entanglement follows from the Hilbert space structure. For a composite quantum system, a state ρ is entangled, if it can not be written in the following form,

$$\rho = \sum_i p_i \rho_i^{A_1} \otimes \rho_i^{A_2} \otimes ... \otimes \rho_i^{A_n}, \tag{1.1}$$

where, A_1, A_2,...A_n denote the subsystems. If the state can be written in the above form, it is called a separable state. A state of the form : $\rho = \rho_i^{A_1} \otimes \rho_i^{A_2} \otimes ... \otimes \rho_i^{A_n}$, is known as product state. Entanglement, as a spooky action at a distance was first recognized by Einstein, Podolosky and Rosen (EPR) in their famous EPR paper [1]. Schrödinger coined the term "Entanglement" [30] in 1935 by calling it "Verschränkung". In 1964, John. S. Bell showed that [2] entanglement is the reason behind the incompatibility of some correlations in QM with LHV model. Along with these developments, entanglement stands as a potential resource for many information processing tasks, that are impossible with classical correlations. Therefore, it is of utmost importance to understand the mathematical structure of entanglement in greater detail. Characterization, quantification, manipulation and detection of entanglement seem to be the questions to be answered. This needs an operational point of view to formalize the concepts, giving rise to the resource theory of entanglement [11]. A resource theory [12] has a common structure consisting of three ingredients : Resource states, Free states and Free operations. Resource states are the states which overcome the constraints posed by the free operations that can not be lifted by the free states. In the case of entanglement theory, free operations are the Local operation and classical communications (LOCC), free states are the separable states and resource states are the Entangled states. The physical motivation behind the restricted operation LOCC [31] is that the composite quantum system under study is distributed among many parties and each party is restricted to manipulate his/her own system (LO) and communicate classically with the other parties (CC). The states, which can be generated by the application of only LOCC operations are the separable states and thus they are the free states in the resource theory of entanglement. Any other states, which can not be prepared by LOCC only, are the entangled states and hence the resource states. So, operationally entanglement is a sort of quantum correlation, which can not be created by LOCC alone. This operational characterization of entanglement paves the way for its quantification. There are two ways to quantify entanglement. One is from the perspective of state transformation via

LOCC and the other is axiomatic quantification. I first discuss these briefly for a system comprising of two subsystems. Then in the next subsection, I will discuss the scenario in multipartite settings.

1.2.1 Bipartite Scenario

First, we note some general properties of entanglement regardless the ways of its quantification.

- Separable states contain no entanglement. They are the free states. All non-separable states contain some amount of entanglement and they are the resource states.
- Amount of entanglement in a state does not increase under LOCC and remains constant under Local Unitary (LU) operations. Two states, which are connected via local unitaries contain same amount of entanglement.

If, there is a notion for maximally entangled state, in the sense that all other states can be prepared from this via LOCC, an ordering among the states according to their entanglement is obtained. In bipartite settings, Bell states (and their LU equivalent states) serve the purpose of maximally entangled state for $d = 2$. But, the notion of a unique maximally entangled state is absent in multipartite scenario. Let's first concentrate on the bipartite settings. Any state, LU equivalent to the state,

$$|\psi_{max}\rangle = \frac{1}{\sqrt{d}} \sum_{i=1}^{d} |i\rangle |i'\rangle , \tag{1.2}$$

is a maximally entangled state. Any state of dimension d can be prepared from this state deterministically via LOCC operation only. As, LOCC does not increase the amount of entanglement in a state, the state in Eq. (1.2) has the maximal amount of entanglement and hence it is a maximally entangled state. So, this prompts the thought that, between two states ρ and σ, the state ρ is more entangled than σ, if σ can be obtained from ρ via LOCC only. Nileson's Majorisation criteria [32] gives a necessary and sufficient criteria for deterministic LOCC inter-convertibility between two bipartite pure states. Let's say that two bipartite pure states are written in their Schmidt decomposed [8] form as,

$$|\psi_1\rangle = \frac{1}{\sqrt{d}} \sum_{i=1}^{d} \alpha_i |i_A\rangle |i_B\rangle , \text{ and } |\psi_2\rangle = \frac{1}{\sqrt{d}} \sum_{i'=1}^{d} \alpha'_i |i'_A\rangle |i'_B\rangle , \tag{1.3}$$

where, α_i's and α'_i's are the Schmidt coefficients, such that, $\alpha_1 \geq \alpha_2 \geq .... \geq \alpha_d$ and $\alpha'_1 \geq \alpha'_2 \geq .... \geq \alpha'_d$. Now, $|\psi_1\rangle$ can be deterministically converted to $|\psi_2\rangle$ via LOCC iff, for all $1 \leq l \leq d$,

$$\sum_{i=1}^{l} \alpha_i \leq \sum_{i=1}^{l} \alpha'_i. \tag{1.4}$$

But, this Majorization criteria does not always hold for dimension $d > 2$, as there are incomparable states in higher dimension such that neither of the states can be converted to another with unit probability by LOCC. Vidal introduced [33, 34] a method for obtaining optimum probability for converting one pure state to another, where deterministic transformation is not possible by LOCC. So, we may think that if $|\psi_1\rangle$ and $|\psi_2\rangle$ are two incomparable states and probability of getting $|\psi_2\rangle$ from $|\psi_1\rangle$, denoted by $P(|\psi_1\rangle \rightarrow |\psi_2\rangle)$ is greater than the probability of getting $|\psi_1\rangle$ from $|\psi_2\rangle$, denoted by $P(|\psi_2\rangle \rightarrow |\psi_1\rangle)$, then $|\psi_1\rangle$ is more entangled than $|\psi_2\rangle$. But this intuition fails [33]. So, in the single copy scenario, we only get some partial order among the states according to the entanglement from the state transformation via LOCC. Situation changes in the many copy scenario. In the many copy transformation scenario, there may arise two approaches : exact and asymptotically exact state transformation. In exact case, we ask whether $\rho^{\otimes n} \rightarrow \sigma^{\otimes m}$ is perfectly attainable for a given finite value of m and n. In the asymptotic regime, we consider the case where in the limit $n \rightarrow \infty$ and for fixed $r = m/n$, the output state goes arbitrarily close to $\sigma^{\otimes m}$. Now, exact state transformation being too restrictive, the suitable approach is to allow some imperfection in the target state and in the asymptotic limit this error becomes vanishingly small. In this asymptotic limit, a unique measure of entanglement is obtained giving the entanglement order in all pure states. It is discussed below.

- *Distillable Entanglement E_D* : It is the maximum rate at which input states ρ, can be converted approximately to the two-qubit maximally entangled states via LOCC, such that asymptotically, the transformation becomes arbitrarily precise. Formally, it is given by,

$$E_D = \sup\left\{r : \lim_{n\rightarrow\infty}\left[\inf_{\Lambda} D(\Lambda(\rho^{\otimes n}), \Phi(2)^{\otimes m})\right] = 0\right\}, \tag{1.5}$$

  where, $D(\sigma, \eta)$ is a suitable measure of distance between two quantum states σ and η, $\Lambda(\rho^{\otimes n})$ denotes the LOCC transformation on n copies of the input state ρ, $\Phi(2)$ denotes a maximally entangled state for two qubits, i.e., L.U equivalent to a Bell state, and $m = rn$. In the asymptotic limit, i.e. when $n \rightarrow \infty$, the approximation in the output states become vanishingly small.

- *Entanglement Cost* E_C : It is the maximum rate at which, for a given state ρ, two-qubit maximally entangled states can be converted approximately to ρ, via LOCC, such that asymptotically, the transformation becomes arbitrarily precise. Formally, it is given by,

$$E_C = \sup\left\{r : \lim_{n\to\infty}\left[\inf_{\Lambda} D(\rho^{\otimes n}, \Lambda(\Phi(2)^{\otimes m}))\right] = 0\right\}, \qquad (1.6)$$

where all the notations are same as the before. From the definition, it is evident that E_C is defined by the reverse of the protocol, which defines E_D.

The next question is whether these two measures are equal or not. For, bipartite pure state transformations only this two measures are equal [7, 11] and equal to the Entropy of entanglement defined as $E(|\phi\rangle\langle\phi|) = S(Tr_A|\phi\rangle\langle\phi|) = S(Tr_B|\phi\rangle\langle\phi|)$ for a pure bipartite state $|\phi\rangle$, where $S(\rho) = -Tr[\rho\log\rho]$ is the Von-Neumann entropy [8] for the state ρ. So, in the asymptotic limit, for pure state transformation only (i.e ρ is pure) via LOCC, transformations (one pure state to Bell state and then Bell state to other pure state) becomes reversible and entropy of entanglement becomes the unique currency to quantify the entanglement. But this reversibility is lost for mixed states and therefore there is no unique measure of entanglement. This loss of reversibility in the mixed states is regarded as the presence of inequivalent class of entanglement in asymptotic limit. An example of two asymptotically inequivalent classes of entanglement for bipartite mixed states is Distillable and Bound entanglement. This leads us to consider the axiomatic approach [7, 11] to quantify the entanglement besides the operational approach. In this approach, a real valued function is defined to quantify the entanglement of a quantum state such that the function obeys some basic rules. There are a number of measures defined over the years in this approach. Let's now formalize the concept. A entanglement measure is a mapping from the density matrix to a positive real number : $E : \mathcal{P}^d \to \mathbb{R}^+$, such that it obeys the following properties [7, 11, 35],

- $E(\rho) = 0$, if ρ is a separable quantum state.
- $E(\rho)$ does not increase under LOCC operation. Sometimes, a stronger condition is employed : $E(\rho) \geq \sum_i p_i E(\sigma_i)$, i.e. E does not increase on average under LOCC.
- $E(\rho)$ is normalized by requiring $E(\Phi(d)) = \log_2 d$, where, $\Phi(d)$ is a maximally entangled state for a bipartite system of d dimension.

- $E(\rho)$ reduces to the Entropy of Entanglement, when ρ is a pure state.

A function, $E(\rho)$, which only obeys first three properties is called a Entanglement Monotone (does not increase on average under LOCC) and which obeys all the four is called an Entanglement Measure (does not increase under LOCC deterministically). Though, often in practice both terms are used in similar footings. Along with the above properties, sometimes, other properties are imposed for certain measures, like, Additivity, Convexity and Continuity. In literature, there are many entanglement measures and monotones proposed so far. I discuss some of these measures below. Note that, Distillable Entanglement (E_D) and Entanglement cost (E_C) are two entanglement measures from axiomatic point of view also.

- *Entanglement of Formation* E_F *:* For a mixed state ρ this measure [36] is obtained by the convex roof extension of the measure Entropy of Entanglement for pure states. It is defined as,

$$E_F = \inf\{\sum_i p_i E(|\phi_i\rangle\langle\phi_i|)\}, \tag{1.7}$$

where, $\rho = \sum_i p_i |\phi_i\rangle\langle\phi_i|$ and $E(|\phi_i\rangle\langle\phi_i|)$ denotes the Entropy of Entanglement for the pure state $|\phi_i\rangle$. It is an open question to decide whether E_F is additive or not. Due to the optimization involved in the definition, E_F is extremely hard to compute. For two-qubit scenario, a closed form formula [36, 37, 38] is known for E_F based on a quantity called Concurrence $\mathcal{C}$ [36, 37], defined as,

$$\mathcal{C}(\rho) = max\{0, \lambda_1 - \lambda_2 - \lambda_3 - \lambda_4\}, \quad \lambda_1 \geq \lambda_2 \geq \lambda_3 \geq \lambda_4, \tag{1.8}$$

where, λ_i's are the square root of the eigenvalues of the operator $\rho\sigma_y \otimes \sigma_y\rho^*\sigma_y \otimes \sigma_y$, with ρ^* as the complex conjugate of ρ. Now, E_F is written as,

$$\begin{aligned} E_F = &-\Big(\frac{1+\sqrt{1-\mathcal{C}^2}}{2}\Big)\log_2\Big(\frac{1+\sqrt{1-\mathcal{C}^2}}{2}\Big) \\ &-\Big(\frac{1-\sqrt{1-\mathcal{C}^2}}{2}\Big)\log_2\Big(\frac{1-\sqrt{1-\mathcal{C}^2}}{2}\Big). \end{aligned} \tag{1.9}$$

E_F is a monotonically increasing function of Concurrence. So, in literature Concurrence is often used as a measure of entanglement for the simplification of analysis in two-qubit system. For higher dimension there is no unique definition of Concurrence.

- *Logarithmic Negativity* E_N *:* This measure is based on the negativity of the partial transposition of the density matrix ρ. It is defined as,

$$E_N(\rho) = \log_2 \|\rho^T\|, \tag{1.10}$$

where, ρ^T denotes the partial transpose of ρ, with respect to one of the parties, and $\|A\| = Tr\sqrt{A^\dagger A}$ denotes the trace norm of the operator A. E_N is additive but not convex. One of the advantages to use this measure is that it is very easy to compute unlike E_F.

After quantification of entanglement, the next question comes to the detection of entanglement. Given a quantum state how to determine whether the state is Entangled or not is in general a difficult problem. There are many mathematical criteria [7, 39], which determine whether a known density matrix is separable. One well known example is the PPT [40, 41] criterion, which states that in $2 \otimes 2$ and $2 \otimes 3$ dimension, a state ρ is separable iff it has Positive Partial Transpose (PPT). This criterion is only necessary but not sufficient for higher dimension due to the existence of bound entangled states [42], which are entangled but PPT making them not distillable. Like the PPT criterion, there are many other separability criteria [7, 39] derived over the years. These criteria are all based on the fact that one knows the density matrix and then does some operations on the state to determine separability. On the other hand, to detect the entanglement in an unknown quantum state requires characterization in terms of directly measured observables. Entanglement Witness [39] serves that purpose. An observable $\mathcal{W}$ is called an Entanglement Witness, if $Tr[\rho\mathcal{W}] \geq 0$ for any separable state ρ and $Tr[\sigma\mathcal{W}] < 0$, for at least one state σ, which is entangled. Note that, there may be entangled states for which expectation value of the operator $\mathcal{W}$ gives positive value. But if for some state it gives negative value, then that state is surely entangled. Existence of Entanglement Witness results from the hyperplane separation theorem [43] for convex sets. Separable states form a convex set as a convex hull of product sets. This allows to identify an operator called Witness operator for an entangled state, which lies outside the set of separable states. Bell inequality is also one of the oldest tools to detect entanglement [44] in terms of observable quantities, though it is not an optimal witness, due to the inequivalency of entanglement and nonlocality.

1.2.2 Multipartite Scenario

With the increase in the number of parties, complexity increases both mathematically and practically. In multipartite settings, there exists different forms of entanglement. For example, for a three partite system, there are three classes of states : Fully separable, Bi-separable and Genuinely Entangled state. Generally, a state ρ of a n-partite system is called k-separable, if it can be written as,

$$\rho = \sum_i p_i \rho^{A_1} \otimes \rho_i^{A_2} \otimes ... \otimes \rho_i^{A_k}, \tag{1.11}$$

where, $\sum_i p_i = 1$, and A_1, A_2,...A_k denotes one subsystem or a group of subsystems, such that total number of subsystems in all these k groups is n. Regarding the operational quantification of Entanglement in multipartite scenario, the crucial difference with bipartite scenario is that there is no unique notion of a maximally entangled state in this settings. For example, following the bipartite scenario, a natural choice for a maximally entangled state in three-qubit scenario would be a LU equivalent state of a GHZ state ; $|GHZ\rangle \equiv \sqrt{1/2}(|000\rangle + |111\rangle)$. But, not all tripartite states can be obtained from GHZ state deterministically by LOCC only. W state [45] ; $|W\rangle = \sqrt{1/3}(|001\rangle + |010\rangle + |100\rangle)$ is one of such states. One can not transform a GHZ state to a W state exactly by LOCC even with a small probability. This gives rise to a new scheme of transformation called Stochastic Local Operations and Classical Communications (SLOCC), where state conversions are carried out via LOCC but not deterministically. GHZ and W are the representatives of two SLOCC inequivalent classes [45] called GHZ class and W class respectively. In tripartite scenario, there are six SLOCC inequivalent classes, out of which the above mentioned two classes represent genuine three-partite entanglement. Complexity increases with the number of parties. For four qubits and more there are infinitely many [46, 47] SLOCC inequivalent classes. We can not compare entanglement in two different SLOCC inequivalent classes like GHZ and W for three qubits. But also within same SLOCC class there is no ordering and also no notion of maximally entangled state. Because, there is no state within a SLOCC class, from which any state in that class can be obtained deterministically. Though in many situation, different perspectives other than operational notion (LOCC inter-convertibility) are invoked to call a state maximally entangled. For example, in three-qubit case, GHZ state is considered to be the maximally entangled state in several aspects. Like, when one qubit is traced out, the two-qubit state is maximally mixed, an maximally entangled two-qubit state shared between any two of the three parties can be obtained from a GHZ state deterministically etc. So, one may wonder, what happens in the asymptotic limit. Can an unambiguous ordering and a notion of maximally entangled state be obtained? Unfortunately, there is no reversibility in state transformation even in the asymptotic limit [11]. Unlike the bipartite scenario (for pure states), there are infinitely many inequivalent forms of entanglement in the asymptotic limit even for pure states. Nevertheless, there are many entanglement measures constructed for multipartite states for different purposes. A common measure is average of a certain bipartite entanglement measure over all the bi-partitions of a multipartite state. In my subsequent discussions I will use this kind of measure taking Entanglement Entropy as the measure of one bi-partition. These kind of measures are used to define the Maximally Multipartite Entangled (MME) [48, 51] and Absolutely Maximally Entangled (AME) states [49, 50, 51]. MME are those states, which maximize the average entanglement over all bipartitions and AME are those states for which the reduced state is a maximally mixed state for any bi-partition. Another measure, widely used for three-qubit pure states is three-tangle or residual tangle [52], defined as,

$$\tau_3 = \tau(A:BC) - \tau(A:B) - \tau(A:C), \tag{1.12}$$

where, the $\tau(X : Y)$ denotes the square of Concurrence ($\mathcal{C}$) in the bi-partition $X - Y$. Tangle is zero for bi-separable states and W class, but is strictly positive for all states in GHZ class. Tangle measure has been generalized to more than three parties in Ref. [53]. There also have been efforts [7, 54, 55] to generalize the Concurrence ($\mathcal{C}$) for multipartite states. Like the bipartite scenario, the next important task is to detect different types of entanglement for multipartite states. The characterization of separability is naturally extended [56] in multipartite scenario. There are several other separability criteria in literature [39]. Besides, due to the existence of different types of entanglement, witness operators are constructed aiming to detect specific classes of entanglement. Like there are witness operators constructed to detect [39] states within GHZ class. They can not be used to detect W class states or biseparable states. These witness operators can be generalized [39] to more than three parties using several construction procedures developed over the years.

1.2.3 QIP tasks using Entanglement as a resource

As already mentioned, there are several Quantum Information Processing (QIP) tasks which use entanglement as a resource. I briefly discuss about some of these protocols relevant to this thesis.

Teleportation *:* Quantum teleportation, first put forward in a seminal paper [57] by Bennet *et al.*, is a scheme, where one party sends an unknown quantum state to another spatially separated party. For this protocol to be successful, the two parties called Alice (sender) and Bob (receiver) share a

Bell state and they can classically communicate. Without the use of entanglement this task seems formidable as Alice has to know the state to be sent. Then only she can communicate sufficient information to Bob, such that he can reproduce the state. But gaining information about an unknown quantum state is not possible with a single copy. The best Bob can achieve with Alice's information is make a state which is not a perfect copy of the desired state but matches with it with a maximum fidelity of $2/3$ on average. Now, this seemingly impossible task can be done perfectly with the use of a shared Bell state between them. Let's say that the state which has to be sent to Bob is $|\psi\rangle \equiv \alpha\,|0\rangle + \beta\,|1\rangle$ and the shared Bell state is $|\phi^+\rangle \equiv \sqrt{1/2}\,|00\rangle + \sqrt{1/2}\,|11\rangle$. Total state can be written as,

$$|\Phi\rangle \equiv \frac{1}{\sqrt{2}}\big[(\alpha\,|0\rangle + \beta\,|1\rangle)(|00\rangle + |11\rangle)\big] \equiv \frac{1}{\sqrt{2}}\big[\alpha(|00\rangle\,|0\rangle + |01\rangle\,|1\rangle) + \beta(|10\rangle\,|0\rangle + |11\rangle\,|1\rangle)\big]. \tag{1.13}$$

Alice now makes a joint measurement in the Bell basis on the first two qubits of the above state (one from the state to be sent and other from the shared Bell state) in her possession. The Bell basis are the four Bell states written below,

$$|\phi^+\rangle \equiv \sqrt{1/2}\,|00\rangle + \sqrt{1/2}\,|11\rangle \tag{1.14}$$

$$|\phi^-\rangle \equiv \sqrt{1/2}\,|00\rangle - \sqrt{1/2}\,|11\rangle \tag{1.15}$$

$$|\psi^+\rangle \equiv \sqrt{1/2}\,|01\rangle + \sqrt{1/2}\,|10\rangle \tag{1.16}$$

$$|\psi^-\rangle \equiv \sqrt{1/2}\,|01\rangle - \sqrt{1/2}\,|10\rangle \tag{1.17}$$

Using the expression of the Bell states, one can rewrite the state in Eq. (1.13) as,

$$|\Phi\rangle \equiv \frac{1}{2}\big[(\alpha\,|0\rangle + \beta\,|1\rangle)\,|\phi^+\rangle + (\alpha\,|0\rangle - \beta\,|1\rangle)\,|\phi^-\rangle + (\alpha\,|1\rangle + \beta\,|0\rangle)\,|\psi^+\rangle + (\alpha\,|1\rangle - \beta\,|0\rangle)\,|\psi^-\rangle\big]. \tag{1.18}$$

After measurement Alice projects her qubits to one of the Bell states and communicates the result to Bob over a classical communication channel. Depending upon Alice's information, Bob applies one of the following four operations,

- If Alice projects to $|\phi^+\rangle\langle\phi^+|$, Bob applies $\mathbb{1}$.
- If Alice projects to $|\phi^-\rangle\langle\phi^-|$, Bob applies σ_z.

- If Alice projects to $|\psi^+\rangle\langle\psi^+|$, Bob applies σ_x.

- If Alice projects to $|\psi^-\rangle\langle\psi^-|$, Bob applies $i\sigma_y$.

Suitable operation depending upon Alice's classical information helps Bob to prepare the desired state $\alpha|0\rangle + \beta|1\rangle$. This is the essence of quantum teleportation. Above protocol uses a maximally entangled state as a resource. With a nonmaximally entangled state or a mixed entangled state, teleportation can not be done with unit fidelity and unit probability, but it gives the advantage over the classical limit $2/3$, though some bound entangled state [58] can not achieve a fidelity better than the classical fidelity $2/3$. Recently, in Ref. [59], using a different benchmarking rather than the fidelity between input and output states, authors have shown that all entangled states can demonstrate non-classical teleportation. In experiment, quantum teleportation has been realized [60] using various technologies.

Dense Coding : In Dense coding [61] Alice wants to maximize the rate at which she can send classical information to Bob over a quantum channel (we assume it to be perfect, i.e no loss of information). Without sharing entanglement, the best she can do is to send one classical bit per qubit. If they share a Bell state between them like before, she can send two bits per qubit to Bob. Let's say, they share the Bell state $|\phi^+\rangle = \frac{1}{\sqrt{2}}(|00\rangle + |11\rangle)$ between them. Now Alice performs one of the four operations on her qubit converting the shared state to one of the four orthogonal Bell states.

- $(\mathbb{1}_A \otimes \mathbb{1}_B)|\phi^+\rangle = \frac{1}{\sqrt{2}}(|00\rangle + |11\rangle) \equiv |\phi^+\rangle$.

- $(\sigma_x \otimes \mathbb{1}_B)|\phi^+\rangle = \frac{1}{\sqrt{2}}(|01\rangle + |10\rangle) \equiv |\psi^+\rangle$.

- $(i\sigma_y \otimes \mathbb{1}_B)|\phi^+\rangle = \frac{1}{\sqrt{2}}(|01\rangle - |10\rangle) \equiv |\psi^-\rangle$.

- $(\sigma_z \otimes \mathbb{1}_B)|\phi^+\rangle = \frac{1}{\sqrt{2}}(|00\rangle - |11\rangle) \equiv |\phi^-\rangle$.

After performing the operation, Alice sends her qubit to Bob over a quantum channel. Upon receiving Alice's qubit, Bob can easily distinguish four states by measuring in Bell basis. If the four Bell states are assigned to the bits 00, 01, 10, and 11 respectively, Bob gets two bits of classical information per qubit successfully.

Quantum Key Distribution : Quantum Key Distribution (QKD) was pioneered by Bennet and Brassard [62] in 1984. But this BB84 protocol does not use entanglement to establish a secure key. In

1991, Ekert [14] proposed a protocol for QKD between two parties using Bell state and presented the security analysis using the Bell-CHSH inequality. We discuss the Ekert's protocol here. The original protocol [14, 63] involves a Bell state shared between two parties. In the absence of an eavesdropper, *e.g.* Eve, the protocol is reminiscent of the BB84 protocol. Two parties hold one qubit each and agree on two sets of basis states in which they measure their own qubits randomly. After the measurement step, they announce their choices of the bases. Those data are kept, where the bases are matched and the rest are discarded. So, in half of the cases they get perfectly correlated results and hence can construct a secure key. The secure key rate is $1/2$ in this scenario. But often in a practical scenario, the perfect correlation is not obtained, which indicates noise in the entanglement channel or imperfect measurement or possibly Eve's intervention. Alice and Bob use a part of the matched data to determine the Quantum Bit Error Rate (QBER) and the remaing part is used to build secure key after error correction and privacy amplification. To know Eve's presence, in the Ekert's original protocol, Alice and Bob use one extra set of basis states each that helps in testing the violation of Bell-CHSH inequality. If it is maximally violated then there is no eavesdropper's attack. Let the three measurement settings be (A_1, A_2, A_3) for Alice and (B_1, B_2, B_3) for Bob. This gives rise to nine combinations of measurement operators. Alice's the settings are : $A_1 = \sigma_x$, $A_2 = 1/\sqrt{2}(\sigma_x + \sigma_y)$ and $A_3 = \sigma_y$. Whereas, Bob's measurement settings are : $B_1 = 1/\sqrt{2}(\sigma_x + \sigma_y)$, $B_2 = \sigma_y$ and $B_3 = 1/\sqrt{2}(-\sigma_x + \sigma_y)$. Two combinations used to make the secret key are (A_2, B_1) and (A_3, B_2), because of perfect correlations in these two settings. Four combinations e.g (A_1, B_1), (A_1, B_3), (A_3, B_1) and (A_3, B_3) are required to test the Bell violation. These particular measurement settings give the maximal violation for a Bell state. Remaining combinations of the measurements are discarded. So, in this case the key rate is $2/9$ instead of $1/2$. Over the years there are many generalization of QKD protocols [64] extending it to multipartite scenarios, device independent variants and obviously implementing in experiments.

1.3 Bell Nonlocality

As already mentioned in the introduction that in 1964, John Bell [2] proved that any physical theory satisfying the notion of local causality is incompatible with QM. In this section, I briefly discuss the notion of local causality, what it means, and the construction of Bell inequality. Then I discuss different Bell inequalities in bipartite and multipartite scenarios. First, I introduce the notion of Bell

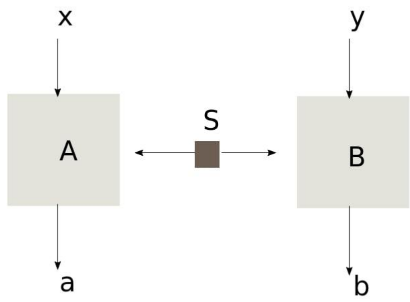

Figure 1.1: Bell experiment with two parties.

experiment. There are two spatially separated parties Alice and Bob, doing local measurements on their respective systems. The measurements are labeled by the inputs x and y respectively. The outputs of their measurements are given by a and b. Local systems of Alice and Bob can be two quantum entangled particles generated from a source S. The joint probability distribution $\mathbf{p} = \{p(ab|xy)\}$ characterizing the Bell experiment is called correlations or behavior. We are interested only in these correlations, anything else is a black box. These joint probability distributions are operational quantities (experimentally reproducible) and we say that they denote a quantum "phenomena". An ontological model which is designed to reproduce the predictions of a quantum phenomena is called A theory. The essence of Bell theorem is that it says certain theories are not compatible with a quantum phenomena. Next section describes this incompatibility.

1.3.1 LHV Model

A theory consists of some ontic variables λ, also called hidden variables which are not accessed by the experiment. The predictions of a quantum phenomena are reproduced by the joint probability distributions of a theory dependent on the hidden variable λ as,

$$p(ab|xy) = \int_{\Lambda} q(\lambda)p(ab|xy, \lambda)d\lambda, \tag{1.19}$$

where, the values of λ are picked from the set Λ with the probability distribution $q(\lambda)$. In addition, we assume that there is "free will" or measurement independence [65], which is expressed as $q(\lambda|xy) = q(\lambda)$ A theory is called Local (L) iff $p(a|x, y, \lambda) = p(a|x, \lambda)$, and deterministic (D) iff $p(ab|x, y, \lambda)$'s are either 0 or 1 [66]. A theory is said to satisfy Local Causality (LC) [66] if $p(a|b, x, y, \lambda) = p(a|x, \lambda)$ and $p(b|a, x, y, \lambda) = p(b|y, \lambda)$. A theory is called factorizable, iff $p(ab|xy, \lambda) = p(a|x, \lambda)p(b|y, \lambda)$.

Mathematically LC is equivalent to factorizability. Local Determinism (LD) is stronger criteria than LC or factorizability. LD implies LC but the converse is not true. We reserve the terminology Local Hidden Variable (LHV) model, for a theory respecting LC.

- ***Bell's Theorem :*** LHV model, a theory which satisfies LC or factorizability is not compatible with some quantum phenomena, i.e. certain correlations in QM can not be decomposed as,

$$p(ab|xy) = \int_{\Lambda} q(\lambda)p(a|x,\lambda)p(b|y,\lambda)d\lambda. \tag{1.20}$$

  It can be shown that, a theory satisfying LC or factorizability satisfies Bell inequality.

As seen above, Bell's theorem is obtained from some ontological criteria. But it can also be derived under operational assumptions [67]. A phenomena is called no-signaling iff,

$$\begin{aligned}\sum_b p(ab|xy) &= \sum_b p(ab|xy'), \forall a, x, y, y' \\ \sum_a p(ab|xy) &= \sum_a p(ab|x'y), \forall a, x, y, y'\end{aligned} \tag{1.21}$$

Next, a phenomena is called Predictable iff, $p(ab|xy)$'s are either 0 or 1. Note that, No-signaling and Predictivity are very similar to the Locality condition and Determinism, but the former notions are in operational level and the later notions are in ontic level. In Ref. [67], authors showed that No-signaling and Predictivity are sufficient to derive Bell inequalities, much like the Locality and Determinism are sufficient (not necessary) to derive Bell inequalities.

1.3.2 Bell inequalities

The set of joint probabilities $p(ab|xy)$ which satisfy the LC relation of Eq. (1.20) is called the set of local correlations $\mathcal{L}$. This set is closed, bounded, convex and forms a polytope. A polytope is a generalization of polygons to any dimension. Mathematically, there are two equivalent definitions [68] of a polytope: V representation and H representation. A V-polytope is the convex hull of a finite set of points $\in \mathbb{R}^d$, which are called vertices. A H polytope is an intersection of a finite number of closed halfspaces in some $\mathbb{R}^d$, which is bounded. So, a polytope is a set of finite number of points $P \subseteq \mathbb{R}^d$, which can be represented as either a V or a H polytope. The dimension of a polytope is the dimension of its affine hull. The elements of $\mathbf{p}$ belong to the set of quantum correlations $\mathcal{Q}$ if,

$p(ab|xy) = Tr(\rho_{AB} M_{a|x} \otimes M_{b|y})$, where $M_{a|x}$ and $M_{b|y}$ are POVM elements of corresponding measurements. Set of quantum correlations is closed, bounded and convex, but it is not a polytope as there are infinite number of extremal points. No-signaling correlations also form a polytope, which consist of both local and nonlocal vertices. Both $\mathcal{L}$ and $\mathcal{Q}$ satisfy the no-signaling constraints, but there are $\mathcal{NS}$ correlations which do not satisfy locality and also do not belong to $\mathcal{Q}$. Any local behavior admits a quantum description and hence belongs to $\mathcal{Q}$. But there are quantum correlations which do not belong to $\mathcal{L}$. So, finally we have, $\mathcal{L} \subset \mathcal{Q} \subset \mathcal{NS}$, which is shown in the Fig. (1.2). Though, the set of quantum correlations is not so simple as it may appear from the schematic diagram. Recently, in [69] authors have investigated the nontrivial geometry of set of quantum correlations. From hyperplane separation theorem [43], for each behavior $\mathbf{p}$ which is not the part of $\mathcal{L}$ or $\mathcal{Q}$ or $\mathcal{NS}$, there is a hyperplane that separates this $\mathbf{p}$ from the corresponding set. If the set is $\mathcal{L}$ then this is nothing but a Bell inequality. This Bell inequality is also called facet Bell inequality. From the Fig. (1.2), it is

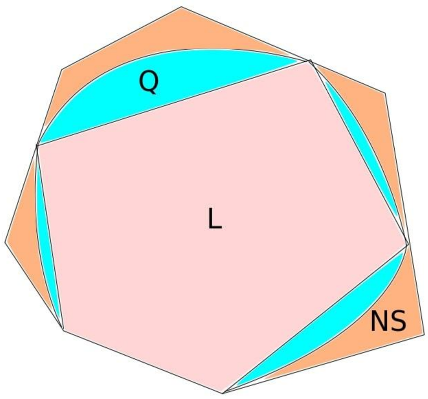

Figure 1.2: Schematic diagram of different type of correlations.

evident that a facet Bell inequality is the tight or optimal Bell inequality for a set of local correlations. One can in principle construct Bell inequalities which are not facets of the local polytope, but these would not be optimal in the sense that there may be some quantum correlations which are nonlocal w.r.t a facet Bell inequality, but do not violate the non-optimal one. In literature [3], there are many Bell inequalities which are useful for different purposes but they are not facet Bell inequalities. I now give some well known examples of Bell inequalities.

Bipartite scenario : Perhaps the most famous example in bipartite settings is the Clauser-Horner-Shimony-Holt (CHSH) inequality [70], which is the only nontrivial facet inequality for two parties and two dichotomic measurement settings per party. With the measurement settings A_1, A_2 at one side and B_1, B_2 at the other side, it has a very simple structure as written below,

$$A_1B_1 + A_1B_2 + A_2B_1 - A_2B_2 \leq 2. \tag{1.22}$$

The left-hand side should be thought of as the expectation value of the observables. Maximum quantum violation of this inequality is $2\sqrt{2}$, which is known as the Tsirelson's bound [71]. Bell states show this maximal violation for specific measurement settings. For example, for the state $\frac{1}{\sqrt{2}}(|00\rangle + |11\rangle)$, the expectation value of the Bell-CHSH operator in Eq. (1.22) is $2\sqrt{2}$ for $A_1 = \sigma_x$, $A_2 = \sigma_z$, $B_1 = \frac{1}{\sqrt{2}}(\sigma_x + \sigma_z)$, and $B_2 = \frac{1}{\sqrt{2}}(\sigma_x - \sigma_z)$. With the local unitary operators, one can find the suitable measurement settings for the Bell states to achieve the maximal violation. Gisin showed that [72, 73] any pure bipartite state of arbitrary dimension violates Bell-CHSH inequality for suitable measurement settings. This is known as Gisin's theorem. There have been many efforts [74, 75, 76, 77] from different approaches to extend this theorem to multipartite scenario. In Ref. [78], authors provided the optimal quantum violation of Bell-CHSH operator and the corresponding measurement settings for a general two-qubit mixed state. Complexity increases with the increase in the dimensions of the Hilbert spaces. For arbitrary dimension d and two measurement settings per party, Collins-Gisin-Linden-Massar-Popescu (CGLMP) inequality [79] is notable. In Ref. [80] it was shown that CGLMP inequality is also a facet Bell inequality. But astonishingly, states [81] that violate CGLMP inequality maximally are not the maximally entangled states. Recently, Bell inequalities for arbitrary dimensions and arbitrary measurement settings have been constructed [82], which give maximal violation for maximally entangled state, but they are not facet inequalities as expected. There is a huge literature of Bell inequalities [3] both facet and non-facet constructed for various purposes.

Multipartite scenario : Multipartite scenario is more complex due to the presence of different types of entanglement even in pure states. Like the famous Mermin-Ardehali-Belinskii-Klyshko (MABK) inequalities [83, 84] were designed for GHZ states. GHZ state violate the inequalities maximally. But it can not be used to guarantee that it certifies genuine entanglement, because bi-separable states also violate the MABK inequalities. Svetlichny inequality [85] is a famous example of a Bell inequality constructed for genuinely entangled three-qubit states. But the definition of genuine nonlocality used by Svetlichny was stronger. A strictly weaker definition was introduced in Ref. [86]. Nonetheless, the equivalence of genuine tripartite entanglement and genuine tripartite nonlocality is an open question [86] even for pure states. As there is no notion of maximally entangled states in multipartite scenario, different Bell inequalities are constructed looking at different states. In Ref. [87] authors constructed a Bell inequality, which is violated maximally by a four-qubit cluster state [88]. Depending upon purposes people have constructed many variants of multipartite Bell inequalities. In Ref. [89] authors constructed the set of correlation Bell inequalities for n parties and two dichotomic measurement per party. These inequalities are also facet inequalities. Śliwa constructed [90] all facet Bell inequalities for three parties and two dichotomic measurements per party. In [91] authors used the Bell inequalities from [89] to show that W states are more robust against noise compared to the GHZ states. In [92, 93] Bell inequalities were devised to discriminate between multipartite entangled states. There are many such bell inequalities constructed for multipartite settings (with arbitrary dimension and measurement settings also) [3] each designed for different purposes.

1.4 Entanglement in Quantum Thermodynamics

Quantum Thermodyanmics [94] is the study of thermodynamic properties of microscopic system, specifically quantum systems. The laws of thermodynamics, originally formulated for macroscopic systems require careful re-investigation in the quantum regime as the miniaturization of current technology demands. Emergence of thermodynamic laws from quantum dynamics gives a close correspondence between two most successful physical theories. There are many facets [95] of Quantum Thermodynamics, like foundations of statistical mechanics, thermalization, quantum heat machines, information thermodynamics, open quantum system, and resource theory of thermodynamics. In each of these areas, the distinguishing quantum effects like Coherence, quantum correlations play important roles and yet to classify what is genuinely quantum [96] in Quantum Thermodynamics is a difficult question. In this section, I will briefly discuss some developments in understanding the effect of quantum correlation, specifically quantum entanglement in Quantum Thermodynamics. There are varied scenarios and thermodynamic protocols, where quantum correlations are valuable resources. Not only that, how the thermodynamic laws are getting modified or reformulated in the presence of correlation is an important question to ask.

1.4.1 Different forms of Quantum correlation

I have discussed Entanglement [7] and Bell nonlocality [3] that capture features of quantum correlations. Bell Nonlocality is a stronger form of correlation than entanglement. Interestingly, separable states also contain some kind of correlation, which is not entirely classical. Actually, there is no unique way to define classical-quantum version. If one consider Local Causality (LC) as one way to define classical correlations then Bell nonlocality characterizes non-classical correlations or genuinely quantum correlation. Likewise, entanglement is the non-classical correlation with respect to LOCC. More generally, information theoretic measures capture features of correlations that go beyond entanglement. Discord is one of such examples. The amount of correlation between two classical random variables A and B is quantified by the mutual information $I(A, B)$ [8, 97],

$$I(A, B) = H(A) + H(B) - H(A, B), \tag{1.23}$$

where, $H(X)$ is the Shanon entropy [97] of the probability distribution $p(X)$ of the random variable X. Quantum generalization of this quantity, written as $\mathcal{I}(A, B) = S(A) + S(B) - S(A, B)$, where $S(X)$, is the Von-Neumann entropy of a density matrix ρ_X. An equivalent form of mutual information in Eq. (1.23) can be written in terms of the conditional entropy $H(X|Y) = H(X, Y) - H(Y)$, as $J(A, B) = H(A) - H(A|B)$. For classical random variables, $I(A, B) = J(A, B)$. But for quantum case, definition of conditional entropy is not unique. One way to define the quantum version $S(A|B)$ of the conditional entropy $H(A|B)$ is to consider a set of POVM $\{E_b\}$ on the subsystem B. The conditional state of the subsystem A, after the measurement on B is given by, $\rho_{A|b} = Tr_B(E_b\rho_{AB})/p_b$, where, $p_b = Tr(E_b\rho_{AB})$ is the probability of the outcome b. Now, the quantum version of conditional entropy is defined as $S(A|B) = S(A) - S(A|\{E_b\})$, where, $S(A|\{E_b\}) = \sum_b p_b S(\rho_{A|b})$. Then one defines [98, 99] for the state ρ_{AB}, conditional entropy $\mathcal{J}(A, B) = S(A) - \max_{\{E_b\}} S(A|\{E_b\})$. And unlike the classical case, $\mathcal{J}(A, B)$ and $\mathcal{I}(A, B)$ are not same. Indeed the difference between these two is the quantifier of quantum correlation present in the state ρ_{AB} and is called discord $D(A, B) = \mathcal{I}(A, B) - \mathcal{J}(A, B)$ [100]. This difference is coming from the fact that quantum measurement disturbs the state. If one state is such that it is perturbed by the measurement on side A and not on the side B, then discord for this state is zero for measurement on B. Such states are called quantum-classical or classical-quantum upon exchanging the role of A and B. A state is classical-quantum state iff

$\rho_{AB} = \sum_i p_i |i\rangle \langle i| \otimes \rho_i^B$, where $\{|i\rangle\}$ is an orthogonal set of vectors. This shows that in general a separable state of the form $\rho_{AB} = \sum_i p_i \rho_i^A \otimes \rho_i^B$ contains non-zero quantum discord, a form of quantum correlation which is weaker than entanglement. For pure states all forms of correlations are manifested as entanglement. In literature [9, 10] there are various other measures to quantify the genuine quantum correlation. Notable measures are Measurement-induced disturbance, Work-deficit, Relative entropy of discord and dissonance, etc.

1.4.2 Thermodynamic laws and correlation

In macroscopic thermodynamics, the interaction between system and the environment (thermal bath) is negligible [101] and they are like the isolated parts of a composite system. But when it comes to quantum system the correlation between two systems (one is the concerned system and other is the bath) becomes important. An uncorrelated state of systems A and B is given by the product state $\rho_A \otimes \rho_B$. But, if the total state can not be written in this form, the systems are correlated and the conventional definitions of thermodynamic quantities like work, heat are no longer valid [101, 102, 103, 104]. The second law of thermodynamics tells that, the entropy of a subsystem can never decrease. However, this thermodynamic arrow of time does not hold [105, 106, 107], if the system and bath is initially correlated. Consequently, the laws of thermodynamics need a reformulation through the redefinition of thrmodynamic quantities [102, 103, 104, 108] in the presence of quantum correlation. Recently, experiment has also been performed [109] to observe this violation of classical thermodynamics.

1.4.3 Correlation advantageous or not

As discussed above, quantum correlations give rise to some anomalous situations. But it can also be helpful from operational and practical point of view. One of the most important aims of Thermodynamics is extracting useful work from a system. Unification of seemingly different heat engines in terms of efficiency started in early 19th century with Sadi Carnot [110]. From then onward, converting heat with increasing efficiency into useful work for practical and industrial purposes got a thrust. With the advent of quantum heat engines [169] a lot of new possibilities came up. Using genuine quantum effects for the betterment of engine's performance started getting attention. Indeed, when the working medium of a quantum engine constitutes more than one subsystems, correlations come into the play. The correlation include quantum effects beyond entanglement as captured by, e.g., discord. In Ref. [112], it was shown that quantum discord is an essential resource in a photo carnot engine, as the efficiency can exceed the classical value exploiting the correlation. In other works like in Ref. [113, 114, 115, 116, 117, 118, 119], quantum Otto engines and Carnot engines with correlated (entanglement or discord can be present) working medium are shown to be more effective than the uncorrelated ones in terms of work extraction and efficiency. In a recent work [120], quantum Otto engine is designed with two qubits as the working medium, coupled to local and common baths, which may be out of equilibrium. They showed a monotonic dependence of the extracted work on discord and entanglement, establishing the advantage of quantum correlation. Another scenario one can consider is the work extraction from a system isolated from thermal bath, and undergoing a cyclic unitary process controlled externally. Maximum work extracted from the system in this situation is called Ergotropy [121]. States, form which no work can be extracted are called passive states. A state is passive [122] iff it commutes with the system Hamiltonian and its eigenvalues are arranged from larger to smaller values with energy. A thermal state is obviously a passive state. But it has also another property which is called completely passive. A state σ is completely passive iff $\sigma^{\otimes n}$ is passive [122] for the Hamiltonian $H = H_1 + H_2 + ... + H_n$. The crucial thing that happens for this many copy tarnsformation is that the Unitary can now be entangling. Indeed authors in Ref. [122] showed that an entanglement generating unitary extracts more work than an independent one. Though subsequent work [123] showed that entanglement generation is not necessary for optimal work extraction, but there is a trade off. Generation of less entanglement leads to more number of required operations and hence time. In Ref. [124], authors computed optimum extractable work from general entangled states, separable states and states with a constant entropy. They showed that for small quantum ensembles entanglement gives an advantage for work extraction but this advantage vanishes when the number of systems in the ensemble is large. In this aspect, recently, it has been shown that [125] non-zero quantum discord between the system and an ancilla helps to increase the ergotropy. In the regime of Information Thermodynamics, entanglement can be used for the betterment of the performance of Szilard engine [126, 127, 128], where one can extract work from a single temperature exploiting the information. It was shown that [129, 130, 131, 132], entanglement between different subsystems, like engine and bath or the engine and observer or two parts of engine can be used to extract work beyond classical regime. In Ref. [133], authors showed that the engine can be driven only by quantum discord. On the other hand in Ref. [134, 135] Thermodynamic perspective was used to quantify the quantum correlation. The difference between global and local work extraction using LOCC is named as "work deficit". For a pure state, this boils down exactly to the Distillable Entanglement of the state. This shows an intimate connection between quantum correlation and quantum thermodynamics. Not only that, there are works, where extracted work is used to detect the entanglement in the system. In Ref. [136], authors showed that one can extract more work from a heat bath using entangled system than using classically correlated systems. Extending that idea to tripartite scenario [137], a protocol was devised to distinguish GHZ, W, and separable states in terms of work extraction using LOCC. In a recent work [138], authors showed that bipartite Gaussian entanglement can be detected by the amount of work extraction in a continuous variable Szilard engine. Despite the fact that, quantum correlation is advantageous in work extraction in a varied scenarios, still a general consensus regarding the advantages of quantum correlation in heat machines and other thermodynamic protocols does not exist in a model independent way. Maximum works that have been done are suited for some particular models and settings. Moreover, the quantum-classical transition in quantum thermodynamics and recognizing the genuine quantum effects [139] is another difficult problem to address.

1.5 Plan of the thesis

The thesis is arranged as following. In the second chapter, I discuss different aspects of the set of six new Bell inequalities for three-qubit pure states. They are violated by all generalized GHZ states and give rise to the special situation, e.g. n parties, two dichotomic measurements for two parties and one for the rest. But they are not facet Bell inequalities in this scenario. In the next chapter, I introduce the facet Bell inequalities for this scenario and discuss their properties. In the fourth chapter, I talk about a new QIP protocol, which we name as Co-operative Quantum Key Distribution (CoQKD) and introduce the multipartite resource states suitable for this scheme. We discuss the CoQKD protocol and Conference key protocol with the new resource states. In the fifth chapter I discuss the role of entanglement in a measurement driven quantum heat engine operating at single temperature. We show that the presence of coupling in the working medium helps to increase the efficiency beyond classical limit. In the last chapter I conclude.

CHAPTER 2

New Bell inequalities for multi-qubit pure states

2.1 Introduction

Unlike a pure bipartite state, the relationship between Bell nonlocality and entanglement is far from simple [140]. For three-qubit states, we will adopt following terminology. A state $|\psi\rangle$ is a pure separable or product state if it can be written in the form $|\psi_1\rangle \otimes |\psi_2\rangle \otimes |\psi_3\rangle$, a pure biseparable state if it can be written as $|\psi_1\rangle \otimes |\psi_{23}\rangle$ or in other permutations and is genuinely entangled if it cannot be written in a product form. Above classification is based on types of entanglement present in the state. Idea of non-separability according to Bell locality comes from the inability of construction of a LHV model for observed correlations. In this case, the quantum mechanical description is not presupposed. For a system of three particles, if the joint probability can be written as,

$$P(a_1, a_2, a_3) = \int d\lambda \rho(\lambda) P_1(a_1|A_1, \lambda) P_2(a_2|A_2, \lambda) P_3(a_3|A_3, \lambda),$$

where, $P_i(a_i|A_i\lambda)(i = 1, 2, 3)$ is the probability of yielding the result a_i, when a measurement A_i is done on the particle with the local hidden variable λ, then the model is the well known LHV model. The intermediate case is the hybrid local-nonlocal model, first considered by Svetlichny [85], where there is an arbitrary nonlocal correlation between two of the three particles but only local correlations between these two and the third particle. The last situation is genuine tripartite nonlocality, where three particles are allowed to share arbitrary correlations. Whereas Svetlichny's inequality allowed arbitrary nonlocal correlation between two parties, a more refined and strictly weaker definition of genuine tripartite nonlocality was introduced in [86]. By analyzing the no-signalling polytope, they found a set of 185 inequivalent facet inequalities and numerically conjectured that every genuine tripartite entangled states show violations within this set and hence they are also genuinely tripartite nonlocal according to their definition.

In the case of three qubits, violation of Mermin-Ardehali-Belinskii-Klyshko (MABK) inequalities [83, 141] gives sufficient criteria to distinguish separable states from entangled ones. But it is not a necessary condition as there are states, which do no violate MABK inequalities but have genuine tripartite entanglement [142]. Śliwa [90] constructed the Bell polytope i.e all tight Bell inequalities for three parties and two dichotomic measuements per party, where Mermin inequality is one of the facets. More precisely, in [142] it was shown that the n-qubit state, $|\psi\rangle = \cos\alpha\,|0...0\rangle + \sin\alpha\,|1...1\rangle$ (we will call it generalized GHZ state) would not violate MABK inequalities for $\sin 2\alpha \leq 1/\sqrt{2^{N-1}}$. Furthermore, in [143] authors showed that generalized GHZ states within a specified parameter range for odd number of qubits do not violate Werner-Wolf-Żukowski-Brukner (WWŻB) inequalities [89]. These inequalities form a complete set of correlation Bell inequalities for n parties, with two measurement settings per party and two outcomes per measurement. Interestingly, tight Bell inequalities can be constructed [144] for more than two measurement settings per party such that generalized GHZ states violate these for the whole parameter range. So, the question naturally arises whether one can construct some Bell inequalities with maximum two measurements per party such that the problematic generalized GHZ state will violate them for the entire parameter range.

In this chapter, one of our motivations is to construct Bell inequalities [145] to answer this question affirmatively. This is achieved by making different number of measurements on different qubits. It is unlike other previous major inequalities. The second motivation is to attempt to link nonlocality with the entanglement. We characterize nonlocality of a state by the maximum amount of violation of a Bell inequality. Both notions of entanglement and nonlocality are fluid for multipartite states. There exist a wide array of Bell inequalities, and multiple characterizations of entanglement. In this chapter, we are able to link entanglement and nonlocality, for the class of generalized GHZ states. The third motivation is to be able to discriminate between separable, biseparable, and genuinely entangled pure states using Bell inequalities. In general, it is very difficult to discriminate between biseparable and genuinely entangled states. MABK inequalities give a sufficient condition to distinguish them

[140, 141, 146]. However as the condition is only sufficient but not a necessary one, biseparable and genuinely entangled states cannot always be distinguished by means of these inequalities. Using our Bell inequalities, one can always distinguish between separable, biseparable and genuinely entangled three-qubit pure states from the pattern of their violations. We have also provided numerical evidence that any pure entangled state will violate one or more inequalities from the set. Analytical proof is difficult due to many parameters in the state and possible measurement settings. Our conjecture is similar in spirit to a few previous works [86]. The discussion is organized as follows. In the next section, we introduce a set of Bell inequalities for three-qubit states and discuss some of their properties. In the subsequent section, we prove a number of propositions for three-qubit states. We then generalize these inequalities to the case of n qubits. The last section has conclusions.

2.2 A set of Bell inequalities

We consider a three-qubit system, with a qubit each with Alice, Bob and Charlie. In the Bell inequalities that we introduce, two of the parties will make two measurements, while the third party will make only one measurement. This third party can be either Alice, Bob, or Charlie. A general state need not have any symmetry, therefore we will be considering a set of Bell inequalities, rather than one inequality. The one measurement by one of the parties is necessary. We note that in the original Bell inequality [2], one of the two parties makes only one measurement. We first list the set of six inequalities, and later explain the motivation.

$$A_1B_1(C_1+C_2)+B_2(C_1-C_2) \leq 2, \quad (2.1)$$

$$A_1B_1(C_1+C_2)+A_2(C_1-C_2) \leq 2, \quad (2.2)$$

$$(B_1+B_2)C_1+A_1(B_1-B_2)C_2 \leq 2, \quad (2.3)$$

$$A_1(B_1+B_2)+A_2(B_1-B_2)C_1 \leq 2, \quad (2.4)$$

$$(A_1+A_2)B_1+(A_1-A_2)B_2C_1 \leq 2, \quad (2.5)$$

$$(A_1+A_2)C_1+(A_1-A_2)B_1C_2 \leq 2. \quad (2.6)$$

In this list, the left-hand side should be thought of as the expectation value of the observables. In the first and third inequalities, Alice makes one measurement given by observable A_1, Bob measures the observables B_1 and B_2, and Charlie measures observables C_1 and C_2. These are dichotomic observables, with values $\{-1, 1\}$. In the inequalities (2) and (6), Bob measures only one observable, B_1, while in the inequalities (4) and (5), Charlie measures only one observable, C_1. Other parties measure two observables. To find the maximal violation of these inequalities for a state, one has to consider all possible measurements. Therefore, inequalities obtained by interchange of A_1 and A_2 will give identical maximal violation. Same will be true for other set of observables. Because of this, we do not include such inequalities in our set. In quantum mechanics, the maximal value of these Bell operators can be $2\sqrt{2}$. This has been proved along the same line as the Tsirelson's bound for Bell-CHSH operator.

2.2.1 Quantum bound for the inequalities

We will obtain the bound for the first inequality and the analysis will be similar for others. Let us call the corresponding Bell operator for the first inequality as,

$$\mathcal{B} = A_1 B_1 (C_1 + C_2) + B_2 (C_1 - C_2) \tag{2.7}$$

If we take the square of this expression we get,

$$\mathcal{B}^2 = 4I + A_1 [C_1, C_2][B_1, B_2]. \tag{2.8}$$

Here, we have used ${A_1}^2 = {B_1}^2 = {B_2}^2 = {C_1}^2 = {C_2}^2 = I$. We know that, for two bounded operators X and Y,

$$\| [X, Y] \| \leq 2 \| X \| \| Y \|, \tag{2.9}$$

where, "$\| \ \|$" is the sup norm of a bounded operator. Using this relation, we notice that the maximum value will be obtained when $\mathcal{B}^2$ is $8I$ and hence $\| \mathcal{B} \| \leq 2\sqrt{2}$. This proves our claim.

2.2.2 Motivation behind the inequalities

To motivate these inequalities, our starting point will be the Bell-CHSH inequality. This inequality reads as, $A_1B_1+A_1B_2+A_2B_1-A_2B_2 \leq 2$, where A_1, A_2 are the measurement observables for Alice, B_1, B_2 are the measurement observables for Bob and 2 is the local-realistic value. Again in left-hand side, expectation value is implicit. From Tsirelson's bound [71], maximum value of this operator can achieve for quantum states is $2\sqrt{2}$. This value is achieved for the maximally entangled states - Bell states. Let us consider the state $|\phi^+\rangle = \frac{1}{\sqrt{2}}(|00\rangle+|11\rangle)$. This state is useful for generalization to GHZ state. For a suitable choice of measurements, for example, $A_1 = \sigma_x$, $A_2 = \sigma_z$, $B_1 = 1/\sqrt{2}(\sigma_x + \sigma_z)$ and $B_2 = 1/\sqrt{2}(\sigma_x - \sigma_z)$, we obtain the maximal violation of $2\sqrt{2}$. For this choice of measurements, the Bell-CHSH operator takes the form $\sqrt{2}(\sigma_x \otimes \sigma_x + \sigma_z \otimes \sigma_z)$. The state $|\phi^+\rangle$ is its eigenstate with eigenvalue $2\sqrt{2}$ [147]. With local unitary transformations, we can find other forms of this operator, of which other Bell states will be eigenstates with maximal eigenvalue. Now, we want to construct an operator for three-qubit pure states such that, the GHZ state of three qubits will be the eigenstate of this operator with highest eigenvalue. Like the Bell-CHSH operator, we can construct an operator such that its maximum eigenvalue will be $2\sqrt{2}$. The GHZ state, $\frac{1}{\sqrt{2}}(|000\rangle + |111\rangle)$, is the eigenstate of the operator $\sqrt{2}(\sigma_x \otimes \sigma_x \otimes \sigma_x + \sigma_z \otimes \sigma_z \otimes I)$ with eigenvalue $2\sqrt{2}$. We can write other forms of this operator where identity operator acts on other qubits. We clearly see that we have even number of σ_z; here it is one fewer than the number of qubits. This suggests that we need to make only one measurement on one of the qubits. With the help of this operator, we can construct the simplest set of Bell inequalities. We need a set to take care of asymmetric situations. This set is given above. To look at it from a different point of view, identity in one place of the aforementioned operator gives us hint to construct non-correlation Bell inequality. Also from previous discussion, it is clear that to obtain violations for all pure entangled states, correlation Bell inequalities are not enough. So, it seems that non-correlation Bell inequalities may work. We show below by first considering generalized GHZ states and then arbitrary three-qubit states that it is indeed true.

2.3 Three-qubit states

In this section, we will consider three different classes of states – product states, pure biseparable states, and states with genuine tripartite entanglement. We will see how our inequalities can distin-

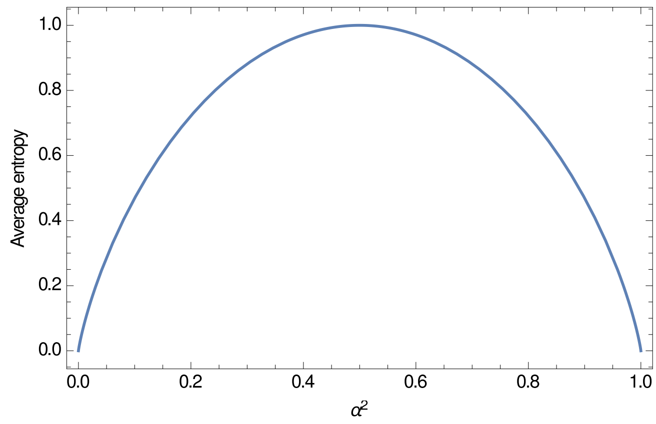

Figure 2.1: Average Von Neumann entropy over the three bipartitions vs α^2 plot.

guish these classes of states. In addition, we shall consider generalized GHZ states. Theses states are symmetric under the permutation of particles; so we can pick any of the inequalities. All will be violated in the same manner.

Proposition 1: *All generalized GHZ states violate all six inequalities of this set.*

Proof: Let's consider the three-qubit generalized GHZ state, which is written as following,

$$|GGHZ\rangle = \alpha\,|000\rangle + \beta\,|111\rangle\,. \tag{2.10}$$

These states have been problematic for different inequalities. However, as our Bell inequalities were designed for GHZ states, all of these generalized GHZ states violate all our inequalities. In the spirit of generalized Schmidt decomposition, we can take α and β to be real and positive numbers. Quantification of entanglement in multipartite scenario is a messy business. Unlike pure bipartite system, there is no unique measure of entanglement for multipartite states [11, 51]. One uses different measures depending upon different purposes. Von Neumann entropy uniquely captures and quantify the entanglement for a pure bipartite system in the asymptotic limit. For a pure multipartite state one can use the average of Von Neumann entropy over each bipartition as a suitable measure of multipartite entanglement [51]. For three-qubit pure state, there are three bipartitions namely, $1-23$, $2-31$ and $3-12$. Average of Von Neumann entropy for generalized GHZ state as defined in equation (3.8) over these bipartitions is $-\alpha^2\log_2\alpha^2 - \beta^2\log_2\beta^2$. This is also the entropy for each bipartition for these states as the states are symmetric. We have plotted this average entropy with α^2 with $\alpha^2+\beta^2=1$, in figure (2.1). Since the states are symmetric under the permutations of particles,

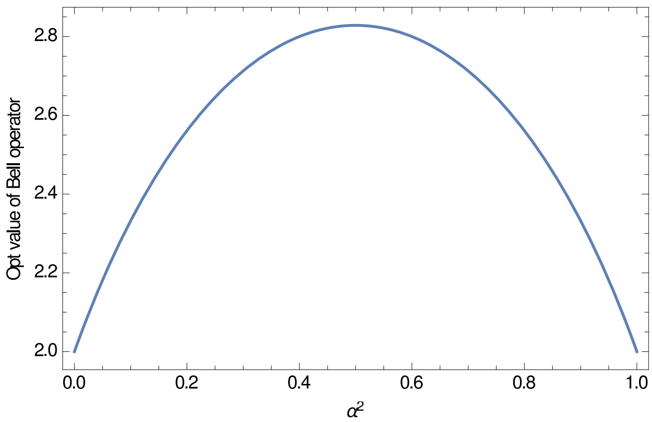

Figure 2.2: Maximum expectation value of the Bell operator for a generalized GHZ state vs α^2 plot.

we can choose any Bell inequality from the set. We choose the inequality,

$$A_1(B_1 + B_2) + A_2(B_1 - B_2)C_1 \leq 2. \tag{2.11}$$

Let us recall that the expectation value for the left-hand side is implicit. We choose the following measurement settings, $A_1 = \sigma_z$, $A_2 = \sigma_x$, $B_1 = \cos\theta\sigma_x + \sin\theta\sigma_z$, $B_2 = -\cos\theta\sigma_x + \sin\theta\sigma_z$, $C_1 = \sigma_x$. For these measurement settings, the expectation value of the above Bell operator for the generalized GHZ state is

$$\langle GGHZ| \, A_1(B_1 + B_2) + A_2(B_1 - B_2)C_1 \, |GGHZ\rangle \, . \tag{2.12}$$

Its value is $2[2\alpha\beta\cos\theta + (\alpha^2 + \beta^2)\sin\theta] = 2[2\alpha\beta\cos\theta + \sin\theta]$. Now, $a\sin\phi + b\cos\phi \leq \sqrt{a^2 + b^2}$. Therefore $\langle GGHZ| \, A_1(B_1 + B_2) + A_2(B_1 - B_2)C_1 \, |GGHZ\rangle$ is less than or equal to $2\sqrt{1 + 4\alpha^2\beta^2}$, which is always greater than 2 for nonzero α, β and gives maximum value $2\sqrt{2}$ for the conventional GHZ state. The upper bound on the expectation value can be written as $2\sqrt{1 + \mathcal{C}^2}$, where $\mathcal{C}^2 = 4\alpha^2\beta^2$ is nothing but the tangle of the generalized GHZ state. The quantity $\mathcal{C}$ is also like concurrence for a two-qubit bipartite state. We have also plotted the optimized expectation value of the Bell operator with α^2 in figure (2.2). From these two plots, it is clear that, the entanglement measure (average Von Neumann entropy over the bipartitions) and the maximum amount of Bell violation for generalized GHZ states are monotonically related to each other. In a different way, we can say that for the generalized GHZ state, the expectation value of the Bell operator depends on the amount of entanglement. The more is the entanglement of a state, the more Bell nonlocal it is. This concludes the proof. As discussed earlier, this is the class of states which was creating problem for MABK, Svetlichny and moreover for all correlation Bell inequalities for a particular range of α and β. However, all states in this class violate all the inequalities in our set.

Proposition 2: *All biseparable pure three-qubit states violate exactly two inequalities within the set and the amount of maximal violation are same for both.*

Proof: This can be proved by observing the form of the inequalities. We can rewrite any biseparable state as an equivalent form of $|0\rangle(\alpha|0\rangle|0\rangle + \beta|1\rangle|1\rangle)$ by local unitary transformations. (We can relabel qubits such that number '2' and '3' are entangled. This state is separable in $1-23$ bipartition. So, those inequalities, which can explore the entanglement between the second and the third qubit will be violated. For example, for the above mentioned state, $A_1B_1(C_1+C_2)+B_2(C_1-C_2) \leq 2$ will be violated, because a Bell-CHSH type operator for second and third qubits is embedded in this operator. So, the amount of violation will be exactly same as in the case of two-qubit entangled state and the Bell-CHSH operator. Not only this inequality, but there is another inequality within this set, which will also be violated in this case. This inequality is, $(B_1 + B_2)C_2 + A_1(B_1 - B_2)C_1 \leq 2$. So, there are two inequalities, which will be violated for a given pure biseparable state. Also, as all the two operators have the same form (the Bell-CHSH form) in second and third particle, the amount of maximal violations will be same in two cases. And the last important fact is that, no other states (except biseparable pure states) will have same kind of violations, i.e exactly two violations of the same maximal amount. This concludes the proof. Until now, we have considered special classes of three-qubit states. One would like to show that any genuinely entangled tripartite state will violate one of our inequalities. For this, we will be presenting numerical evidence, using a general parametrized form of a three-qubit state.

Conjecture 3: *For all genuine tripartite pure entangled states, we have violation within the set.*

We do not have an analytical proof for this proposition. But we present supporting numerical evidence. Any genuinely entangled three-qubit pure state can be written in a canonical form [148] with six parameters. This form includes the GHZ and W class states [45] for three qubits. For biseparable pure states, we have already provided proof for the violation of inequalities within the set. The canonical form of a general three-qubit state is,

$$|\psi\rangle = \lambda_0 |0\rangle |0\rangle |0\rangle + \lambda_1 e^{i\phi} |1\rangle |0\rangle |0\rangle + \lambda_2 |1\rangle |0\rangle |1\rangle + \lambda_3 |1\rangle |1\rangle |0\rangle + \lambda_4 |1\rangle |1\rangle |1\rangle \,, \qquad (2.13)$$

where $\lambda_i \geq 0$, $\sum_i {\lambda_i}^2 = 1$, $\lambda_0 \neq 0$, $\lambda_2 + \lambda_4 \neq 0, \lambda_3 + \lambda_4 \neq 0$ and $\phi \in [0, \pi]$. We have randomly generated 25,000 states and tested our set of Bell inequalities. The expectation value of a Bell operator is optimized by considering all possible measurement settings for all observables. Starting from the inequality (1) from the set, we continued with other inequalities one after one until all the generated states violate one inequality from the set. Results are displayed in figures (2.3-2.7). At first, Bell

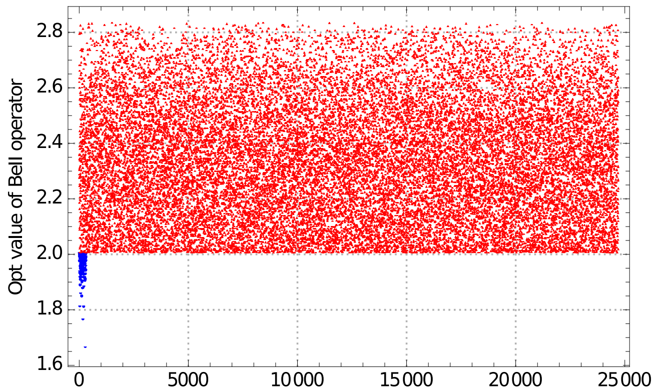

Figure 2.3: Optimum value of the Bell operator (1). Out of 25000 states, 297 states do not violate this inequality. States which violate the inequality are shown by red points and those do not are shown by blue points.

inequality (1) was tested for these randomly generated states and out of 25000 states, 297 states do not violate this inequality, as shown in figure (2.3). Then using the inequality (2) with these 297 states, number of states which do not violate these first two inequalities was further reduced to 59 states, as shown in figure (2.4). Similarly, applying the other Bell inequalities from the proposed set one by one the number of states showing no violation for those inequalities can be reduced to zero. We have shown in figures (2.3-2.7), starting from 25000 random states, violation for each state has been obtained using first five inequalities from the proposed set.

However, this random generation of states would not be setting any of the parameters as zero. But we should consider those states also for numerical checking. So, we have generated 5000 states each for 9 more classes of states, by setting some of the parameters as zero. These classes are obtained as, only $\lambda_1 = 0$, only $\lambda_2 = 0$, only $\lambda_3 = 0$, only $\lambda_4 = 0$, only $\lambda_1, \lambda_2 = 0$, only $\lambda_1, \lambda_3 = 0$, only, $\lambda_1, \lambda_4 = 0$, only, $\lambda_2, \lambda_3 = 0$, Only, $\lambda_1, \lambda_2, \lambda_3 = 0$. For each of theses class, ϕ is arbitrary. We have

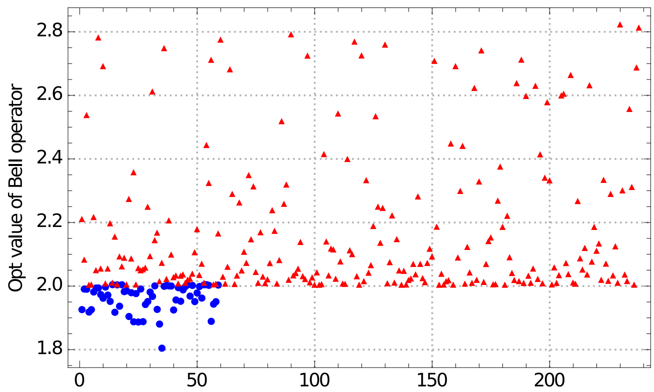

Figure 2.4: Optimum value of the Bell operator (2). Out of 297 states, 59 states do not violate this inequality. States which violate the inequality are shown by red points and those do not are shown by blue points.

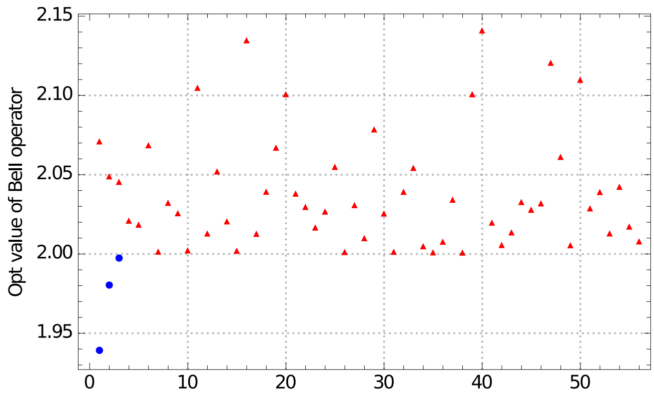

Figure 2.5: Optimum value of the Bell operator (3). Out of 59 states, 3 states do not violate this inequality. States which violate the inequality are shown by red points and those do not are shown by blue points.

taken 5000 random values of each parameter for each class and found violations within the set of 6 inequalities in each case. Based on this and the fact that all generalized GHZ class states violate each inequality (already proved), we expect that this set can certify genuine pure tripartite entanglement.

To conclude the case of tripartite scenario, we have established that all generalized GHZ states violate all the inequalities within the set and with the help of propositions 1,2 and 3 one can always distinguish between separable, biseparable and genuinely entangled pure states from the pattern of their violations of inequalities from the set.

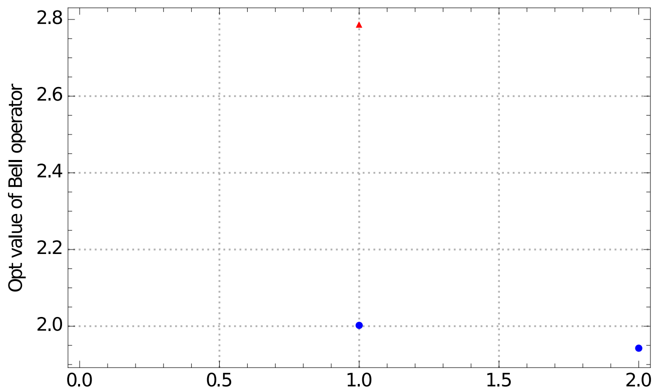

Figure 2.6: Optimum value of the Bell operator (4). Out of 3 states, 2 states do not violate this inequality. States which violate the inequality are shown by red points and those do not are shown by blue points.

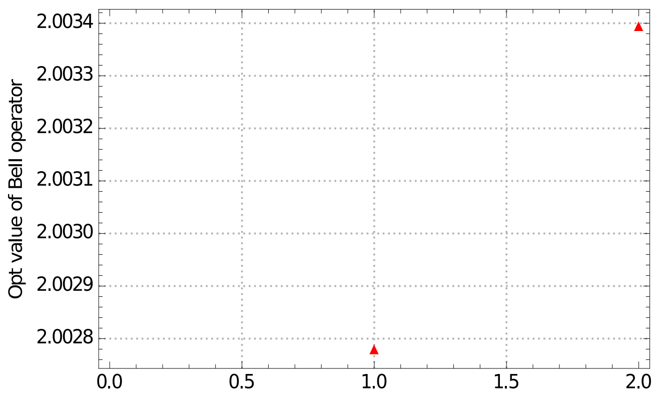

Figure 2.7: Optimum value of the Bell operator (5). Out of 2 states, all the states violate this inequality. So, there are 2 red points and no blue points.

2.4 Multi-qubit states

We have established that our set of inequalities are violated by any entangled three-qubit pure state. We can generalize this set of inequalities to n-qubit states. This extension for multi-qubit scenario is straight-forward. One will have to distinguish between two cases – odd number of qubits and even number of qubits. Starting from the operator, of which GHZ state is an eigenstate, one can construct different Bell inequalities. For even n, there will be a set of n inequalities; while for odd n, the number will rise to $n(n-1)$. The set is larger for odd number of qubits, because we have choice of making one measurement on any of n qubits; while in the case of even n, two measurements are made on all qubits. Therefore, we have to construct different types of inequalities for even and odd number of particles. We have already seen that the GHZ state of three qubits is eigenstate of the operator $\sqrt{2}(\sigma_x \otimes \sigma_x \otimes \sigma_x + \sigma_z \otimes \sigma_z \otimes I)$ with the highest eigenvalue $2\sqrt{2}$. This form of the operator can be generalized for any n-qubit GHZ state, when n is odd. n-qubit GHZ states is the eigenstate of the operator $\sqrt{2}(\sigma_x \otimes \sigma_x \otimes \sigma_x \otimes \cdots \otimes \sigma_x^{nth} + \sigma_z \otimes \sigma_z \otimes \cdots \otimes \sigma_z^{(n-1)th} \otimes I)$ with the highest eigenvalue $2\sqrt{2}$. So, like the three-qubit case, we have to consider non-correlation Bell inequalities when n is odd. The first two Bell inequalities (1) and (2) can be easily generalized for n-qubit pure states as,

$$A_1A_2A_3A_4A_5..(A_n + A'_n) + A'_2A'_3A'_4A'_5..(A_n - A'_n) \leq 2, \tag{2.14}$$

and

$$A_2A_3A_4A_5..(A_n + A'_n) + A_1A'_2A'_3A'_4A'_5..(A_n - A'_n) \leq 2. \tag{2.15}$$

Here, A_i and A'_i are two dichotomic observable for i^{th} party. In these inequalities, one measurement has been made on first qubit. Similarly one can make single measurement on $(n-2)$ other qubits. This will lead to $(n-1)$ inequalities. We can write n such $(n-1)$ inequalities with $(A_i \pm A'_i)$ for i^{th} qubit, giving a set of total $n(n-1)$ inequalities. For three-qubit the number of inequalities in the set is six. For finding maximal violation, we consider all allowed A_i and A'_i, therefore their positions in the inequalities can be interchanged. The above set of inequalities can be used to characterize the entanglement of n-qubit states for odd n. In the case of generalized n-qubit GHZ states, any one of these generalized inequalities is enough. One can show that for odd number of qubits these non-correlation Bell inequalities are violated by all generalized GHZ states with maximum violation of $2\sqrt{2}$ for the conventional GHZ state. The proof is similar to the three-qubit case. Situation changes when one considers GHZ like states with even number of qubits. Because now, like the Bell states, the conventional GHZ state of n qubits (n is even) is the eigenstate of the operator $\sqrt{2}(\sigma_x \otimes \sigma_x \otimes \sigma_x \otimes \cdots \otimes \sigma_x^{nth} + \sigma_z \otimes \sigma_z \otimes \cdots \otimes \sigma_z^{(n-1)th} \otimes \sigma_z)$ with highest eigenvalue $2\sqrt{2}$. This suggests that correlation Bell inequalities are required in this case. For example, one can generalize the first correlation Bell inequality as,

$$(A_1 + A'_1)A_2A_3A_4A_5..A_n + (A_1 - A'_1)A'_2A'_3A'_4A'_5..A'_n \leq 2. \tag{2.16}$$

Similarly, n such inequalities with $(A_i \pm A'_i)$ can be written. Again, among these correlation Bell inequalities any one of them can be used for generalized GHZ states. The proof that any generalized GHZ state with even number of qubits violates these inequalities can be carried along the same line as for the three-qubit case. The fact that generalized GHZ states with even number of qubits violate a correlation Bell inequality within the set of all correlation Bell inequalities [89] was known [143]. But it is important to note that, the correlation Bell inequality violated by the generalized GHZ state with even number of qubits, may not be MABK inequalities. Here, we have introduced a set of correlation Bell inequalities which must be violated by all generalized GHZ states with even number of qubits. Like three-qubit states, one may expect that any n-qubit pure state for odd value of n will violate one of the $n(n-1)$ inequalities like in (2.14) and (2.15), while for even n, one of the n inequalities like in (2.16) will be violated.

Proposition 4: *Multiqubit extension of the inequalities are violated by all multiqubit generalized GHZ states.*

Proof: Let's consider the generalized n-qubit GHZ state

$$|GGHZ\rangle_n = \alpha\,|00.....00\rangle + \beta\,|11.....11\rangle\,. \tag{2.17}$$

In this state, first term represents all n qubits in the '0' state and the second term is for all n qubits in the '1' state. The proof follows exactly same steps as in the proposition 1. The result is also identical. In the case of both even and odd n, the maximal violation would be $2\sqrt{1+\mathcal{C}^2}$, where $\mathcal{C} = 2\alpha\beta$. For the n-qubit GHZ state $\mathcal{C} = 1$ and the maximal violation is $2\sqrt{2}$.

2.5 Conclusion

We have presented a new set of six Bell inequalities. Separable three-qubit pure states do not violate any of these inequalities and biseparable pure three-qubit states violate exactly two of them with same maximal amount. A generalized GHZ state violates all the inequalities in the set, with conventional GHZ state giving maximum amount of violation, which is $2\sqrt{2}$. Furthermore, for this class of states, our inequalities provide a link between nonlocality and entanglement. More entangled state will violate the inequalities more. We have also provided numerical evidence that any genuine tripartite entangled pure state will give violation within this set.

A key point of this set of inequalities is that one will make only one measurement on one of the qubits. For violation this measurement is necessary. It is similar to the original Bell inequality. It can also be used to distinguish between separable, biseparable and genuinely entangled pure three qubit states. So this inequality can serve as a entanglement witness (considering the numerical conjecture) for a three qubit pure state. From the measurement point of view it is very efficient. Because the simplest way to determine whether a pure state is entangled is to measure the purities of the subsystems. This will require atleast three measurement settings per party (single qubit tomography), where these inequalities only require two measurements for two parties and only one for the rest.

One can also examine the three-qubit mixed states, where one may expect to find the phenomenon of hidden nonlocality with respect to our set of inequalities. These inequalities have also been generalized for multiqubit scenario. Each of these inequalities will be violated by a generalized multiqubit GHZ state. It is highly likely that a set of inequalities similar to three-qubit states can detect and characterize the entanglement of multiqubit states. However in the absence of a parametrized form of a pure entangled states beyond three-qubit case, we cannot do numerical analysis for the whole set.

CHAPTER 3

Minimal scenario facet Bell inequalities

3.1 Introduction

In the previous chapter, we noted a particular limitation of Mermin-Ardehali-Belinskii-Klyshko (MABK) [83] inequalities. Particularly, the n-qubit state, $|\psi\rangle = \cos\alpha\,|0...0\rangle + \sin\alpha\,|1...1\rangle$ (generalized GHZ state) does not violate MABK inequalities [142] for $\sin 2\alpha \leq 1/\sqrt{2^{N-1}}$. Not only that in [89] all correlation Bell inequalities were constructed for n qubits, and in [143] it was shown that again generalized GHZ states do not violate those inequalities for the whole parameter range. As already mentioned in the previous chapter that this drawback can be mended by considering alternative Bell inequalities designed for different settings. Like in [144] authors have constructed multipartite tight Bell inequalities for more than two measurement settings per party. In this extended scenario, they showed that generalized GHZ states now violate the inequalities for the whole parameter range. But if we restrict our-self to the scenario, where maximum two measurement settings are allowed per party, then can we construct Bell inequalities, for which this shortcoming can be lifted? This was the main motivation in the previous chapter based on our paper [145], where we constructed a set of six inequalities each of which is violated by generalized GHZ states for the whole parameter range. Also with the help of this set of inequalities we can distinguish between pure biseparable and pure genuinely entangled states. This distinction can not also be done with MABK inequalities, as they give only sufficient criteria [140, 141, 146] to distinguish them. These six inequalities could be obtained from two inequalities after permutations of qubits. One important fact of those inequalities was the scenario we considered, i.e three parties, two dichotomic measurement settings for two parties and one dichotomic measurement for the remaining. But our inequalities were not facet inequalities for this particular scenario. Question naturally arises what about the facet inequalities for this scenario. Will they also circumvent the obstacle posed by the MABK inequalities regarding the violation in the whole parameter range for generalized GHZ states and order them according to their entanglement? Besides, construction of facet Bell inequalities in this scenario is itself very interesting, as it is the minimal scenario, where one can generate facet Bell inequalities. We need minimum two parties performing two dichotomic measurements, to have some nontrivial facet inequalities, also called facet Bell inequalities. In literature, complete set of facet inequalities is known only for few cases [3]. Like, for two parties with three dichotomic measurements per party, there are only two [149, 150] facet Bell inequalities, but already for four measurement settings the complete set is not known [151]. In multipartite case, as already mentioned, the result of Sliwa [90] gives the set of all facet Bell inequalities for three qubits, with two dichotomic measurement settings per party. But except this result, to my knowledge there is no other scenario in multipartite settings, where the complete list is known. Even for two parties, with two measurement settings per party but with more than two outcomes, complete list of facet Bell inequalities is not known. To compute all the facet Bell inequalities for a given scenario is a highly non-trivial task and many techniques are being developed in this direction [3]. We first explicitly construct [152] the facets of the local polytope for three qubits and find only one nontrivial facet inequality upto the relabelling of indices. With permutation of qubits, the number is three. Interestingly, this facet inequality is equivalent to the lifted version [153] of Bell-CHSH inequality for more parties. This shows that to uncover the nonlocality of a three-qubit, or multiqubit (as discussed below) system, one facet Bell inequality, and its permutations, may be enough. This inequality involves multipartite correlations; so it explores multipartite nonlocality.

In this chapter, we have first constructed the facet Bell inequalities for three qubits explicitly and found only one non-trivial facet upto the relabeling of indices. This facet inequality is equivalent to the lifted Bell-CHSH inequality for more parties. We compare the results with that for other well known inequalities. We have also considered a few noisy mixed states. We also constructed the facets for four- and five-qubit cases for the same minimal measurement settings where, only two parties are doing two dichotomic measurements and the remaining parties are doing one dichotomic measurement each. For each of these four- and five-qubit scenarios, there is again only one non-trivial facet, upto the relabeling of indices, with similar structure as the three-qubit scenario. This is expected from the result of the Ref. [153]. This observation enabled us to generalize our facet Bell inequality to n-qubit systems. We show that generalized GHZ states of n qubits violate the facet inequality for the whole parameter range.

The facet Bell inequality we obtained is not maximally violated by a maximally entangled state. The notion of a maximally entangled state for a mutipartite state is not straightforward. However, for a three-qubit system GHZ-state, for all practical purposes, can be considered to be maximally entangled. We find that the facet Bell inequality of our scenario is not maximally violated by the GHZ-state.

The chapter is organized as follows. In the next section, we obtain facet Bell inequalities in the case of three qubits for our minimal scenario. In Sections 3.3 to 3.6, we discuss various aspects of these inequalities. In Section 3.7, we generalize the three-qubit facet Bell inequalities to multipartite case. In the last section, we present our conclusions.

3.2 Facet Inequalities

In the first chapter, I have discussed about what a facet Bell inequality is. It is an optimal Bell inequality with respect to the local polytope. So, it is always desirable to find facet Bell inequalities for a set of local correlations. In literature, facet Bell inequalities have been constructed for many scenarios [3], like for higher dimensions, different measurement settings, multipartite settings etc. As we have seen, one of the important features of a local polytope is that only local correlations are inside it. Quantum correlations are outside it. Therefore, quantum correlations are expected to violate at least one of the facet inequalities of a given local polytope. From this point of view, it is of value to consider a local polytope with smallest number of nontrivial facet inequalities. As stated in the introduction, we first construct facet Bell inequalities for three parties, two dichotomic measurements for two parties and one measurement for the rest. For this case we have a local polytope with 17 vertices in V representation. By converting this V-representation to H-representation with the software cdd [154] we obtained total 48 facet inequalities. Among 48 inequalities, 32 are just the positivity conditions for probabilities. Remaining 16 inequalities are the variations of four non-trivial facet inequalities. The four inequalities upto relabeling of indices are given below. In terms of the well known Bell-CHSH inequality, these four can be written more simply as,

$$-I_{CHSH} - I_{CHSH}C_1 - 2C_1 \quad \leq 2, \tag{3.1}$$

$$I_{CHSH} + I_{CHSH}C_1 - 2C_1 \quad \leq 2, \tag{3.2}$$

$$-I_{CHSH} + I_{CHSH}C_1 + 2C_1 \quad \leq 2, \tag{3.3}$$

$$I_{CHSH} - I_{CHSH}C_1 + 2C_1 \quad \leq 2, \tag{3.4}$$

where, $I_{CHSH} \equiv (-A_2B_2+A_2B_1+A_1B_2+A_1B_1)$. In this list, the left-hand side should be thought of as the expectation value of the observables. But, these four inequalities are not in-equivalent. We can see that if we make the interchange of the indices as, $A_1 \to A_2$, $A_2 \to -A_1$, $B_1 \to B_2$, $B_2 \to -B_1$ in the first inequality (Eq.(3.1)), then it goes to the second inequality (Eq.(3.2)). Similarly, one can see that with this type of interchange all the above inequalities are equivalent. So, finally we have only one inequality. We will choose the form of second inequality (if not mentioned) to do the rest of the analysis. With no surprise this inequality is equivalent to the lifted version of Bell-CHSH inequality (Eq. (2) of Ref. [153]) for more parties. Now other than Charlie, one can choose either Alice or Bob doing one measurement and rest are doing two dichotomic measurements. For each case we get one facet Bell inequality. In this way, there are three inequalities, where in our previous paper we had six inequalities. These three inequalities are,

$$I_1 = I_{CHSH} + I_{CHSH}A_1 - 2A_1 \leq 2 \tag{3.5}$$

$$I_2 = I_{CHSH} + I_{CHSH}B_1 - 2B_1 \leq 2 \tag{3.6}$$

$$I_3 = I_{CHSH} + I_{CHSH}C_1 - 2C_1 \leq 2 \tag{3.7}$$

It is easy to note that each of the above inequalities has the LHV lower bound -6. In the following, we analyze these facet Bell inequalities for different purposes.

3.3 Three-Qubit generalized GHZ states

First, we show that with the facet Bell inequalities, we can again have violation for all generalized GHZ states like our previous paper's inequalities. Then we show that amount of violation of the facet inequalities are in accordance with the amount of entanglement present in the generalized GHZ states, i.e more entangled a state is, more will be its violation. We will be using average Von Neumann entropy over each bi-partition as a measure of entanglement. One can take any other measure, and would get the same result. Let us consider the three-qubit generalized GHZ state,

$$|GGHZ\rangle = \alpha\,|000\rangle + \beta\,|111\rangle\,. \tag{3.8}$$

Without loss of generality, for simplicity, we take α and β to be real and positive numbers, as the method will be same even if they are complex. Average Von Neumann entropy for generalized GHZ state as defined above over these bi-partitions is $-\alpha^2\log_2\alpha^2 - \beta^2\log_2\beta^2$, which is also the entropy for each bi-partition for these states. Now to see the Bell violation by these states for the facet inequality, let's take the facet inequality, $I_B = I_{CHSH} + I_{CHSH}C_1 - 2C_1 \leqslant 2$. We choose $A_1 = \sigma_z$, $A_2 = \sigma_x$, $B_1 = \cos\theta\sigma_x + \sin\theta\sigma_z$, $B_2 = -\cos\theta\sigma_x + \sin\theta\sigma_z$ and $C_1 = \sigma_x$. For the generalized GHZ state $|GGHZ\rangle = \alpha\,|000\rangle + \beta\,|111\rangle$, the expectation value of the operator I_B is calculated to be,

$$\langle GGHZ|\, I_B\, |GGHZ\rangle = 2\sin\theta + 4\alpha\beta\cos\theta \tag{3.9}$$

As, $a\sin\theta + b\cos\theta \leqslant \sqrt{a^2+b^2}$, we have $\langle I_B\rangle_{|GGHZ\rangle} \leqslant 2\sqrt{1+4\alpha^2\beta^2} = 2\sqrt{1+\mathcal{C}}$, where $\mathcal{C} = 4\alpha^2\beta^2$ is nothing but the tangle [52] of the generalized GHZ state. The quantity $\mathcal{C}$ is also like concurrence for a two-qubit bipartite state. Maximum is achieved when we choose $\sin\theta = \frac{1}{\sqrt{1+4\alpha^2\beta^2}}$ and $\cos\theta = \frac{2\alpha\beta}{\sqrt{1+4\alpha^2\beta^2}}$. Therefore, it is obvious that as long as the state is entangled i.e α and β are not zero, the generalized GHZ states will violate the facet Bell inequality. This proves our first claim. Now, from this measurement setting, the maximum violation for the GHZ state is again $2\sqrt{2}$. Numerically, we have maximized the expectation value of the Bell operator for GHZ state and it is coming out to be $2\sqrt{2}$. So, this is the optimal measurement settings for GHZ state. Interesting fact is that there are many other states (not generalized GHZ states) which give violation greater than $2\sqrt{2}$. Interestingly, we have numerically checked that the generalized GHZ states do not violate the lower bound of the inequalities. Even the GHZ state does not show the violation of the LHV lower bound, which is -6. Next, if we plot the entanglement (as calculated above) and the amount of optimal violation of the Bell inequality, we would get similar kind of plots such that they are monotonically related (see [145] for more details and the plots). So, more entangled a generalized GHZ state is more will be the violation of the facet Bell inequality. One question may now arise that for this particular measurement settings, we are getting the expression of optimal violation which is a monotonic function of $\mathcal{C}$. If we choose other measurement settings, will this type of relation emerge? To answer this question, let us consider a general measurement settings as below,

$$A_1 = \sin\theta_{a1}\cos\phi_{a1}\sigma_x + \sin\theta_{a1}\sin\phi_{a1}\sigma_y + \cos\theta_{a1}\sigma_z$$
$$A_2 = \sin\theta_{a2}\cos\phi_{a2}\sigma_x + \sin\theta_{a2}\sin\phi_{a2}\sigma_y + \cos\theta_{a2}\sigma_z$$
$$B_1 = \sin\theta_{b1}\cos\phi_{b1}\sigma_x + \sin\theta_{b1}\sin\phi_{b1}\sigma_y + \cos\theta_{b1}\sigma_z$$
$$B_2 = \sin\theta_{b2}\cos\phi_{b2}\sigma_x + \sin\theta_{b2}\sin\phi_{b2}\sigma_y + \cos\theta_{b2}\sigma_z$$
$$C_1 = \cos\phi_{c1}\sigma_x + \sin\phi_{c1}\sigma_y$$

With these measurement settings we get,

$$\langle I_B\rangle_{|GGHZ\rangle} = X + \mathcal{C}Y, \tag{3.10}$$

where $X = \cos\theta_{a2}(\cos\theta_{b1} - \cos\theta_{b2}) + \cos\theta_{a1}(\cos\theta_{b1} + \cos\theta_{b2})$, $Y = \cos(\phi_{a1}+\phi_{b1}+\phi_{c1})\sin\theta_{a1}\sin\theta_{b1} + \cos(\phi_{a2}+\phi_{b1}+\phi_{c1})\sin\theta_{a2}\sin\theta_{b1} + \cos(\phi_{a1}+\phi_{b2}+\phi_{c1})\sin\theta_{a1}\sin\theta_{b2} - \cos(\phi_{a2}+\phi_{b2}+\phi_{c1})\sin\theta_{a2}\sin\theta_{b2}$ and $\mathcal{C} = 2\alpha\beta$. From the above relation, it is clear that for fixed values of X and Y, the amount of violation is again monotonic in C. So, no matter what the measurement settings, we will get more violation for a more entangled state, as long as we use same measurement settings for the states.

3.3.1 Comparison with Mermin inequality

Mermin inequality [83] can also track the entanglement, i.e violation of Mermin inequality will be more for more entangled generalized GHZ states. Mermin inequality is

$$I_{\mathrm{M}} = A_1B_1C_2 + A_1B_2C_1 + A_2B_1C_1 - A_2B_2C_2 \leq 2. \tag{3.11}$$

In this case if we choose the same general measurement settings as described above with $C_2 = \cos\phi_{c2}\sigma_x + \sin\phi_{c2}\sigma_y$. The expectation value of the operator I_{M} for the generalized GHZ state,

$$\begin{aligned}
\langle I_{\text{M}}\rangle_{|GGHZ\rangle} &= \mathcal{C}\Big(\cos(\phi_{a1}+\phi_{b1}+\phi_{c2}) sin\theta_{a1}\sin\theta_{b1}\cos(\phi_{a2}+\phi_{b1}+\phi_{c1})\sin\theta_{a2}\sin\theta_{b1} + \\
&\quad + \cos(\phi_{a1}+\phi_{b2}+\phi_{c1}) sin\theta_{a1}\sin\theta_{b2} - \\
&\quad \cos(\phi_{a2}+\phi_{b2}+\phi_{c2}) sin\theta_{a2}\sin\theta_{b2}\Big). \qquad (3.12)
\end{aligned}$$

So, expectation value of the Bell-Mermin operator is again a monotonic function of $\mathcal{C}$. But the problem is that it does not show violation for the whole range of generalized GHZ states. So, for those states which do not violate Mermin inequality, this relation between entanglement and nonlocality has no meaning. But this relation can be used to measure the entanglement.

3.3.2 Comparison with Svetlichny inequality

Svetlichny first introduced [85] a definition of genuine tripartite nonlocality. Based on that definition he gave an inequality to detect genuine tripartite nonlocality and was generalized for n parties in [140]. But Svetlichny inequality is not violated [155, 156] by some tripartite genuinely entangled states, revealing that Svetlichny's definition of genuine tripartite nonlocality is not equivalent to genuine tripartite entanglement, but a bit stronger. A strictly weaker definition of genuine tripartite nonlocality was given in [86], and the authors conjectured that every genuinely entangled tripartite pure state is also genuinely nonlocal according to their definition. But, if some state violates Svetlichny inequality, it must be a genuinely entangled state. This is not the case with Mermin inequality, as biseparable state also violate the Mermin inequality. This is also true for our facet and previous inequalities. They do not detect genuine entanglement, as biseparable states also violate them. But the class of states [155, 156] for which the Svetlichny inequality is not violated, our facet inequality and also the previous inequalities get violated. There are two classes of states which do not violate Svetlichny inequality,

$$I_{\text{S}} = A_1D_1C_1 + A_1D_2C_2 + A_2D_2C_1 - A_2D_1C_2 \leq 4, \qquad (3.13)$$

where $D_1 = B_1 + B_2$ and $D_2 = B_1 - B_2$. One class is generalized GHZ class and another class is,

$$|\psi_{gs}\rangle = \alpha\,|000\rangle + \beta\,|11\rangle\,(\cos\phi\,|0\rangle + \sin\phi\,|1\rangle) \tag{3.14}$$

For this class of states with the measurement settings chosen earlier, i.e $A_1 = \sigma_z$, $A_2 = \sigma_x$, $B_1 = \cos\theta\sigma_x + \sin\theta\sigma_z$, $B_2 = -\cos\theta\sigma_x + \sin\theta\sigma_z$ and $C_1 = \sigma_x$, the expectation value of our facet operator,

$$\begin{aligned}\langle I_B\rangle_{|\psi_{gs}\rangle} &= 4\alpha\beta\cos\phi(\cos\theta + \sin\theta) + 2(1 + \beta^2\sin 2\theta)\sin\phi - 2\beta^2\sin 2\theta \leq \\ &\quad 2\Big[\sqrt{\alpha^2(\beta^2 + \beta^2\sin 2\theta) + (1 + \beta^2\sin 2\theta)^2} - \beta^2\sin 2\theta\Big].\end{aligned} \tag{3.15}$$

It is clear from the expression that for any α and β, above expectation value is always greater than two. Therefore, our inequalities are also violated by those states, which do not Svetlichny inequality. Nevertheless our previous and facet inequalities can not be used to detect genuine tripartite entanglement just like Mermin inequality.

3.3.3 More Violation by a non-maximally entangled state

Unlike our previous inequalities, which are violated maximally by GHZ state by an amount $2\sqrt{2}$, our facet Bell inequalities are violated more by other genuinely entangled states. One very simple example is W state. Numerically we have found that W state gives maximum violation of 3.105 for the inequality, where Charlie makes one measurement. Obviously, there is no ordering of violation of the facet Bell inequality according to the entanglement within W class. Like the state $\sqrt{1/6}\,|001\rangle + \sqrt{3/6}\,|010\rangle + \sqrt{2/6}\,|001\rangle$ has average entropy 0.856 and violation of 3.33. And $\sqrt{1/10}\,|001\rangle + \sqrt{4/10}\,|010\rangle + \sqrt{5/10}\,|001\rangle$ has average entropy 0.813 and violation 3.475. Also, the later state violates (found numerically) the lower LHV bound but not the former as well as the W state. Not only that, there are state within GHZ class, which violates the facet inequality more than the conventional GHZ state. Like the state $|\psi\rangle = \sqrt{22/50}\,|000\rangle + \sqrt{3/50}\,|100\rangle + \sqrt{2/50}\,|101\rangle + \sqrt{21/50}\,|110\rangle + \sqrt{2/50}\,|111\rangle$ has maximum expectation value 3.377 (found numerically) and also belongs to the GHZ class. More interestingly, it also violates the lower LHV bound. For this state it is -7.02. Ordering is valid only for generalized GHZ states, not for whole GHZ class and obviously W class. For three-qubit systems, GHZ-state can be considered to be maximally entangled state in the sense that, the subsystems are maximally mixed. Furthermore, for a number of communication protocols, the GHZ state is a task-oriented maximally entangled state [157]. But we see, that a facet Bell inequality is not maximally violated by this state. Non facet inequalities like in reference [145] and Mermin inequalities are violated maximally by the GHZ-state.

3.3.4 Three-qubit pure bi-separable states

The three facet Bell inequalities explore the entanglement of three types of bi-separable pure states like our previous inequalities. For example, the state which is separable in $1-23$ bi-partition will violate that facet inequality, which can explore the entanglement between the second and the third qubit. So in this case, the inequality Eqn.(3.5), i.e $I_{CHSH} + I_{CHSH}A_1 - 2A_1 \leq 2$ will be violated. Similarly, other two types of bi-separable states will violate other two inequalities. But we can not distinguish between bi-separable and genuinely entangled pure states like our previous set of inequalities. Because we had six inequalities for the previous paper and bi-separable state would violate exactly two inequalities from the state with same amount of optimal violation. But in the case of facet Bell inequalities bi-separable states will violate only one out of the three, and that optimal violation may be exhibited by some genuinely entangled state also. So, by a violation, we can not say whether it is for a bi-separable pure state or for a genuinely entangled pure state.

3.4 Violation for three-qubit genuinely entangled states

In the previous subsection, we have shown that any bi-separable pure state will violate one of our three facet Bell inequalities, depending upon in which bi-partition they are separable. In this section, we will investigate the case for genuinely entangled pure states. A genuinely entangled three-qubit pure state can be written in a canonical form [148] with six parameters as,

$$|\psi\rangle = \lambda_0 |0\rangle |0\rangle |0\rangle + \lambda_1 e^{i\phi} |1\rangle |0\rangle |0\rangle + \lambda_2 |1\rangle |0\rangle |1\rangle + \lambda_3 |1\rangle |1\rangle |0\rangle + \lambda_4 |1\rangle |1\rangle |1\rangle , \tag{3.16}$$

where $\lambda_i \geq 0$, $\sum_i {\lambda_i}^2 = 1$, $\lambda_0 \neq 0$, $\lambda_2 + \lambda_4 \neq 0, \lambda_3 + \lambda_4 \neq 0$ and $\phi \in [0, \pi]$. As there are many parameters involved (state parameters plus the parameters for the measurement operators), we don't have any analytical claim for three-qubit genuinely entangled pure states. But we do have numerical evidence that all genuinely entangled pure states violates atleast one of the three inequalities listed above. We have generated 25000 random states and checked the expectation value of the facet-Bell operator. We numerically optimized the expectation value by considering all possible measurement settings and in each case we got a violation. In support of this we will provide some results for some special cases of pure three-qubit states. In section 3.3, we have shown that all three inequalities are violated for the whole range of generalized GHZ states. We consider another class of GHZ state, i.e., $|\psi\rangle_{GG} = \sin\alpha\cos\beta\,|000\rangle + \sin\alpha\sin\beta\,|101\rangle + \cos\alpha\,|111\rangle$. We find the expectation value of all three inequalities and then find out the maximum ($I_G = \max[I_1, I_2, I_3]$) among them. We plot I_G with β for some values of α in Fig.(3.1). Fig.(3.1) shows that $|\psi\rangle_{GG}$ violate at least one of the three inequalities

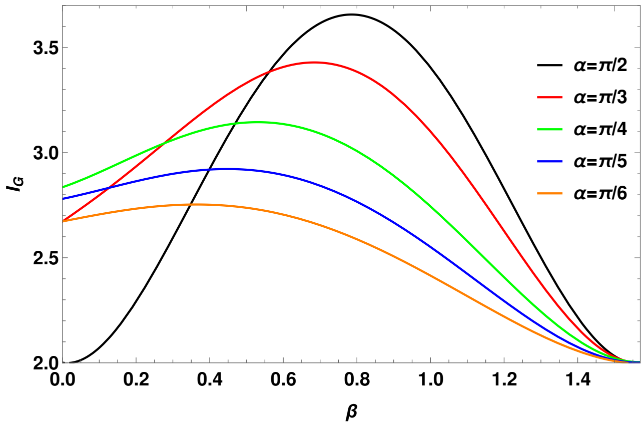

Figure 3.1: Variation of I_G with β, where $I_G = \max[I_1, I_2, I_3]$.

except for cases $\beta = 0$; $\alpha = \frac{\pi}{2}$ and $\beta = \frac{\pi}{2}$ where the states are product states. Next, we consider generalized W state of the form $|\psi\rangle_{GW} = \sin\alpha\cos\beta\,|001\rangle + \sin\alpha\sin\beta\,|010\rangle + \cos\alpha\,|100\rangle$. Again for this class of states we find out the maximum ($I_W = \max[I_1, I_2, I_3]$) among the three inequalities. In Fig.(3.2) we plot I_W with β for some fixed values of α. From this figure it is evident that at least

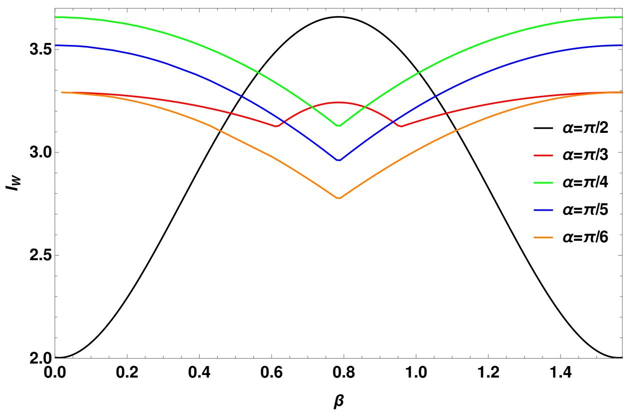

Figure 3.2: Variation of I_W with β, where $I_W = \max[I_1, I_2, I_3]$.

one of the three inequalities is violated by the generalized W state $|\psi\rangle_{GW}$ except when $\beta = 0$; $\alpha = \frac{\pi}{2}$ and $\beta = \frac{\pi}{2}$; $\alpha = \frac{\pi}{2}$ as they are product states.

3.5 Quantum to classical ratio

In this section, we study quantum to classical ratio and compare our inequalities with the well-known Mermin inequality. Quantum to classical ratio has a meaning in the sense that if quantum to classical ratio is large then the inequality is better suitable for an experiment. In our case, we define the quantum to classical ratio as $\frac{I}{2}$, where $I = \max[I_1, I_2, I_3]$. For generalized GHZ state ($|GGHZ\rangle = \sin\beta\,|000\rangle + \cos\beta\,|111\rangle$) our inequalities are not as good as Mermin. However, there is one drawback of Mermin inequality. It is not violated by the whole range of generalized GHZ state. In this sense our inequalities are better than Mermin inequalities. In Fig.(3.4), we compare our results for generalized

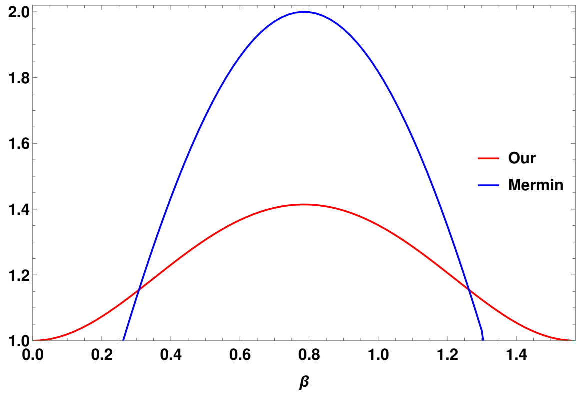

Figure 3.3: Variation of quantum to classical ratio with β for generalized GHZ state.

W state of the form $|\psi\rangle_{GW} = \sin\alpha\cos\beta\,|001\rangle + \sin\alpha\sin\beta\,|010\rangle + \cos\alpha\,|100\rangle$, where we consider the case $\alpha = \frac{\pi}{4}$. From this figure it is clear that our facet Bell inequalities are better than of Mermin inequalities. Therefore, for experimental studies our inequalities are better.

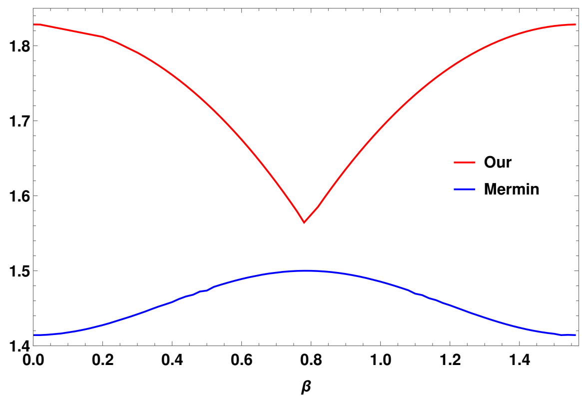

Figure 3.4: Variation of quantum to classical ratio with β for generalized W state with $\alpha = \frac{\pi}{4}$.

3.6 Mixed state scenario

Mixed states present different challenges. There is a phenomenon of hidden nonlocality. We have the modest goal to examine where the facet Bell inequalities of this paper may be more useful. We consider a few noisy states, like noisy GHZ states, noisy W states with both white and colored noise, to see whether any advantages are there for our facet Bell inequalities over the Mermin inequality for mixed states. First we take a Werner like state for three qubits, which is GHZ state with white noise.

$$NoisyGHZ = p\,|GHZ\rangle\langle GHZ| + \frac{(1-p)}{8}\mathbb{1}, \tag{3.17}$$

The identity can be written as the sum of all orthogonal variants of GHZ state as written below,

$$\begin{aligned} \mathbb{1} &= |\psi_0^+\rangle\langle\psi_0^+| + |\psi_0^-\rangle\langle\psi_0^-| + |\psi_1^+\rangle\langle\psi_1^+| + |\psi_1^-\rangle\langle\psi_1^-| \\ &+ |\psi_2^+\rangle\langle\psi_2^+| + |\psi_2^-\rangle\langle\psi_2^-| + |\psi_3^+\rangle\langle\psi_3^+| + |\psi_3^-\rangle\langle\psi_3^-| \end{aligned} \tag{3.18}$$

and the expression of the orthogonal variants are as following,

$$|\psi_0^+\rangle = |GHZ\rangle = \sqrt{1/2}(|000\rangle + |111\rangle) \tag{3.19}$$

$$|\psi_0^-\rangle = \sqrt{1/2}(|000\rangle - |111\rangle) \tag{3.20}$$

$$|\psi_1^+\rangle = \sqrt{1/2}(|010\rangle + |101\rangle) \tag{3.21}$$

$$|\psi_1^-\rangle = \sqrt{1/2}(|010\rangle - |101\rangle) \tag{3.22}$$

$$|\psi_2^+\rangle = \sqrt{1/2}(|100\rangle + |011\rangle) \tag{3.23}$$

$$|\psi_2^-\rangle = \sqrt{1/2}(|100\rangle - |011\rangle) \tag{3.24}$$

$$|\psi_3^+\rangle = \sqrt{1/2}(|110\rangle + |001\rangle) \tag{3.25}$$

$$|\psi_3^-\rangle = \sqrt{1/2}(|110\rangle - |011\rangle). \tag{3.26}$$

For this noisy GHZ state, we have numerically obtained the optimal expectation value of the facet Bell operator for the whole range of p ($0 \leq p \leq 1$) and plotted them. The noisy GHZ states start violating our facet Bell inequality after $p = 0.71$. Now, let us see what is the scenario for Mermin inequality for the same noisy GHZ states. We see that for Mermin operator, the violation starts after

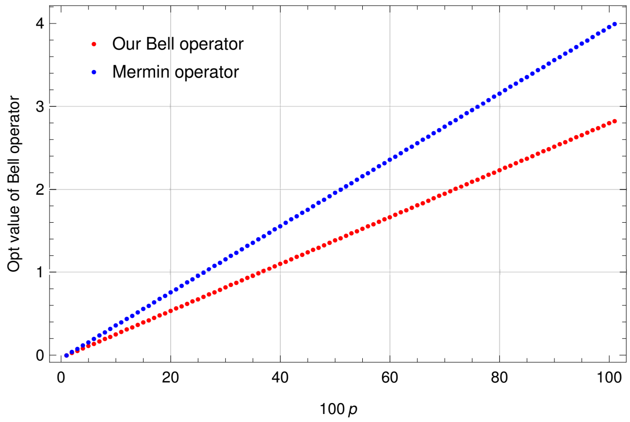

Figure 3.5: Maximum expectation value of the our Bell operator and Mermin operator for a noisy GHZ states vs p plot.

$p = 0.51$. So, for this noisy GHZ states, our facet Bell inequality presents no advantage. One of the reasons for this is that, Mermin inequality is optimally constructed for GHZ states, giving a violation 4, whereas, our facet inequality gives only $2\sqrt{2}$ for GHZ states. Let us now consider noisy W states

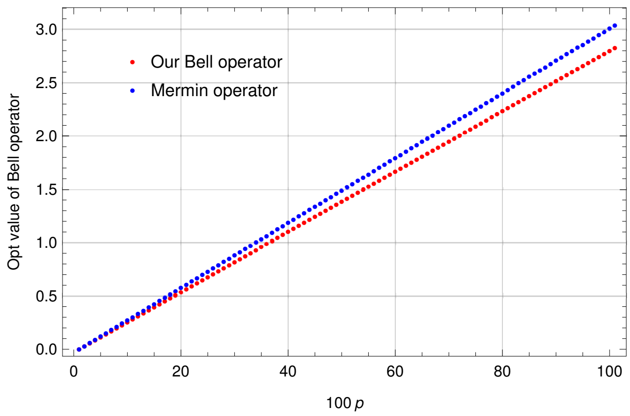

Figure 3.6: Maximum expectation value of our Bell operator and the Mermin operator for a noisy GHZ states vs p plot.

to analyze the same thing. We take,

$$NoisyW = p\,|W\rangle\,\langle W| + \frac{(1-p)}{8}\mathbb{1} \tag{3.27}$$

For this case, we see that nosy W states start to violate our facet Bell inequality after $p = 0.70$. For Mermin inequality violation starts after $p = 0.65$. So, in this case also Mermin inequality gives advantage over the our inequality, but as compared to the noisy GHZ state, the advantage is much less. If we take colored noise and different noisy states, we can see that sometimes our inequality has advantage over the Mermin. In the following we give a table listing the results we have obtained numerically. In the above table we have used the following notations for the states,

	Minimum p for violation	
States	Facet	Mermin
$p\lvert GHZ\rangle\langle GHZ\rvert + \frac{(1-p)}{8}\mathbb{1}$	0.71	0.51
$p\lvert GGHZ3\rangle\langle GGHZ3\rvert + \frac{(1-p)}{8}\mathbb{1}$	0.80	0.69
$p\lvert GGHZ2\rangle\langle GGHZ2\rvert + \frac{(1-p)}{8}\mathbb{1}$	0.81	0.73
$p\lvert GGHZ1\rangle\langle GGHZ1\rvert + \frac{(1-p)}{8}\mathbb{1}$	0.83	0.97
$p\lvert GHZ\rangle\langle GHZ\rvert + \frac{(1-p)}{5}col$	0.64	0.38
$p\lvert W\rangle\langle W\rvert + \frac{(1-p)}{8}\mathbb{1}$	0.70	0.65
$p\lvert W1\rangle\langle W1\rvert + \frac{(1-p)}{8}\mathbb{1}$	0.61	0.68

Table 3.1: Noisy states and Bell violation

$$|GGHZ_1\rangle = \sqrt{8/9}\,|000\rangle + \sqrt{1/9}\,|111\rangle \tag{3.28}$$

$$|GGHZ_2\rangle = \sqrt{25/29}\,|000\rangle + \sqrt{4/29}\,|111\rangle \tag{3.29}$$

$$|GGHZ_3\rangle = \sqrt{21/25}\,|000\rangle + \sqrt{4/25}\,|111\rangle \tag{3.30}$$

$$col = |\psi_0^+\rangle\langle\psi_0^+| + |\psi_1^+\rangle\langle\psi_1^+|$$

$$+ |\psi_1^-\rangle\langle\psi_1^-| + |\psi_2^+\rangle\langle\psi_2^+| + |\psi_2^-\rangle\langle\psi_2^-| \tag{3.31}$$

$$|W\rangle = \sqrt{1/3}\,|001\rangle + \sqrt{1/3}\,|010\rangle + \sqrt{1/3}\,|100\rangle \tag{3.32}$$

$$|W1\rangle = \sqrt{1/6}\,|001\rangle + \sqrt{2/6}\,|010\rangle + \sqrt{3/6}\,|100\rangle\,. \tag{3.33}$$

In the above, we have taken col to be colored noise and $|GGHZ_1\rangle$, $|GGHZ_2\rangle$, $|GGHZ_3\rangle$ are generalized GHZ states and $|W1\rangle$ is a W class state. Evidently, our inequality gives advantages for noisy W states. For noisy GHZ states Mermin is better except for the cases starting from the close vicinity of the parameter range $\theta = 15^\circ$ $i.e$ $\sin\theta \sim 0.25$, where Mermin does not get violated. From the table it is evident that when $\sin\theta = \sqrt{1/9} = 0.33$, the noisy state violates Mermin when it is almost pure. Obviously in those regions our inequality is advantageous, because they are violated for all generalized GHZ states i.e GGHZ states. One can in principle check for other mixed states. We have analyzed the noisy ones, because they are experimentally relevant. Whenever one tries to prepare a GHZ or W state in lab, unavoidable noises add up, making the states noisy.

3.7 Extension to multipartite scenario

In this section, we will be extending the previous facet inequalities to more than three parties. First, we will be dealing with four-qubit scenario and then with five qubits. After that results will be generalized for n qubits, where $n \geq 3$. In all these scenarios we will be restricting our calculations for the situations, where two parties are making two dichotomic measurements and rest are making only one dichotomic measurement. For this particular scenario, we will find nontrivial facets of the local polytope. Let's start with four qubits.

3.7.1 Four-qubit scenario

For this case we have 35 vertices for the local polytope, where two parties are making two dichotomic measurements and remaining two parties are making one dichotomic measurement each. We again convert this V-representation of the polytope to the H-representation using the software cdd [154] and obtain a total of 96 facets. Out of which 64 facets are just the positivity conditions on the probabilities. So, we get 32 nontrivial facet inequalities. But, interestingly, these 32 inequalities are just the variants of one single inequality, upto the relabelling of indices. So, like the three-qubit scenario, we again get only one single inequality.

$$(-2 + A_1(B_1 + B_2) + A_2(B_1 - B_2))(1 + C_1)(1 + D_1) \leq 0 \tag{3.34}$$

All the 32 facet inequalities are equivalent to this inequality upto the relabelling of indices. The form of this inequality is very similar to the inequality for the three-qubit case. Because one can write the inequality given by the Eq. (3.7) as,

$$(-2 + A_1(B_1 + B_2) + A_2(B_1 - B_2))(1 + C_1) \leq 0,$$

which has the exactly similar structure like the four-qubit inequality except the extra party denoted by D. Next we will explore whether five-qubit case has also the similar structure.

3.7.2 Five qubits or more

In this case, again we have two parties performing two dichotomic measurements and the remaining parties are performing only one dichotomic measurement. For this case, we have a total of 71 vertices. Converting from the V representation to H representation for this local polytope, we obtain total of 192 facets. Out of which, 128 inequalities are just the positivity conditions for the probabilities. Remaining 64 inequalities again give only one non-trivial inequality upto the relabeling of the indices.

$$(-2 + A_1(B_1 + B_2) + A_2(B_1 - B_2))(1 + C_1)(1 + D_1)(1 + E_1) \leq 0 \tag{3.35}$$

Again for five-qubit case also, we have the same structure of the inequality like three- and four-qubit cases, with the addition of a new term for the party E. So, after exploring these three cases extensively, we can generalize this structure to more qubits. For n number of qubits, we can generalize the structure as,

$$(-2 + A_1(A_2 + A_2') + A_1'(A_2 - A_2'))(1 + A_3)(1 + A_4)...(1 + A_n) \leq 0, \tag{3.36}$$

where A_1 and A_1' are the two measurement choices for the party A_1 and similarly for A_2. If we just expand this we will get,

$$(A_1(A_2{+}A_2'){+}A_1'(A_2{-}A_2'))(1{+}A_3)...(\mathbb{1}{+}A_n){-}(2A_3{+}2A_4{+}...2A_3A_4{+}...2A_3A_4..A_n) \leq 2. \tag{3.37}$$

So, the facet Bell inequalities have very simple and intuitive structure. Important point is that we have only one facet Bell inequality in our minimal scenario for any number of qubits, which can also be obtained by lifting [153] the Bell-CHSH inequality to n parties. This Bell inequality involves multipartite correlations. We can permute the parties that make two dichomotic measurements to obtain the complete set. We now show that all n-qubit generalized GHZ state violate this n-qubit facet Bell inequality.

3.7.3 Violation by n-qubit GGHZ state

Here, we will show that the n-qubit facet Bell inequality for n qubits will be violated by the generalized GHZ states for the whole parameter range. To show this, we take the n-qubit generalized GHZ state to be, $|GGHZn\rangle = \alpha\,|00..0_n\rangle + \beta\,|11..1_n\rangle$ and the similar measurement settings as the three-qubit scenario, i.e we choose, $A_1 = \sigma_z$, $A_1' = \sigma_x$, $A_2 = \cos\theta\sigma_x + \sin\theta\sigma_z$, $A_2' = -\cos\theta\sigma_x + \sin\theta\sigma_z$ and all other measurement settings to be σ_x, i.e $A_3 = \sigma_x$, $A_4 = \sigma_x$,...$A_n = \sigma_x$. Now for these measurement settings the expectation value of the facet-Bell operator given by the Eq. (3.37) is $(2\sin\theta + 4\alpha\beta\cos\theta)$, which is exactly equal to the previously obtained expectation value for the three-qubit scenario. So, the generalized GHZ state will violate the n-qubit facet inequality for all the range of parameters, giving the maximum violation of $2\sqrt{1+4\alpha^2\beta^2}$ for the GHZ state for this measurement settings.

3.8 Conclusion

In this chapter, we have considered a specific measurement scenario. This scenario may be thought of as minimal scenario that involves multipartite correlations. In this scenario, there are two dichotomic measurement settings for two parties and one dichotomic measurement setting for each of the remaining parties. Interestingly, there is just one facet Bell inequality (up to permutation of parties) for n qubits. This is the lifted version [153] of Bell-CHSH inequality. This is like the two-qubit scenario where only Bell-CHSH inequality is the facet Bell inequality. This suggests that we need only one facet Bell inequality that uses multipartite correlations to detect the nonlocality of a multipartite state. This gives significant advantage over the other scenarios.

We first constructed facet Bell inequalities, in this scenario, for a three-qubit system. This was motivated by our previous work [145] described in the last chapter. Then, we showed that the three facet inequalities give similar advantages like our previous inequalities [145]. However, the facet Bell inequalities are now not violated maximally by the GHZ states, which can be considered as maximally entangled three-qubit state. We then computed the facets for four and five qubits in the minimal scenario. We found that each of these two cases again give only one non-trivial facet inequality upto the relabeling of indices as expected from the results of the Ref. [153]. We then extended our results to n parties and shown that the n-qubit facet Bell inequality is violated by all n-qubit generalized GHZ states. We have compared minimal-scenario facet three-qubit inequalities with Mermin and Svetlichny inequalities and also analyzed some cases of mixed states, including noisy GHZ and W states. We have demarcated where these facet Bell inequalities present advantages. Inequalities in this chapter can be tested experimentally as our previous ones [158].

CHAPTER 4

Co-operative Quantum Key Distribution (CoQKD)

4.1 Introduction

Usefulness of entanglement as a resource in cryptography was demonstrated by Ekert [14] in a protocol. This protocol is an extension of the seminal BB84 protocol [62]. I have already discussed the Ekert's protocol in the first chapter. Since then many variants of this protocol have been proposed [63, 64] using bipartite and multipartite entanglement. We are mainly interested in a variant of Ekert's protocol with multipartite entangled state, where we consider two scenarios. In the first scenario, a key is established between two par- ties, say Alice and Bob, with other parties controlling this key generation. This protocol of cooperative (controlled) QKD was introduced in the Ref. [159]. In the second scenario, a key is established among all parties, so that there can be secret communication among all of them. For the first case, the need for control may arise for a number of different reasons. Some of them could be: i) one of the two parties may be dishonest, ii) one of the two parties may be compromised by some eavesdropper, iii) the communication may be done only under some supervision. In this protocol, the controller/supervisor determines the state that Alice and Bob can share. This state can be a product state, a partially entangled state, or a maximally entangled state. The nature of this state will determine if a key can be established or not, and what will be the key rate and security. We mention the suitable resource states to carry out CoQKD and introduce a protocol to implement the same. we also generalize the scheme for more than three parties. In the second scenario, the key, that is established among all parties, is known as conference key. Using the new resource state we give a protocol to establish a conference key. We discuss the security of this key using our Bell inequalities [145, 152] introduced in last two chapters. The chapter is organized as follows. In Sections 4.2, 4.3, and 4.4 we cover the three qubit scenario in detail. Specifically, in the section 4.2, we introduce the CoQKD protocol. Then, we discuss the CoQKD protocol using the new resource states in the section 4.3. In the section 4.4, we show the generation of the conference key by these states. In the section 5.2, we explore further for the suitable structure of states useful in CoQKD beyond three qubits and in next section 5.3 we conclude.

4.2 CoQKD scheme

In this section, we illustrate the CoQKD protocol using three-qubit GHZ state. The goal of this new protocol is to establish a secret key between two parties with the involvement of the other parties. As discusses earlier, there could be multiple reasons for the involvement of other parties. One of the parties with the final secret key is not trustworthy, and wants to disrupt the key creation. Specifically, in the key forming procedure, the dishonest party can deliberately make false statements in the public declaration rounds and affect the secret key. Moreover, he/she can be compromised by an external attacker, such that they two collaborate to act dishonestly. If there is a supervisor who can control the shared entangled state between the two parties and supervises the key generation then a party cannot cheat or be compromised by any external eavesdropper. Specifically, the supervisor knows exactly which state the two parties are sharing and what the optimal key rate should be. Here, by optimum key rate we mean the maximum possible key rate possible with a given state between two parties assuming no noise in the communication channel. If the parties report the controller/supervisor a smaller key rate than the optimal, then there is a cheating involved and that run of the key generation is discarded. The supervisor is also a controller. All the parties share a multipartite entangled state and the controller does a measurement on his/her system to initiate the key generation process. There may be more than one controller and one controller may have more than one qubit in his/her possession.

In this protocol, there are N ($N \geq 3$) parties, among which $N-2$ parties control the secret key generation by two remaining parties, say Alice and Bob. To illustrate the protocol clearly, we consider a simple scenario of three parties who share a three-qubit GHZ state, $|GHZ\rangle = \frac{1}{\sqrt{2}}(|000\rangle + |111\rangle)$. If the controller Charlie performs measurement on his qubit in Hadamard basis, then the collapsed state between Alice and Bob is a Bell state: $|\psi^{\pm}\rangle = \frac{1}{\sqrt{2}}(|00\rangle \pm |11\rangle)$. Then Charlie publicly announces his measurement basis such that, following the Ekert's protocol, Alice and Bob can establish a perfect secret key with optimal key rate between them, *i. e.* without any Quantum Bit Error rate (QBER). After establishing the key, Alice and Bob both report the key rate to Charlie. If it is not optimal, then Charlie knows that there has been a cheating. We assume here that the communication takes place over a noiseless classical channel. Moreover, without the measurement performed by Charlie, Alice and Bob can not establish a key, as their qubits are in maximally mixed state. So, Charlie also supervises the starting of the key generation process, which allows him to control the whole process. If Charlie makes a measurement in a basis other than the Hadamard basis, shared state between Alice and Bob is not a Bell state, but a partially entangled state. With this state, perfect key generation with optimal key rate would not be obtained. If the key rate reported to Charlie is less than the optimal w.r.t the shared state between Alice and Bob, Charlie knows that there is a cheating involved and that run of key making is discarded. Therefore, for a particular basis of Charlie, Alice and Bob can

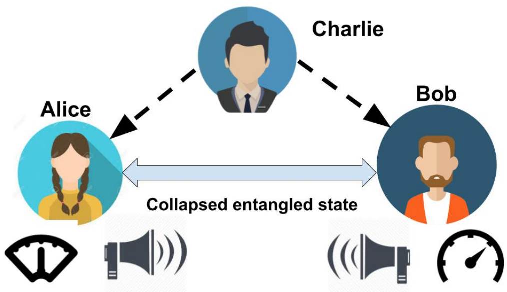

Figure 4.1: CoQKD: Charlie, the controller supervises and initiates the secret key making procedure shared between Alice and Bob.

establish a perfect secret key with optimal key rate, as the collapsed state between Alice and Bob is a maximally entangled state. If Charlie performs the measurement in a general basis, the secret key rate is not optimal. Advantage of this protocol is that Charlie can detect if there is a cheating involved in the establishment of the secret key and also he can control the optimal key rate and QBER between Alice and Bob. In the above illustration, we find that GHZ state can be used for *maximal* CoQKD, i.e, the generation of a perfect secret key with optimal key rate. We also note that the states with two maximally mixed marginals [160], are also suitable for maximal CoQKD. For three qubits if one of the marginals is non-maximally mixed, we call it NMM-state, $|NMM\rangle$ (similarly, the MMN or MNM). These are class of one parameter state and for a specific value of the parameter, these state becomes the GHZ-state. Particularly, the GHZ state is MMM-state, $|MMM\rangle$ because its marginals are maximally mixed. Note that these four classes of states belong to the GHZ class states. Next, we extend these protocols for four qubit states. For four qubits, there exist MMNN-states, MMMN-states, or MMMM-states (like GHZ-state, or cluster state) for CoQKD. Two cases may arise, where each party has one qubit each, or one of the parties have more than one qubit. We discuss this and the further generalizations in subsequent sections.

4.3 CoQKD protocol with NMM state

In this section, we put forward a scheme for cooperative QKD using NMM-state written as following,

$$|NMM\rangle = \sqrt{p}\,|0\rangle_C\,|\phi^+\rangle_{AB} + \sqrt{1-p}\,|1\rangle_C\,|\phi^-\rangle_{AB}\,. \tag{4.1}$$

If $p = 1/2$, the state is LU equivalent to the GHZ state. The qubit Charlie holds is not maximally mixed, where Alice and Bob holds the maximally mixed qubits. Now, depending upon the measurement basis of Charlie, the collapsed state shared between Alice and Bob will be either maximally entangled or partially entangled or product state. With maximally entangled state one can carry out the Ekert's protocol. But as in general the shared state between Alice and Bob is not a maximally entangled state, we introduce a protocol which uses partially entangled state as the resource. To establish the protocol, we use the fact that given a non-maximally entangled two-qubit pure state, we can always specify the measurement settings [78, 161] for which Bell-CHSH [70] inequality shows the optimal violation. Now the steps are following. Charlie first publicly announces his choice of measurement basis, such that Alice and Bob know the shared state between them. Suppose, the collapsed state between Alice and Bob is $|\psi\rangle = \alpha\,|00\rangle + \beta\,|11\rangle$. Then, Alice and Bob choose the following three measurement settings each giving rise to nine combinations.

$$A_1 = \sigma_z,\;\; A_2 = \cos\theta\sigma_z + \sin\theta\sigma_x,\;\; A_3 = \sigma_x,$$

$$B_1 = \cos\theta\sigma_z + \sin\theta\sigma_x,\; B_2 = \sigma_x,\; B_3 = \cos\theta\sigma_z - \sin\theta\sigma_x,$$

where, $\cos\theta = 1/\sqrt{1+4\alpha^2\beta^2}$. Like before, the combination (A_2, B_1) and (A_3, B_2) can be used to generate the secret key and the combination (A_1, B_1), (A_1, B_3), (A_3, B_1) and (A_3, B_3) can give the optimal Bell violation, which is $2\sqrt{1+4\alpha^2\beta^2}$. Remaining combinations are thrown out. So, if the

Bell violation is less than the optimum value $2\sqrt{1+4\alpha^2\beta^2}$, Eve's presence is detected. In the case of a partially entangled state, perfect correlation are not obtained, which leads to nonzero QBER. After the protocol, Alice and Bob inform Charlie about the key rate and QBER. If there is a discrepancy between the expected QBER (and key rate) and reported QBER (and key rate), then Charlie knows that there is a cheating and that run of secret key making is rejected. Moreover, without Charlie's measurement Alice and Bob can not establish a key, as their reduced state is a maximally mixed state. So, the whole key making process is initiated and supervised by a controller Charlie and thus making it more secure and trustworthy.

Remarks.– In the above, we see that if, the reduced density matrices of Alice and Bob have entropy one from the beginning, then by making a measurement in a right basis Charlie can reduce the state between Alice and Bob to a maximally entangled state. So, the question arises that, if the qubits held by Alice and Bob do not have entropy one (*i.e.*, maximally mixed) but less than one from the beginning, can a measurement by Charlie make them maximally mixed? In the following, we show that this is not possible. To show this, we start with the state of the form of Eq. (4.1). But this time Charlie makes a measurement on a qubit, which has entropy one. Then we show that it is not possible to increase the entropy of the qubit, which has entropy less than one. Considering the state in Eq. (4.1), let us say, Charlie makes a measurement on the second qubit in the general basis given below,

$$|+_n\rangle = \frac{|0\rangle + n\,|1\rangle}{\sqrt{1+|n|^2}}, \;\; |-_n\rangle = \frac{-n^*\,|0\rangle + |1\rangle}{\sqrt{1+|n|^2}}, \tag{4.2}$$

where $n \in \mathbb{C}$ and $0 \leq |n|^2 \leq 1$. In terms of this basis, we can write the resource state as,

$$\begin{aligned} |NMM\rangle = N/\sqrt{2}\Big[\sqrt{p}\,|00\rangle + n^*\sqrt{p}\,|01\rangle + \sqrt{1-p}\,|10\rangle - n^*\sqrt{1-p}\,|11\rangle\Big]\,|+\rangle \\ +N/\sqrt{2}\Big[-n\sqrt{p}\,|00\rangle + \sqrt{p}\,|01\rangle - n\sqrt{1-p}\,|10\rangle - \sqrt{1-p}\,|11\rangle\Big]\,|-\rangle \end{aligned} \tag{4.3}$$

For two outcomes of Charlie's measurement, the collapsed states between Alice and Bob are,

$$|\phi^+\rangle \;=\; \sqrt{p}\,|0\rangle\,\Big[N[|0\rangle + n^*\,|1\rangle]\Big] + \sqrt{1-p}\,|1\rangle\,\Big[N[|0\rangle - n^*\,|1\rangle]], \tag{4.4}$$

$$|\phi^-\rangle \;=\; \sqrt{p}\,|0\rangle\,\Big[N[-n\,|0\rangle + |1\rangle]\Big] + \sqrt{1-p}\,|1\rangle\,\Big[N[-n\,|0\rangle - |1\rangle]]. \tag{4.5}$$

Probabilities of getting these collapsed states are $1/2$ for each. It is evident from the expression that, for the collapsed state to be a Bell state, we must have $n = 1$ and $p = 1/2$. This eventually makes the starting state to be a GHZ state. Maximum entropy we can achieve for the qubit held by Bob is what we had from the beginning and that can be attained when $n = 1$. This shows that we must have atleast two qubits to have entropy one, on which measurements are not being done. We can do CoQKD with a partially entangled state, but then key rate would not be maximal.

4.4 Conference QKD with NMM-state

In the previous section, we discussed the cooperative QKD scheme, where one party's role was to do the measurement and supervising the establishment of a secret key between the remaining two parties. We discussed the structure of the states optimal for this scheme. In this section, we discuss the protocol for establishing a secret key among all three parties, also called a conference key, with the states introduced in the previous section. There are several conference key protocols using multipartite entanglement [162, 163, 164, 165]. Here, we are closely following the scheme introduced in the Ref. [163]. We show that one can generate conference key using the NMM-state with some non-zero QBER. Before going to describe the protocol, first we note the following equivalences, without invoking any local unitary,

$$\sqrt{1/2}\big[\,|+_x\rangle\,|\phi^+\rangle + |-_x\rangle\,|\phi^-\rangle\,\big] = \sqrt{1/2}(|000\rangle + |111\rangle) = \sqrt{1/2}\big[\,|+_y\rangle\,|\Phi^-\rangle + |-_y\rangle\,|\Phi^+\rangle\,\big] \quad (4.6)$$

where, $|+_x\rangle = \sqrt{1/2}(|0\rangle + |1\rangle)$ and $|-_x\rangle = \sqrt{1/2}(|0\rangle - |1\rangle)$ are the eigenstates of σ_x, $|+_y\rangle = \sqrt{1/2}(|0\rangle + i\,|1\rangle)$ and $|-_y\rangle = \sqrt{1/2}(|0\rangle - i\,|1\rangle)$ are the eigenstates of σ_y, $|\Phi^+\rangle = \sqrt{1/2}(|00\rangle + i\,|11\rangle)$ and $|\Phi^-\rangle = \sqrt{1/2}(|00\rangle - i\,|11\rangle)$. One can also show that,

$$|\phi^+\rangle = \sqrt{1/2}(|+_x\rangle\,|+_x\rangle + |-_x\rangle\,|-_x\rangle = \sqrt{1/2}(|+_y\rangle\,|-_y\rangle + |-_y\rangle\,|+_y\rangle). \quad (4.7)$$

$$|\Phi^+\rangle = \sqrt{1/2}(|+_x\rangle\,|+_y\rangle + |-_x\rangle\,|-_y\rangle) = \sqrt{1/2}(|+_y\rangle\,|+_x\rangle + |-_y\rangle\,|-_x\rangle), \quad (4.8)$$

and similarly for $|\phi^-\rangle$ and $|\Phi^-\rangle$. Above equations show that whenever odd number of σ_x and even number of σ_y are measured, one gets perfect correlations. This is because the GHZ state is the simultaneous eigenstate of the stabilizer group containing eight elements, [164] which are

σ_x	σ_x	σ_x
$+$	$+$	$+$
$+$	$-$	$-$
$-$	$+$	$-$
$-$	$-$	$+$

σ_x	σ_y	σ_y
$+$	$+$	$-$
$+$	$-$	$+$
$-$	$+$	$+$
$-$	$-$	$-$

σ_y	σ_x	σ_y
$+$	$+$	$-$
$+$	$-$	$+$
$-$	$+$	$+$
$-$	$-$	$-$

σ_y	σ_y	σ_x
$+$	$+$	$-$
$+$	$-$	$+$
$-$	$+$	$+$
$-$	$-$	$-$

Table 4.1: Correlation and anti-correlation tables.

$\{III, XXX, ZZI, IZZ, ZIZ, -YXY, -YYX, XYY\}$. This observation is crucial for the protocol of conference QKD. First, one of the party, say, Alice starts with a three-qubit GHZ-state and makes a measurement on one qubit, either in σ_x or σ_y basis. Then, keeping that qubit she sends the rest of the two qubits to Bob and Charlie, who in this protocol are partners of Alice, such that a conference key is established among three of them. Then Bob and Charlie make measurements on their respective qubits in σ_x or σ_y basis randomly. For the time being, we are not concerned with Eve's presence. Then all of them including Alice publicly announce their measurement basis choices. They keep the data for which all of them measure σ_x or any two of them measure σ_y. They discard the remaining data. As, their results are now perfectly correlated, they can generate a secret key. Out of eight set of measurements, they keep four of them to generate the key. So, the key rate is $1/2$.

Now, we consider the NMM-state. We take the starting form of the state to be $|\psi\rangle = \sqrt{p}\,|+_x\rangle\,|\phi^+\rangle + \sqrt{1-p}\,|-_x\rangle\,|\phi^-\rangle$. As expected, we would not get perfect correlations; so QBER is not zero. We calculate QBER for this kind of state. Before that, let us first write down the correlation and anti-correlation tables. Note that the starting state, $|\psi\rangle$ is LU equivalent to the NMM-state. The state has perfect correlations for three σ_x measurements. So, QBER is zero for this kind of correlation. Also, when σ_x is measured on the first qubit, it is straightforward to see that,

$$\begin{aligned} &\sqrt{p}\,|+_x\rangle\,|\phi^+\rangle + \sqrt{1-p}\,|-_x\rangle\,|\phi^-\rangle = \\ &\sqrt{p/2}\,|+_x\rangle\,(|+_y\rangle\,|-_y\rangle + |-_y\rangle\,|+_y\rangle) + \sqrt{(1-p)/2}\,|-_x\rangle\,(|+_y\rangle\,|+_y\rangle + |-_y\rangle\,|-_y\rangle). \end{aligned} \tag{4.9}$$

So, for the the measurements XXX and XYY, we have perfect correlations and hence zero QBER. But, the other two measurements do not give perfect correlations. Now, QBER is defined as the probability that they would obtain different outcomes even if the measurement basis states are same. From the chart of correlation and anti-correlation it is evident that remaining two cases *i.e.*, YXY and YYX give same QBER. Let us compute it for the first one. For the table of YYX, the QBER is given by,

$$Tr[(P_+^y \otimes P_+^y \otimes P_+^x)\rho] + Tr[(P_+^y \otimes P_-^y \otimes P_-^x)\rho]$$
$$+ Tr[(P_-^y \otimes P_+^y \otimes P_-^x)\rho] + Tr[(P_-^y \otimes P_-^y \otimes P_+^x)\rho], \tag{4.10}$$

which comes out to be equal to $1/2(\sqrt{1-p} - \sqrt{p})^2$ and same for the other table. we plot the QBER with p and see that as expected, it is zero for GHZ-state. We see that the NMM-state is useful

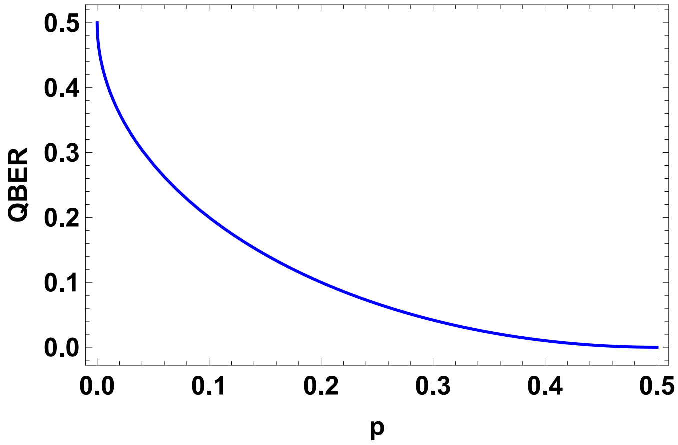

Figure 4.2: Variation of QBER with p

for conference QKD scheme, but with some non-zero QBER. The security of the secret key in the presence of Eve can be analysed with the help of Bell inequalities. We assume that all the three parties between whom the secret key is being established are trusted. It is only an outsider like Eve who wants to jeopardize the protocol. The inequalities [145, 152] previously introduced are useful to check the security of the QKD protocol, as these inequalities are violated by all generalized GHZ-states, the property which is not shown by any correlation Bell inequalities with two measurement choices per party. In the following, we show the protocol in which using the inequalities introduced in [145], we can detect the presence of Eve. We take any inequality out of the set of six inequalities constructed in [145], and see the violation by the NMM-state. We take the following inequality,

$$I = A_1(B_1 + B_2) + A_2(B_1 - B_2)C_1 \leq 2. \tag{4.11}$$

In the following we show that every NMM-state violates the inequality for the whole parameter range. To show this, we choose the following measurement settings,

$$
\begin{aligned}
&A_1 = \sigma_z, \quad A_2 = \sigma_x \\
&B_1 = \cos\theta\sigma_x + \sin\theta\sigma_z, \quad B_2 = -\cos\theta\sigma_x + \sin\theta\sigma_z \\
&C_1 = \sigma_x
\end{aligned}
\tag{4.12}
$$

These measurement settings are similar to the ones used in Ref. [145]. For these measurement settings, the expectation value of the state $|\psi\rangle = \sqrt{p}\,|+_x\rangle\,|\phi^+\rangle + \sqrt{1-p}\,|-_x\rangle\,|\phi^-\rangle$ is $\langle I\rangle = 4\sqrt{p(1-p)}\cos\theta + 2\sin\theta$. From $\alpha\sin\theta + \beta\cos\theta \leq \sqrt{\alpha^2+\beta^2}$, it is evident that, $\langle I\rangle \leq 2\sqrt{1+4p(1-p)}$. This shows that the inequality gets always violated by the NMM-state and when $p = 1/2$ (*i.e.* GHZ-state), the violation is $2\sqrt{2}$. Therefore, for $\cos\theta = 1/\sqrt{1+4p(1-p)}$, the measurement settings we chose is also the optimal measurement settings for the NMM-state. Next, we describe the protocol to detect the presence of Eve. For this, in each round of the protocol, Alice chooses from three measurement settings, Bob chooses from four measurement settings and Charlie chooses from three measurement settings as following,

$$
\begin{aligned}
&A_1 = \sigma_x, \quad A_2 = \sigma_y, \quad A_3 = \sigma_z \\
&B_1 = \sigma_x, \; B_2 = \sigma_y, \\
&B_3 = \cos\theta\sigma_x + \sin\theta\sigma_z, \; B_4 = -\cos\theta\sigma_x + \sin\theta\sigma_z. \\
&C_1 = \sigma_x, \quad C_2 = \sigma_y, \quad C_3 = \mathbb{I},
\end{aligned}
\tag{4.13}
$$

where, $\mathbb{I}$ is an Identity operator, and $\cos\theta = 1/\sqrt{1+4p(1-p)}$. So, there are total 36 combinations, out of which four combinations *e.g.* (A_1, B_1, C_1), (A_1, B_2, C_2), (A_2, B_1, C_2) and (A_2, B_2, C_1) are used to make the key as described before. This gives the key rate of $1/9$. Four combinations, *e.g.* (A_3, B_3, C_3), (A_3, B_4, C_3), (A_1, B_3, C_1) and (A_1, B_4, C_1) are used to check the optimal violation for the inequality in Eq. (4.11), which is $2\sqrt{1+4p(1-p)}$. So, if the expectation value for the inequality is less than $2\sqrt{1+4p(1-p)}$, we can surely say that there is Eve's intervention. Remaining 28 combinations are thrown away for the completion of the protocol.

4.5 Resource structure for multipartite states ($N \geq 4$)

In this section, we explore the resource state structure of four-qubit states that are suitable for maximal CoQKD, *i.e.* CoQKD with maximal key rate (perfect key), for some particular measurement settings by the controllers. In this scenario, there may arise two situations for cooperative QKD. In the first case, there are four parties and each party has one qubit. Second case is when there are three parties and one party (other than the sender and the receiver) has two qubits. We start with the first case.

4.5.1 Case I: Each party has one qubit

Secret key can be established between Alice and Bob, if after the measurements by Charlie and Dennis, they share a Bell state or its LU equivalent state.

Proposition-2 : *Cooperative QKD is successful if, after the measurement by one party say Dennis, the collapsed state between Alice, Bob and Charlie is LU equivalent* $\sqrt{1/2}\big[\,|0\rangle\,|\phi^{+}\rangle + |1\rangle\,(\mathbb{1}\otimes U)\,|\phi^{-}\rangle\,\big]$. *If* $(\mathbb{1}\otimes U)\,|\phi^{-}\rangle$ *is orthonormal to* $|\phi^{+}\rangle$*, then it is LU equivalent to GHZ-state.*

Proof : The proof follows from the Proposition-1 where we proved that for three qubits the structures we presented, *i.e.* LU equivalent to GHZ or LU equivalent to $\sqrt{1/2}\big[\,|0\rangle\,|\phi^{-}\rangle + |1\rangle\,(\mathbb{1}\otimes U)\,|\phi^{+}\rangle\,\big]$, such that $(\mathbb{1}\otimes U)\,|\phi^{-}\rangle$ is not orthonormal to $|\phi^{+}\rangle$ are necessary and sufficient for cooperative QKD to be successful. Therefore, for four qubits, after the measurement by one party, the state must collapse to one of these three-qubit states. The protocol can be generalized for multipartite entangled states also. In analogy with the previous section there may arise three different type of structures for the resource state as listed in the following,

$$|\Phi_1\rangle = \frac{1}{\sqrt{2}}(|0\rangle_4 \otimes |g_0\rangle_{321} + |1\rangle_4 \otimes |g_1\rangle_{321}). \tag{4.14}$$

$$|\Phi_2\rangle = \frac{1}{\sqrt{2}}(|0\rangle_4 \otimes |g_0\rangle_{321} + \frac{1}{\sqrt{2}}\,|1\rangle_4 \otimes |\psi\rangle_{321}). \tag{4.15}$$

$$|\Phi_3\rangle = \frac{1}{\sqrt{2}}(|0\rangle_4 \otimes |\psi\rangle_{321} + \frac{1}{\sqrt{2}}\,|1\rangle_4 \otimes |\psi'\rangle_{321}). \tag{4.16}$$

where, $|g_0\rangle$ is conventional GHZ-state and $|g_1\rangle$ is LU equivalent to the former one, $|\psi\rangle$ and $|\psi'\rangle$ are the states as mentioned in Eq. (4.1) with different coefficients p. The subscripts denote the order of the qubits which we follow throughout our discussion. Notice that, if $|g_0\rangle$ is orthogonal to $|g_1\rangle$, then all the single qubit reduced density matrices of the resource state $|\Phi_1\rangle$ have entropy one, otherwise, the reduced density matrix of the first qubit has entropy less than one, whereas all other single qubit reduced density matrices have entropy one. For the state $|\Phi_2\rangle$, the single qubit reduced density matrices for the last two qubits are maximally mixed, whereas the other qubits have reduced density matrices with entropy less than one. And similarly the state $|\Phi_3\rangle$ has also the similar entropy configuration as $|\Phi_2\rangle$. Therefore, given the entropy structures, we cannot distinguish between $|\Phi_2\rangle$ and $|\Phi_3\rangle$. To distinguish them, we need the collapsed states after the measurement by Dennis. $\square$

To illustrate the above proposition, we find that the cluster states [88] belong to the first category of states with all the single qubit reduced density matrices having entropy one. So, it is a suitable resource state for cooperative QKD. Next example is the following state,

$$|R_1\rangle = \frac{1}{2\sqrt{2}}\Big[|0010\rangle + |0100\rangle + |0001\rangle - |0111\rangle + |1000\rangle + |1100\rangle + |1011\rangle - |1111\rangle\Big].$$

This state has similar entropic structure like the first structure, where $|g_0\rangle$ and $|g_1\rangle$ are not orthogonal as $S(\rho_4) \approx .81$ and $S(\rho_i) = 1$ for $i = 1, 2, 3$. Therefore, this state is also suitable for cooperative QKD. For four-qubits, we see that two maximally-mixed single qubit reduced density matrices are the minimum requirement. Therefore, for four-qubits, this criteria is also a necessary and sufficient for successful cooperative QKD. Other possible structures are sufficient conditions. So, we can generalize it for any N-qubit entangled state with each one holding a single subsystem.

Proposition : *For a successful cooperative QKD with maximal key rate, using a N-qubit entangled state, with each party holding one qubit, the necessary and sufficient condition for the resource state is that it has at least two maximally-mixed single qubits.*

4.5.2 Case II: One party has more than one qubit

Let us now consider the second situation, where one party, *e.g.* Charlie, has two qubits in his possession. We know that for CoQKD the state must be either NMM (necessary and sufficient) or GHZ (sufficient) along the cut Charlie-(Alice and Bob). Now, Charlie holds two qubits, say first two qubits, and makes measurement in the orthonormal computational basis :$\{|00\rangle, |01\rangle, |10\rangle, |11\rangle\}$. We require that after the joint measurement, the collapsed state between Alice and Bob is LU equivalent state to a Bell state. Therefore, the most general structure of the resource state is,

$$|\Psi\rangle = \frac{1}{2}(|00\rangle \otimes |\phi_1\rangle + |01\rangle \otimes |\phi_2\rangle + |10\rangle \otimes |\phi_3\rangle + |11\rangle \otimes |\phi_4\rangle), \tag{4.17}$$

where, $|\phi_1\rangle$, $|\phi_2\rangle$, $|\phi_3\rangle$ and $|\phi_4\rangle$ are LU equivalent to Bell states, though not necessarily orthonormal to each other. All states of the form of Eq. (4.14), Eq. (4.15) and Eq. (4.16) can be recast as Eq. (4.17) and vice versa. It can be shown very easily, by observing that $\sqrt{1/2}(|0\rangle \otimes |\phi_1\rangle + |1\rangle \otimes |\phi_2\rangle)$ and $\sqrt{1/2}(|0\rangle \otimes |\phi_3\rangle + |1\rangle \otimes |\phi_4\rangle)$ are the NMM states. So, $|\Psi\rangle$ has the similar structure like $|\Phi_1\rangle$, $|\Phi_2\rangle$ and $|\Phi_3\rangle$. Therefore, the states which are useful for CoQKD as described in the case I, can also be used as a resource in the present case II.

4.5.3 QBER for the state between Alice and Bob

As the structure of the resource states is similar for two scenarios, we can start with any of the above written forms of the resource states. We choose the form of the state to be Eq. (4.17). First we start with the scenario, when each party has one qubit with them. In this case there are two controllers *e.g.* Charlie and Dennis. As before in the three-qubit scenario, collapsed state between Alice and Bob depends upon the measurement basis chosen by the controllers.

Without the loss of generality, we consider that Dennis and Charlie choose to measure in the basis given by Eq. (4.2). So after the measurement of Dennis, the collapsed state between Charlie, Alice and Bob corresponding to the outcome $|+\rangle$, is given by,

$$|\Psi^+_{CAB}\rangle = \frac{|0\rangle\,(|\phi_1\rangle + \beta\,|\phi_3\rangle) + |1\rangle\,(|\phi_2\rangle + \beta\,|\phi_4\rangle)}{\sqrt{2(1+|\beta|^2)}} \tag{4.18}$$

where β determines the measurement basis chosen by Denis and the probability that Dennis obtains $|+\rangle$ outcome is $1/2$. Thus the collapsed state is partially entangled three-qubit state. So there is non-vanishing QBER in the protocol. It is to be noted that there is a collapsed state corresponding to the measurement outcome $|-\rangle$ but the analysis is same as the present case. Now, Charlie would measure in the general basis as before resulting a collapsed state between Alice and Bob. Corresponding to the outcome $|+\rangle$, we find that the state is given by,

$$|\Psi^+_{AB}\rangle = \frac{|\phi_1\rangle + \alpha\,|\phi_2\rangle + \beta\,|\phi_3\rangle + \alpha\beta\,|1\rangle\,|\phi_4\rangle}{\sqrt{(1+|\alpha|^2)(1+|\beta|^2)}}, \tag{4.19}$$

where α is the measurement parameter of Charlie and Charlie obtains the outcome $|+\rangle$ with probability $1/2$. Now, the collapsed state between Alice and Bob involves two parameters arising from the measurement basis of Charlie and Dennis. We take these two parameters to be real. As the state is not maximally entangled there is non-vanishing QBER even in the absence of any eavesdropper. When $|\phi_1\rangle$, $|\phi_2\rangle$, $|\phi_3\rangle$ and $|\phi_4\rangle$ are four Bell states, we find the QBER of the protocol as given by,

$$Q_1 = \frac{\beta^2}{1+\beta^2} + \frac{\alpha^2}{1+\alpha^2} \tag{4.20}$$

There are two parameters in QBER which are controlled by Dennis and Charlie. The behavior of QBER with respect to the measurement parameters are displayed in Fig. 4.3. We have plotted the QBER with the parameter α, for different values of β's. From the expression of QBER, it is evident that plot with β for different α's is similar. We can see from Eq. (4.18) and Eq. (4.19) that if Dennis

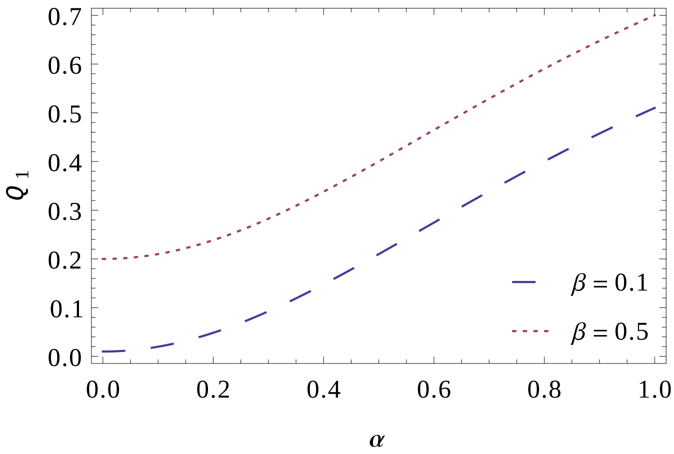

Figure 4.3: Variation of QBER with α for different β's.

and Charlie measure in the computational basis the collapsed states are three-qubit GHZ-state and Bell state respectively. Therefore, we find vanishing QBER which can be seen in the above plot. Next, we consider the second scenario, where there is one controller *e.g.* Charlie, who holds two qubits. Charlie now can use an entangled basis for the measurement. We show that for the measurement in entangled basis, the collapsed state between Alice and Bob is not a Bell state. For the resource state in Eq. (4.17), Charlie performs a joint measurement using Generalized Bell Basis (GBS), written as,

$$\begin{aligned} |\chi_m^+\rangle &= \frac{|00\rangle + m\,|11\rangle}{\sqrt{1+|m|^2}}, \quad |\chi_m^-\rangle = \frac{m^*\,|00\rangle - |11\rangle}{\sqrt{1+|m|^2}}, \\ |\zeta_m^+\rangle &= \frac{|01\rangle + m\,|10\rangle}{\sqrt{1+|m|^2}}, \quad |\zeta_m^-\rangle = \frac{m^*\,|01\rangle - |10\rangle}{\sqrt{1+|m|^2}}, \end{aligned} \tag{4.21}$$

Then, the collapsed state between Alice and Bob is given by,

$$|\Psi^{+}_{AB}\rangle = \frac{|\phi_1\rangle + m\,|\phi_4\rangle}{\sqrt{1+m^2}}, \tag{4.22}$$

corresponding to the outcome $|\chi^{+}_{m}\rangle$, which occurs with probability $1/4$. The collapsed state is partially entangled state and as before we find QBER of the protocol,

$$Q_2 = \frac{m^2}{1+m^2}, \tag{4.23}$$

where, we have considered m as real. If Charlie measures in computational basis the collapsed state is a Bell state which yields a vanishing bit error rate. We plot the QBER in this case with the parameter m in Fig. 4.4.

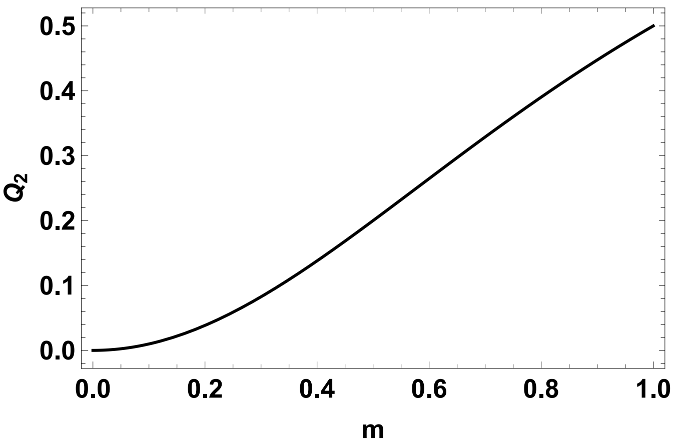

Figure 4.4: Variation of QBER with the parameter m.

4.6 Conclusion

We have considered the protocol for Co-operative QKD, where a secret key is established between two parties with the control of other parties. The advantage of this protocol is that one or more parties can supervise the secret key making, thus reducing the chance of cheating. For a given multipartite state, it is not always obvious whether this state can be used for Co-operative QKD or Co-operative teleportation. In this chapter, we have provided resource states for successful cooperative QKD, *i.e.* Co-QKD with maximal key rate. The efficiency of the protocols depends on the choice of the measurement basis by the controlling parties. We have explicitly shown the dependence of the key rate of CoQKD protocol with Charlie's choice of measurement basis. Efficiency of the protocol (key rate or fidelity) is controlled by Charlie. If he chooses a basis set wisely then the protocol can be carried out maximally, *i.e.* maximal key rate or fidelity. For arbitrary choice of basis by Charlie, the collapsed state between Alice and Bob is non-maximally entangled. We also introduce a novel protocol for QKD with the non-maximally entangled state in the same line of Ekert's protocol. Apart from CoQKD, we have shown how to generate a conference key with the resource state. It turns out that our recently introduced Bell inequalities can be used to determine the security of the conference key protocol. We have also gone beyond three-qubit scenario, and constructed suitable resource states for four-qubit states. We hope that our discussion would lead to experimental observations of these cooperative schemes.

CHAPTER 5

Measurement based quantum heat engine with coupled working medium

5.1 Introduction

For a standard heat engine working cyclically between two heat baths of temperature T_1 and T_2 ($T_2 < T_1$), efficiency of the heat engine is upper bounded by $\eta = 1 - T_2/T_1$, the Carnot efficiency [166]. Second law of thermodynamics puts this fundamental limitation on the extent of work that can be converted from heat. The laws of thermodynamics are empirical and were first adopted for classical macroscopic system. Naturally, the validity of the laws of thermodynamics are questionable and subject to verification in the quantum regime. Moreover, quantum mechanics gives the dynamical viewpoint of thermodynamics [167, 168], describing the emergence of thermodynamic laws from quantum mechanics.

The idea of quantum heat engine first appeared in a paper by Scovil and Schulz-DuBois [169], where the authors demonstrated that three level masers can be treated as a working medium for heat engines. Today, study of heat engine in quantum domain is an active area of research both due to the gradual miniaturization of current technology and its theoretical richness.

Within the quantum engines scenario, quantum analog of the classical heat engines [170, 171] and many other generalizations [172, 173, 174, 175] have been studied. Analysis of finite power quantum heat engines also have a significant amount of literature, references [176, 177, 178, 179, 180, 181, 182] to name a few. With the onset of the quantum effects, many interesting phenomena like the increase of efficiency beyond Carnot's limit [112, 183, 184] may occure. Nevertheless in reference [185], it was shown that if one accounts for the work cost to maintain the non-equilibrium reservoir, Carnot's limit can not be surprassed and hence not violating the second law of thermodynamics. Still, understanding quantum thermodynamic machines [96] and the role of quantum effects in Quantum Thermodynamics [24, 95] is far from fully understood. Where quantum effects set a limit to our ability [186] for practical purposes and where we can actually use the quantum resources are still parts of ongoing research field. The approach to resource theory of quantum thermodynamics [187] tells us about the fundamental corrections to the laws of thermodynamics setting the limit to the performance of quantum heat engines.

Previously it was shown that [114, 116] a quantum Otto engine with coupled working medium leads to a higher efficiency than that of an uncoupled one. In addiion, in Information heat engine, e.g the Szilard engine, where one can extract work from a single temperature [126, 127, 128, 133], exploiting the information, it was shown that [129, 130, 131, 132] entanglement can be used to extract work beyond the limit, which is possible using classical correlation only.

Recently, in Ref. [188], the authors have introduced a new kind of single temperature quantum heat engine without feedback control. The essential part of the engine which replaces feedback is a non-selective quantum measurement on the working medium, changing the energy of the system, and thus, enabling one to extract useful work. This engine is much like a quantum Otto cycle [189, 190, 191, 192] with one thermalization stroke being replaced by a quantum non-selective measurement, whereas in Maxwell's demon and Szilard engine [126, 127] work is extracted from a single heat reservoir using feedback control. Another version of Maxwell's demon engine was introduced in [193, 194], where without the presence of any thermal bath, work can be extracted using measurement and feedback control. So, quantum measurment plays an important role in Quantum Thermodynamics. Energetic cost for performing a measurement [195, 196, 197, 198, 199] and using the average energy change due to the measurement for extracting useful work are two important facets of Quantum Thermodynamics. In a subsequent work [200], the authors calculated the detailed fluctuation of work and heat in the measurement driven single temperature heat engine without feedback and also considered the finite power scenario. So, the next question that can be raised is whether quantum correlations play any role in this particular type of heat engine. Can we use correlations to enhance the performance of this engine? In this chapter, we analyze the role of coupled working medium [201] in the single temperature measurement driven quantum heat engine without feedback control [188]. Taking a coupled one-dimensional Heisenberg model as the working medium, we show an advantage for the efficiency over the uncoupled one. First, we start with a one-dimensional Heisenberg model of two spin-1/2 particles and then generalize that for two spin-d particles, where d can take values of 1/2, 1, and 3/2. We note that, for different choices of non-selective measurements, the efficiency of the heat engine changes. In addition, in the higher-dimensional scenario, another interesting feature is observed: we can either extract work from the engine cycle or have to invest work to run the cycle depending upon the spin configuration we choose. By judiciously choosing all the conditions, such as measurement choices, coupling constant and the dimension of the Hilbert spaces, one can optimize the engine performance, which is better than the uncoupled one in terms of efficiency.

The chapter is organized as follows. In the next section, we give a short introduction about the single temperature measurement-based heat engine as introduced in the Ref. [188]. In sections 5.3 and 5.4, we present our result for the coupled measurement based heat engine taking the working medium to be the Heisenberg model of two spin half particles. In section 5.5 we consider the higher dimensional scenario. In the next section (namely, section 5.6), we present an analysis of the global and local work, and finally we conclude in section 5.7.

5.2 Single temperature measurement driven heat engine

In this section we briefly discuss the recently introduced measurement-based single temperature quantum heat engine without feedback control [188]. It is very similar to the Otto cycle except for one isochoric branch. One thermalization step is replaced by a non-selective quantum measurement. Now, if it had been a classical system, in principle, there would be no subsequent effect of the measurement on the system. But quantum mechanical system is generally disturbed by measurement and hence average energy of the system changes. Judiciously choosing the measurement operators as discussed in [188], we can extract work form this type of engine. We will now briefly describe the parts of the engine cycle.

The working system of the heat engine has a Hamiltonian $H(\lambda)$, which is a function of an external control parameter λ. The system starts from a thermal state of temperature T. This can be achieved with the help of a heat bath of temperature T, which is the only heat bath to be used throughout the action of the engine. The system is brought to the contact with the bath and let to thermalize. After a long enough time when the system attains equilibrium thermal state, the heat bath is detached and it gets ready for the first cycle of our heat engine. So, the initial state of the system is, $\rho_{int} = e^{-\beta H(\lambda_{int})}/Z = \sum_n (e^{-\beta E_n(\lambda_{int})}/Z) |n(\lambda_{int})\rangle \langle n(\lambda_{int})|$, where, $Z = \sum_n e^{-\beta E_n(\lambda_{int})}$, while, $|n(\lambda)\rangle$ and $E_n(\lambda)$ are respectively the n^{th} eigenstate and eigenvalue of the Hamiltonian $H(\lambda)$. Now, the engine strokes are as following,

First stroke : The first stroke of the cycle is an adiabatic compression process. The working system is isolated from the heat bath and the Hamiltonian is changed quasi-statically from $H(\lambda_{int})$ to $H(\lambda_{fin})$. For a system defined by a density matrix ρ and Hamiltonian H, its internal energy or average energy is defined as $U = Tr[\rho H]$. Change in internal energy is the sum of two contributions [24], one is heat, defined as $dQ = Tr[H d\rho]$ and another is work, defined as $dW = Tr[\rho dH]$. Though, this identification of heat and work is not always valid, especially in strong system bath coupling [101, 202]. We will be considering the weak system bath coupling scenario, such that the above definition is valid. Although, during a general adiabatic process, the state of the working medium changes, for the model of engine cycle we consider in this paper, the state of the working medium does not change throughout the adiabatic stroke. Hence, in the first stroke, change in the internal energy of the system is, $W_1 = Tr[\rho_{int}(H(\lambda_{fin}) - H(\lambda_{int}))]$, which can also be written as, $W_1 = \sum_n [E_n(\lambda_{fin}) - E_n(\lambda_{int})] p_n(\lambda_{int})$, where $p_n(\lambda_{int}) = (e^{-\beta E_n(\lambda_{int})}/Z)$. If this is positive then this is the energy gained by the system. So, the average work extracted from this stroke is $-W_1$.

Second stroke : Next stroke is the most crucial and special one, which involves a non-selective measurement. A measurement [32] corresponding to an observable $\hat{G}$ can be described by a POVM, $\{G_n\}$, where, $G_n \geq 0$ are the POVM effects, $\sum_n G_n = \mathbb{1}$ and $Tr[\rho G_n]$ is the probability of getting n^{th} outcome denoted here as α_n. If in addition the POVM elements satisfy $G_m G_n = \delta_{mn} G_n$, then they are projectors and the observable $\hat{G}$ can be written as $\hat{G} = \sum_n \alpha_n G_n$ (spectral value decomposition), where α_n's are now the eigenvalues of $\hat{G}$. Equivalently, measurement can be completely described by a set of measurement operators $\{M_n\}$, with $M_n^\dagger M_n = G_n$. As mentioned in the first chapter, corresponding to a particular POVM, there exists infinite sets of measurement operators, each connected by a unitary. Now, given a set of measurement operators $\{M_n\}$, if the state of the system before the measurement is $|\phi\rangle$, then corresponding to the n^{th} outcome, the state of the system after measurement is, $\frac{M_n|\phi\rangle}{\sqrt{p_n}}$ or $\frac{M_n \rho_\phi M_n^\dagger}{p_n}$, where $\rho_\phi = |\phi\rangle\langle\phi|$ and $p_n = Tr[\rho_\phi M_n^\dagger M_n] = \langle\phi| M_n^\dagger M_n |\phi\rangle$ is the probability of getting n^{th} outcome. In a non-selective measurement i.e., if the outcomes of the measurements is not recorded, then the state after measurement is $\sum_n M_n \rho_\phi M_n^\dagger$. So, after the first stroke, we do a non-selective measurement described by the measurement operators $\{M_\alpha\}$ on the system state giving the post-measurement state as $\rho_M = \sum_\alpha M_\alpha \rho_\phi M_\alpha^\dagger$. Now, in this stroke, the Hamiltonian of the system is unchanged at $H(\lambda_{fin})$. So, the average energy change of the system is given by, $Q_M = Tr[(\rho_M - \rho_{int})H(\lambda_{fin})]$, which is a reminiscent of heat can also be written as [188],

$$\begin{aligned}
Q_M &= \sum_{m,n} [E_m(\lambda_{fin}) - E_n(\lambda_{fin})] T_{m,n} p_n(\lambda_{int}) \\
&= \sum_n \langle n(\lambda_{fin})| H_M(\lambda_{fin}) - H(\lambda_{int}) |n(\lambda_{fin})\rangle \, p_n(\lambda_{int}).
\end{aligned}$$

where, $T_{m,n} = \sum_\alpha |\langle n(\lambda_{fin})| M_\alpha |m(\lambda_{fin})\rangle|^2$, is the transition probability from a eigenstate labeled n before the measurement to an eigenstate labeled m after the measurement, and $H_M(\lambda_{fin}) = \sum_\alpha M_\alpha H(\lambda_{fin}) M_\alpha$. As shown in [188], Q_M is always positive implied by the properties of the transition matrix ; $T_{m,n} = T_{n,m}$ and $\sum_n T_{m,n} = 1$. This fact will be illustrated more explicitly in the next section. It is also noted that, whenever the Hamiltonian of the system does not commute with the measurement operators, we get a nonzero Q_M.

Third stroke : This is the second adiabatic process, which is now a quasi-static expansion. The Hamiltonian $H(\lambda_{fin})$ is very slowly changed back to the initial Hamiltonian $H(\lambda_{int})$. Like the previous adiabatic stroke, the average change in energy of the system is, $W_2 = Tr[\rho_M(H(\lambda_{int}) - H(\lambda_{fin}))]$, as the state of the system is unchanged throughout the stroke. This is nothing but $\sum_n [E_n(\lambda_{int}) - E_n(\lambda_{fin})] p_n^M$, where, $p_n^M = \langle n(\lambda_{fin})| \rho_M |n(\lambda_{fin})\rangle = \sum_m p_m(\lambda_{int}) T_{m,n}$ is the probability of finding the n^{th} eigenstate of $H(\lambda_{fin})$ in ρ_M. So, the work extracted form this adiabatic stroke is $-W_2$, which follows from the similar argument given in the description of the first stroke.

Fourth stroke : In this last stroke of the cycle, the system is brought into contact with the heat bath of temperature T, while keeping the Hamiltonian fixed at $H(\lambda_{int})$ and allowed to thermalize, until it goes back to the initial thermal state ρ_{int}. So, heat transfer for this stroke is given by, $Q_T = Tr[(\rho_{int} - \rho_M)H(\lambda_{int})]$, as the Hamiltonian is fixed in this stroke. This can be written as,

$Q_T = \sum_n E_n(\lambda_{int})[p_n(\lambda_{int}) - p_n^M]$ and shown to be negative in [188]. This means that heat is going to the heat bath from the working medium at this stage.

The signs of each of these quantities e.g. W_1, Q_M, W_2, and Q_T will be analyzed explicitly in the next section in the case of coupled working medium. So, the whole cycle is like energy Q_M is taken by the system, doing a work $-(W_1 + W_2)$ and dumping energy Q_T to a heat bath. So, we have $Q_M + Q_T = -(W_1 + W_2)$, correctly depicting the first law of thermodynamics, i.e energy conservation. Efficiency of the heat engine is given as the ratio of extracted work $-(W_1+W_2)$ over the average energy change Q_M in the measurement stroke $\eta = \frac{-(W_1+W_2)}{Q_M}$. Authors in the Ref. [188] showed that the extracted work $-(W_1 + W_2)$ is always positive, relying on the fact that work strokes are either adiabatic expansion or compression of the working medium. But we will see in the next section that for a coupled working medium their way of reasoning does not hold good and there can be instances where $-(W_1 + W_2)$ is negative.

5.3 Coupled single temperature measurement engine

In this section we will present an analysis of a coupled measurement-based single temperature heat engine. We consider the working medium of the system to be a one dimensional Heisenberg model of two particles with the following Hamiltonian,

$$H = 8J\vec{S_A}.\vec{S_B} + 2B(S_A^z + S_B^z). \tag{5.1}$$

For two spin half particles, $\vec{S_A} = \vec{S_B} = \frac{1}{2}\vec{\sigma}$, where $\vec{\sigma} = (\sigma_x, \sigma_y, \sigma_z)$ are the Pauli matrices. So, in this case, we can write the Hamiltonian as,

$$H = 2J({\sigma_x}^A \otimes {\sigma_x}^B + {\sigma_y}^A \otimes {\sigma_y}^B + {\sigma_z}^A \otimes {\sigma_z}^B) + B({\sigma_z}^A + {\sigma_z}^B), \tag{5.2}$$

where, J is the coupling constant and B is the external magnetic field. The entanglement between two qubits for this model has been studied in [203]. $J > 0$ and $J < 0$ cases correspond to the anti-ferromagnetic and ferromagnetic interactions respectively. In this paper, we will be restricting ourselves to the anti-ferromagnetic case only. Eigenvalues and eigenstates of this Hamiltonian are listed in Table 5.1, where, $|0\rangle \doteq \begin{pmatrix} 1 \\ 0 \end{pmatrix}$ and $|1\rangle \doteq \begin{pmatrix} 0 \\ 1 \end{pmatrix}$ are the eigenstates of σ_z. First, we will be considering only qubit case, next d-dimensional cases will be considered. As described before, engine cycle of the measurement based heat engine has four steps. First stroke of the cycle is an adiabatic compression, where the Hamiltonian of the working system, as described above, is quasi-statically changed from an initial parameter value to a final parameter value. External magnetic field B is the parameter of the Hamiltonian here. It is changed quasi-statically from the initial value B_1 to the final value B_2. As this process is done adiabatically, the state of the system remains in its instantaneous eigenstate. At the beginning of the cycle, we take the working medium of the heat engine to be in a thermal equilibrium state of temperature T. Thus here, $\rho_{int} = \sum_{n=1}^{4} P_n \left|n(B,J)\right\rangle \left\langle n(B,J)\right|$, where, $P_n = \exp(-E_n/k_BT)/Z$, $Z = \sum_n \exp(-E_n/k_BT)$, E_n's and corresponding $\left|n(B,J)\right\rangle$ are given in Table 5.1. Then in the second stroke of the cycle, the Hamiltonian of the system is kept unaltered

Eigenvalues	Eigenstates
$2J + 2B = E_4$	$\|00\rangle = \|4(B,J)\rangle$
$2J = E_3$	$\sqrt{\frac{1}{2}}(\|10\rangle + \|01\rangle) = \|3(B,J)\rangle$
$2J - 2B = E_2$	$\|11\rangle = \|2(B,J)\rangle$
$-6J = E_1$	$\sqrt{\frac{1}{2}}(\|10\rangle - \|01\rangle) = \|1(B,J)\rangle$

Table 5.1: $S_A = 1/2$,$S_B = 1/2$.

but a measurement of an observable is performed on the system. As, already discussed earlier, the observable has to be non-commutative with the Hamiltonian to get a positive work output. In this case we have a distributed system and we will see that the efficiency of the heat engine will depend on the local measurements we are performing. Detail discussion will follow. Third stroke is again an adiabatic process changing the external magnetic field B_2 back to B_1. The final stage of the cycle is a thermalization step and in this stage the system is brought to contact with a heat bath of the starting temperature T and let the system thermalize for a sufficiently long time, after which it again goes back to the initial thermal equilibrium state. Now, as mentioned before, the initial state of the system is a thermal state of temperature T,

$$\rho_{int} = \sum_{n=1}^{4} P_n \left|n(B,J)\right\rangle \left\langle n(B,J)\right|, \tag{5.3}$$

where, $P_n = \exp(E_n/k_BT)/Z$, $Z = \sum_n \exp(E_n/k_BT)$, E_n and $\left|n(B,J)\right\rangle$'s are the energy eigenvalues and eigenstates respectively as listed in the Table 5.1. From now on, we will be taking $k_BT = 1$ throughout the paper. The energy eigenvalues and hence the probabilities P_n depend on the changing parameter which is external magnetic field B, but the eigenstates are independent of the parameter. So, we will be writing the probabilities and the energy eigenvalues as a function of the parameter B, like $E_n(B)$ and $P_n(B)$. Now, let us do the quantitative analysis of each stroke of the cycle. As discussed in the previous section, the average work in the first adiabatic stroke is

$$W_1 = \sum_n [E_n(B_2) - E_n(B_1)]P_n(B_1), \tag{5.4}$$

as the state remains in its instantaneous eigenstate with same probability. For the system we considered and the initial thermal state of the system, we have,

$$W_1 = \frac{2(B_1 - B_2)(-1 + e^{4B_1})}{1 + e^{2B_1}(1 + e^{2B_1} + e^{8J})}. \tag{5.5}$$

Next comes the most important part of the engine cycle, which is the measurement part. We can choose any arbitrary observable for measurement with only constraint that the observable must be non-commuting with the Hamiltonian. For the time being we restrict ourselves to projective measurements. In our case, for coupled measurement based heat engine, we take most general Von Neumann measurement operators as,

$$M_1 = |+^a\rangle\langle+^a| \otimes |+^b\rangle\langle+^b| \tag{5.6}$$

$$M_2 = |+^a\rangle\langle+^a| \otimes |-^b\rangle\langle-^b| \tag{5.7}$$

$$M_3 = |-^a\rangle\langle-^a| \otimes |+^b\rangle\langle+^b| \tag{5.8}$$

$$M_4 = |-^a\rangle\langle-^a| \otimes |-^b\rangle\langle-^b|, \tag{5.9}$$

where, $|+^a\rangle\langle+^a|$ and $|-^a\rangle\langle-^a|$ are the eigenstate projectors for the observable $\vec{\sigma}.\hat{a}$ for one party and $|+^b\rangle\langle+^b|$ and $|-^b\rangle\langle-^b|$ are the eigenstate projectors for the observable $\vec{\sigma}.\hat{b}$ for the other. Now if the initial state of the working medium is given by Eq. (5.3), then for a non-selective measurement given by the above measurement operators, the post measurement state will be,

$$\rho_M = \sum_{k=1}^{4} M_k \rho_{int} M_k. \tag{5.10}$$

Now, the transition probability is given by,

$$T_{m,n} = \sum_k |\langle\psi_m| M_k |\psi_n\rangle|^2 \ \ \forall m, n \in \{1, 2, 3, 4\}, \tag{5.11}$$

where, $|\psi_m\rangle$ and $|\psi_n\rangle$ denote the eigenstates of the Hamiltonian as written in the Table 5.1 and M_k's are the measurement operators written above. The average energy change of the system during this measurement is,

$$Q_M = \sum_{m,n} [E_n(B_2) - E_m(B_1)] T_{m,n} P_m(B_1). \tag{5.12}$$

Now, for the most general form of the measurement operators, the expressions will be quite complicated. So, we will write the expressions for some special measurements. First case will be when $\vec{\sigma}.\hat{a}$ is σ_x and $\vec{\sigma}.\hat{b}$ is σ_z. For this case,

$$Q_M = \frac{B_2(-1 + e^{4B_1}) - 2[1 + e^{2B_1}(1 + e^{2B_1} - 3e^{8J})]J}{1 + e^{2B_1}(1 + e^{2B_1} + e^{8J})}. \tag{5.13}$$

For $\vec{\sigma}.\hat{a} = \sigma_y$ and $\vec{\sigma}.\hat{b} = \sigma_z$, the expression for the average change in energy remains the same. Another case is when $\vec{\sigma}.\hat{a} = \sigma_x$ and $\vec{\sigma}.\hat{b} = \sigma_y$. In this scenario,

$$Q_M = \frac{2B_2(-1 + e^{4B_1}) - 2[1 + e^{2B_1}(1 + e^{2B_1} - 3e^{8J})]J}{1 + e^{2B_1}(1 + e^{2B_1} + e^{8J})}. \tag{5.14}$$

There are many other different choices of measurement operators, like both are measuring σ_x or σ_y or σ_z etc. In each case, the expression for Q_M will change accordingly. This average energy change is like heat in the conventional quantum heat engine. Now, the third step of the cycle is again a adiabatic process, where the magnetic field B_2 is changed back into B_1 very slowly. For this part of the cycle, the work done is,

$$W_2 = \sum_n [E_n(B_1) - E_n(B_2)] P'_n, \tag{5.15}$$

where $P'_n = \langle\psi_n| \rho_{PM} |\psi_n\rangle = \sum_m T_{m,n} P_m(B_1)$ is the probability of getting n^{th} eigenstate in the post measurement state. When, $\vec{\sigma}.\hat{a} = \sigma_x$ and $\vec{\sigma}.\hat{b} = \sigma_z$, the expression of this work for our system is,

$$W_2 = \frac{(B_1 - B_2)(1 - e^{4B_1})}{1 + e^{2B_1}(1 + e^{2B_1} + e^{8J})}. \tag{5.16}$$

Last step of the cycle is to bring the system in contact with the heat bath of temperature T and let it thermalize back to the initial thermal state ρ_{int}. Heat exchanged in this step is given by,

$$Q_T = \sum_n E_n(B_1)(P_n(B_1) - P'_n). \tag{5.17}$$

Again, for, $\vec{\sigma}.\hat{a} = \sigma_x$ and $\vec{\sigma}.\hat{b} = \sigma_z$, heat dumped into the heat bath in this last step is,

$$Q_T = -6J + \frac{B_1(1 - e^{4B_1}) + 8(1 + e^{2B_1} + e^{4B_1})J}{1 + e^{2B_1}(1 + e^{2B_1} + e^{8J})}. \tag{5.18}$$

So, as discussed in the previous section, the total work that can be obtained from the cycle is given by the sum of the works that can be extracted in the first and third strokes. For $\vec{\sigma}.\hat{a} = \sigma_x$ and $\vec{\sigma}.\hat{b} = \sigma_z$, total extracted work is given by,

$$W_t = -W = -(W_1 + W_2) = \frac{(B_1 - B_2)(1 - e^{4B_1})}{1 + e^{2B_1}(1 + e^{2B_1} + e^{8J})}. \tag{5.19}$$

The quantities we have calculated so far are global (from the perspective of two systems together), i.e., global heat or global work or global energy change. In the next section we will discuss the global efficiency of the heat engine. Also, the measurements we chose are all projective measurements. We investigated some cases of POVM, namely the SIC POVM [204], and some other examples. But in all the cases, we found that projective measurements are more effective so far as the efficiency is concerned. So, we will be restricting ourselves with projective measurements only. A point to note that, we have not optimized the engine over different projective measurements. We have chosen some particular measurement settings and compared the coupled and uncoupled scenarios.

5.4 Efficiency of the heat engine, Global analysis

Now, we will evaluate the efficiency of the measurement based coupled heat engine and compare it with the uncoupled one. Before doing that, it is necessary to determine the signs of the quantities Q_M (Eq. (5.12)), Q_T (Eq. (5.17)), W_1 (Eq. (5.4)) and W_2 (Eq. (5.15)) for this coupled working medium. The average energy change Q_M of the system during this measurement, given in Eq.(5.20) can also be written as [188],

$$Q_M = \frac{1}{2}\sum_{m,n}[E_n(B_2) - E_m(B_1)]T_{m,n}(P_m(B_1) - P_n(B_1)). \tag{5.20}$$

This is obtained by employing the properties of the transition matrix $T_{m,n}$: $T_{m,n} = T_{n,m}$ and $\sum_m T_{m,n} = 1$. From the fact that $T_{m,n} \geq 0$ and the equilibrium occupation probability P_n for an energy level E_n decreases with the increase of energy E_n, it turns out that $Q_M \geq 0$. That means, in the measurement step, heat enters into the working medium. Similarly, the expression for Q_T given in Eq. (5.17) can be written as,

$$Q_T = \frac{1}{2}\sum_{n,m}(E_n(B_1) - E_m(B_1))T_{m,n}(P_n(B_1) - P_m(B_1)). \tag{5.21}$$

By the similar arguments made for Q_M, it is evident that $Q_T \leq 0$, which means that, heat goes from the working medium to the heat bath of temperature T at the last step of the cycle. Now to determine the signs of W_1 and W_2, let's first write down the alternative expression for the work done as was done in Ref. [188].

$$W = -W_t = \frac{1}{2}\sum_{n,m}(\Delta^f_{m,n} - \Delta^i_{m,n})T_{m,n}[P_m(B_1) - P_n(B_1)], \tag{5.22}$$

where, $\Delta^\alpha_{m,n}$ denotes the difference between the m-th and n-th energy eigenvalues and is given by, $\Delta^\alpha_{m,n} \equiv E_m(\lambda_\alpha) - E_n(\lambda_\alpha)$, for $\alpha = i, f$, $\lambda_i = B_1$ and $\lambda_f = B_2$. In Ref. [188], authors designed the adiabatic strokes to be compression and expansion, in the sense that spacing between the energy levels of the Hamiltonian either increases or decreases. Then they argued that for the compression stroke, $\Delta^f_{m,n} \geq \Delta^i_{m,n}$ and as the canonical probability decreases monotonically with the increase of energy, for $\Delta^i_{m,n} > 0$, $P_m(B_1) - P_n(B_1)$ is negative. Together with the fact that $T_{m,n}$ is positive, we have every term of the above expression of W as non-positive and hence the total work extracted $W_t = -W$ is always positive and similarly for the expansion stroke. But for a coupled working medium this argument does not hold good. In the presence of coupling J, the uniform increase or decrease of spacing between the energy levels does not happen. For example, for the two spin-1/2 scenario, the energy eigenvalues are $-6J$, $2J - 2B$, $2J$, $2J + 2B$, which are ordered from low to high for $J > 0$. Throughout the paper we are considering the anti-ferromagnetic case i.e. $J > 0$, as stated earlier. Now energy difference between lowest two energy levels is $8J - 2B$ and highest two energy levels is $2B$. So, for a fixed J, with increasing B, spacing between lowest two energy levels decreases, where, spacing between highest two energy level increases. So, as a whole, we can not say that the adiabatic stroke is compression or expansion for the working medium and consequently the line of reasoning like in Ref. [188] does not hold. We simply say that the work strokes are the first and second adiabatic work strokes.

So whether the extracted work will be positive or negative would depend upon the structure of the energy levels of the Hamiltonian. Let's illustrate this taking the working medium to be a two spin-1/2 system. In Eq. (5.22), some terms are negative and some terms are positive. Sign of the total work

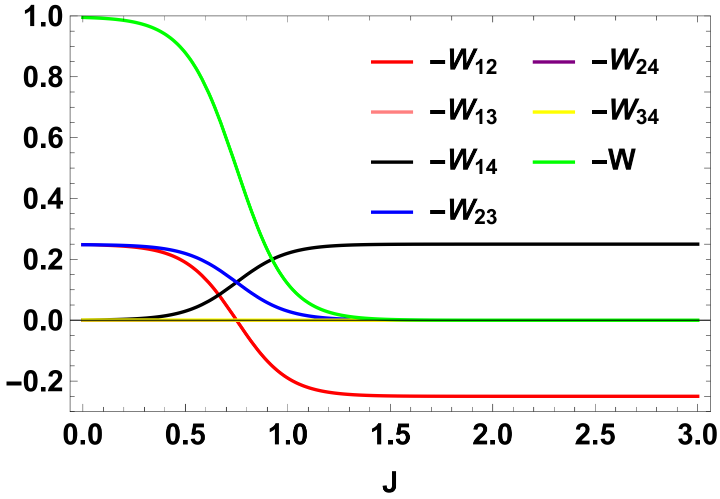

Figure 5.1: (Color online) Work contributions ($-W_{mn}$) and total extracted work ($-W$) vs J plot for $B_2 > B_1$, with $B_2 = 4$, $B_1 = 3$.

will depend upon the positive and negative contributions of these terms. We denote each term of the expression as $W_{mn} = \frac{1}{2}(\Delta^f_{m,n} - \Delta^i_{m,n})T_{m,n}[P_m(B_1) - P_n(B_1)]$ and note that $W_{mn} = W_{nm}$. We have plotted different terms with the coupling constant J in Fig. 5.1. We notice that, $-W_{12}$ ($-W_{21}$) gives negative contributions, $-W_{14}$ ($-W_{41}$), $-W_{23}$ ($-W_{32}$) give positive contributions and other terms are zero. Consequently, the total work output is positive. We also plot the contributions for first and second adiabatic work strokes in Fig. 5.2 and notice that, the contribution of the first work stroke is positive, whereas contribution of the second work stroke is negative but their sum is positive and hence we extract a positive work. Now, the above plots have been generated for the case $B_2 > B_1$ and we got the extracted work W_t to be positive. So, the next question is what happens for the other scenario, i.e., when $B_2 < B_1$. It is important to note that, arguments behind $Q_M \geq 0$ and $Q_T \leq 0$ are independent of the choice of initial and final magnetic field B_1 and B_2 respectively. And indeed

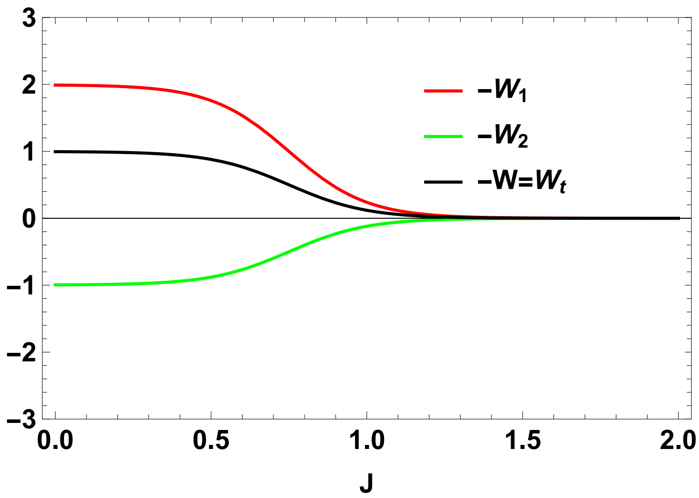

Figure 5.2: (Color online) $-W_1$, $-W_2$ and W_t vs J plot for $B_2 > B_1$, with $B_2 = 4$, $B_1 = 3$. W_t is postive for two spin-$1/2$ particles.

for both $B_2 > B_1$ and $B_2 < B_1$, Q_M is always positive and Q_T is always negative. It is the extracted work W_t, whose sign depends upon B_1 and B_2. From the Eq.(5.19), it is evident that, when $B_2 > B_1$, we extract positive work i.e $W_t \geq 0$ and when $B_2 < B_1$, extracted work is negative for all J. This can be seen from the Fig. 5.2. This plot shows that when the values of B_1 and B_2 are interchanged,

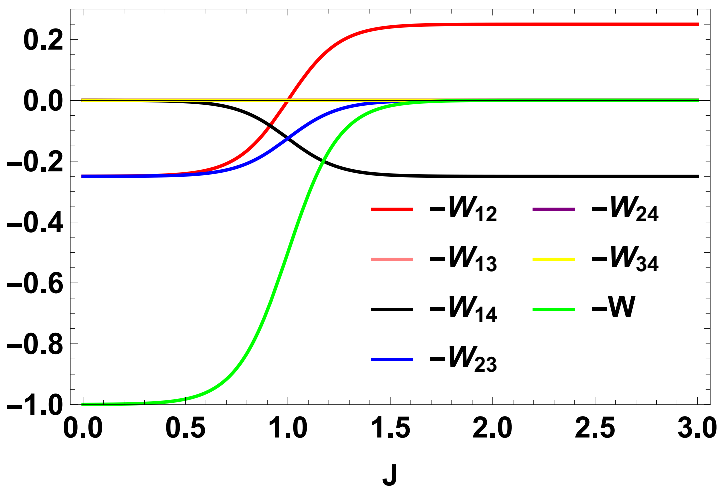

Figure 5.3: (Color online) Work contributions ($-W_{mn}$) and total extracted work ($-W$) vs J plot for $B_2 < B_1$, with $B_2 = 3$, $B_1 = 4$.

i.e., $B_1 = 4$ and $B_2 = 3$, the nature of the plots are just opposite to each other. From the definition of efficiency as the ratio of total extracted work (W_t) over Q_M: $\eta = W_t/Q_M$, it is evident that efficiency can be negative only if the extracted work W_t is negative, which means that we can not extract work from the engine but have to do work to run it. We have seen that for $B_2 > B_1$, the extracted work is positive. For the rest of the analysis we will stick to this scenario. From the expressions derived above, we can have different efficiencies depending upon the measurement choices. When $\vec{\sigma}.\hat{a}$ is σ_z and $\vec{\sigma}.\hat{b}$ is σ_x, we have,

$$\eta = \frac{(B_1 - B_2)(1 - e^{4B_1})}{B_2(-1 + e^{4B_1}) - 2[1 + e^{2B_1}(1 + e^{2B_1} - 3e^{8J})]J}. \tag{5.23}$$

Thus the efficiency depends upon the coupling constant J, where, $J = 0$ corresponds to the uncoupled scenario with efficiency $(1 - \frac{B_1}{B_2})$. As J increases, for a certain range of J, efficiency is also increased over the uncoupled value. Expression for the efficiency remains same as in Eq. (5.23) for $\vec{\sigma}.\hat{a} = \sigma_y$ and $\vec{\sigma}.\hat{b} = \sigma_z$, For, $\vec{\sigma}.\hat{a} = \sigma_x$ and $\vec{\sigma}.\hat{b} = \sigma_y$,

$$\eta = \frac{(B_1 - B_2)(1 - e^{4B_1})}{B_2(-1 + e^{4B_1}) - [1 + e^{2B_1}(1 + e^{2B_1} - 3e^{8J})]J}. \tag{5.24}$$

Now, let us examine those cases when same observables are being measured on both sides, like $\vec{\sigma}.\hat{a} = \vec{\sigma}.\hat{b} = \sigma_z$ or σ_x or σ_y. When both the observables are σ_x, we have,

$$\eta = \frac{(B_1 - B_2)(-1 + e^{4B_1})}{B_2(1 - e^{4B_1}) + (1 + e^{4B_1} - 2e^{2B_1+8J})J}. \tag{5.25}$$

Exactly the same expression is obtained when both the observables are σ_y. When both the observables are σ_z, the work contributions from two adiabatic branches are equal and opposite to each other. Consequently, the total work done is zero and hence the efficiency is zero. After calculating the efficiency for different measurement choices, we plot them in Fig. 5.4 together with, $B_1 = 3$ and $B_2 = 4$. Next, we are plotting the efficiency for a fixed observable σ_z on one side and varying the parameters for the observable on the other side. We can write, $\vec{\sigma}.\hat{m} = \sin\theta\cos\phi\sigma_x + \sin\theta\sin\phi\sigma_y + \cos\theta\sigma_z$. In this case we calculate the efficiency and it turns out to be independent of the parameter ϕ but depends on θ. From the 3-d plot in Fig. 5.5 it is clear that when θ is $\pi/2$, the efficiency is optimum and it is exactly equal to the case where σ_x is measured for one spin and σ_z is measured for the other. Our results show that using non-zero coupling J, we can actually get an advantage over the no-coupling scenario. We have argued that, for $B_2 > B_1$ the extracted work is positive and hence we get a positive efficiency. Now we will show that for any B_1, B_2 $(B_1, B_2 > 0)$ with $B_2 > B_1$, the efficiency of the coupled engine can be greater than that of an uncoupled one, for a certain range of J. To show this

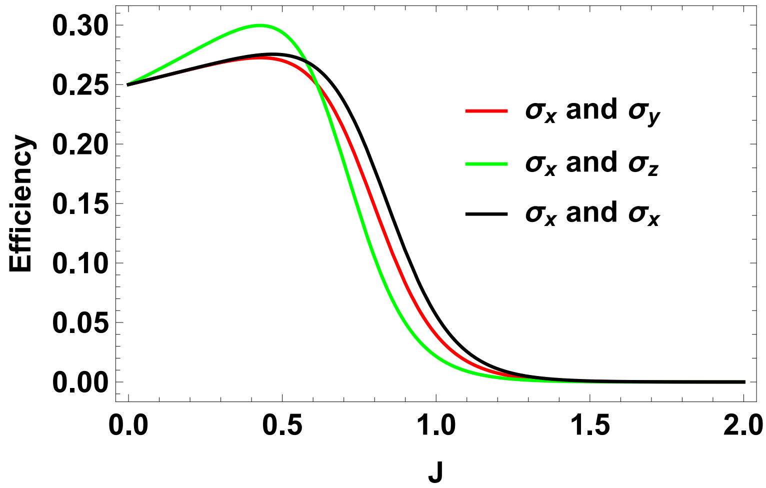

Figure 5.4: (Color online) Efficiency vs J plot for different measurement choices for two spin-$1/2$ particles.

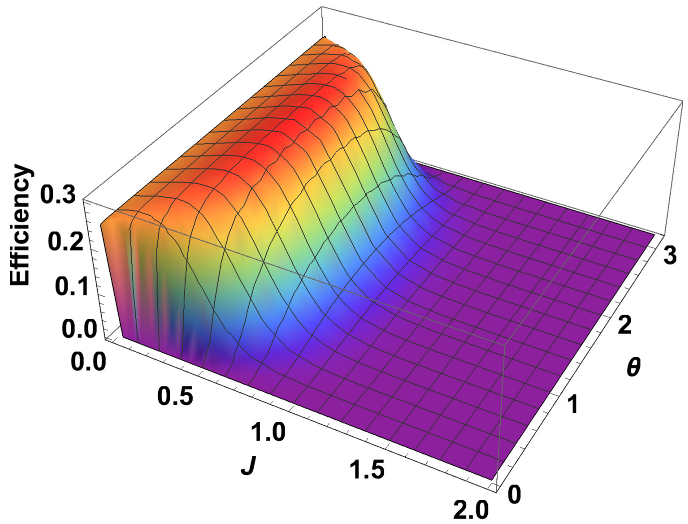

Figure 5.5: (Color online) Efficiency vs J plot for σ_z on one side and arbitrary observable (depends upon θ) on other side.

we rewrite Eq. (5.23) as,

$$\eta = \left(1 - \frac{B_1}{B_2}\right)\left[\frac{(-1+e^{4B_1})}{(-1+e^{4B_1}) - 2B_2[1+e^{2B_1}(1+e^{2B_1}-3e^{8J})]J}\right]. \tag{5.26}$$

As already mentioned, $\left(1 - \frac{B_1}{B_2}\right)$ is the efficiency of an uncoupled ($J = 0$) engine. From the above expression it turns out that the efficiency will be greater than that of the uncoupled one if $2B_2[1 + e^{2B_1}(1 + e^{2B_1} - 3e^{8J})]J > 0$. This implies that,

$$e^{2B_1}(3e^{8J} - e^{2B_1} - 1) < 1. \tag{5.27}$$

From this inequality, it is evident that for any $B_1 > 0$ (B_2 can have any value greater than B_1), we always get a positive value for J, below which we get an advantage for the efficiency over the uncoupled one. To give an example, let's consider a small value of B_1, e.g. $B_1 = 0.1$. When $B_1 = 0.1$, we have to find the value of J for which the above inequality holds. Solving the Eq. (5.27) for $B_1 = 0.1$, one can show that when $J < 0.00166$ approximately, the efficiency will be greater than that for the uncoupled one. For $B_1 = 0.1$, and $B_2 = 4$, the uncoupled efficiency is 0.975. Let's take $J = 0.0014$. For that we have $\eta = 0.975011$ for the same values of B_1 and B_2. So, the coupled engine is still more efficient but it is in such a small region that can not be seen from the plot unless the plot has a very fine scaling. With the increase in the value of B_1 , the cutoff value of J, above which the coupled engine is more efficient increases and less the value of the ratio of B_1 over B_2, more is the efficiency of the engine. For the uncoupled efficiency more and more close to one, the region in which there is an advantage of the coupled engine will be more and more narrow. But, in principle, we always have the coupled engine as the more efficient one, compared to the uncoupled one. Now, the entanglement of formation for the initial thermal state ρ_{int} is given by [203],

$$E_f = -\Big(\frac{1+\sqrt{1-C^2}}{2}\Big)\log_2\Big(\frac{1+\sqrt{1-C^2}}{2}\Big) - \Big(\frac{1-\sqrt{1-C^2}}{2}\Big)\log_2\Big(\frac{1-\sqrt{1-C^2}}{2}\Big), \quad (5.28)$$

where, C is the concurrence given by,

$$C = 0, \qquad \text{if, } e^{8J/k_BT} \leq 3,$$
$$C = \frac{e^{8J/k_BT} - 3}{1 + e^{-2B/k_BT} + e^{2B/k_BT} + e^{8J/k_BT}}, \quad \text{if, } e^{8J/k_BT} > 3.$$

The above relations imply that whenever, $J \leq (k_BT/3)\log_e 3$, Concurrence C (and thereby E_f) vanishes. Also, E_f is a monotonically increasing function of Concurrence. So, one can use Concurrence as a measure of entanglement for the simplification of analysis. Whenever $J \geq (k_BT/3)\log_e 3$, the thermal state has a non-zero entanglement. In the following we have plotted Concurrence and Efficiency vs J in Fig. 5.6. Though the efficiency and the entanglement is not monotonically related, the coupled engine is delivering more efficiency than an uncoupled one due to the correlation present in the working medium. We can have the expressions for C as mentioned above when $e^{8J/k_BT} \geq 3$, which implies $J \geq 0.137$ approximately, setting $k_BT = 1$ as before. In the plot we started the range of J from 0.15. For two spin-1/2 case J it is like another parameter but this parameter is closely

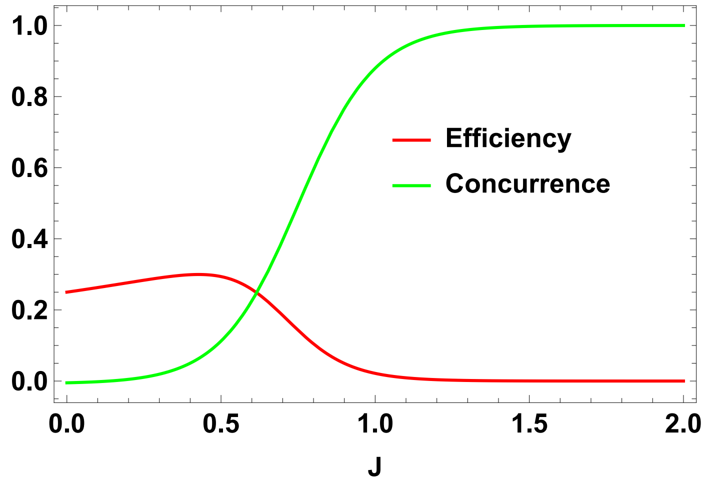

Figure 5.6: Concurrence and Efficiency vs J plot for two spin-$1/2$ particles.

connected to the entanglement of the state. In this respect, it is like the Otto cycle considered in [114, 116], where coupled working medium harnesses more efficiency than that of an uncoupled one. Also, from Fig. 5.4, it is evident that different measurement choices give different efficiencies for the heat engine. Here, choosing σ_x and σ_z or σ_y and σ_z as measurement operators, we get the maximum efficiency. So, judiciously choosing measurement operators is important for optimum performance of the heat engine.

5.5 Higher Dimensional Case

In this section we are interested in the higher dimensional Heisenberg model as considered in [116], where one spin half particle is coupled to a spin s particle. It will be interesting to observe the effect of higher spin as an additional parameter along with the coupling constant. We have the following Hamiltonian,

$$H = 8J\vec{S_A}.\vec{S_B} + 2B(S_A^z + S_B^z), \tag{5.29}$$

where, $\vec{S_A} = (S_A^x, S_A^y, S_A^z)$ and $\vec{S_B} = (S_B^x, S_B^y, S_B^z)$ are two spin operators, J is coupling constant and B is the external magnetic field. Two spin-$1/2$ case has already been discussed. Now, detailed calculation will be carried out for $S_{A/B} = 1$ and $S_{A/B} = 3/2$. One can obviously go on to calculate the cases for 2 and $5/2$ and so on, but the essential points can be observed by studying the following cases : $S_{A/B} = 1$ and $S_{A/B} = 3/2$. We first start with a spin-$1/2$ and a spin-1 operator, which is an asymmetric case in the sense that the spins on two sides are different. We will call it symmetric when two spins at two sides are same. We will deal the different cases one by one. We start with the asymmetric cases.

5.5.1 Asymmetric case

First we take $S_A = 1/2$ and $S_B = 1$. Spin operators for spin-$1/2$ particle are $\frac{1}{2}\vec{\sigma}$, where $\vec{\sigma} = (\sigma_x, \sigma_y, \sigma_z)$ are the Pauli matrices. These spin operators for spin-$1/2$ particle form the fundamental irreducible representation of $SU(2)$. Spin operators for the spin 1 particle are the three dimensional irreducible representation of $SU(2)$. These are listed as following,

$$S^x = \frac{1}{\sqrt{2}}\begin{pmatrix} 0 & 1 & 0 \\ 1 & 0 & 1 \\ 0 & 1 & 0 \end{pmatrix}, S^y = \frac{1}{\sqrt{2}}\begin{pmatrix} 0 & -i & 0 \\ i & 0 & -i \\ 0 & i & 0 \end{pmatrix} S^z = \frac{1}{\sqrt{2}}\begin{pmatrix} 1 & 0 & 0 \\ 0 & 0 & 0 \\ 0 & 0 & -1 \end{pmatrix}$$

With these spin matrices, the Eigenvalues and the eigenstates of the Hamiltonian given in Eq. (5.29) are listed in Table 5.2, where, $|0_A\rangle \doteq \begin{pmatrix} 1 \\ 0 \end{pmatrix}$, $|1_A\rangle \doteq \begin{pmatrix} 0 \\ 1 \end{pmatrix}$, $|0_B\rangle \doteq \begin{pmatrix} 1 \\ 0 \\ 0 \end{pmatrix}$, $|1_B\rangle \doteq \begin{pmatrix} 0 \\ 1 \\ 0 \end{pmatrix}$ and

Eigenvalues	Eigenstates
$-B - 8J = E_1$	$-\sqrt{\frac{2}{3}}\,\|0_A 2_B\rangle + \sqrt{\frac{1}{3}}\,\|1_A 1_B\rangle = \|\psi_1\rangle$
$B - 8J = E_2$	$-\sqrt{\frac{1}{3}}\,\|0_A 1_B\rangle + \sqrt{\frac{2}{3}}\,\|1_A 0_B\rangle = \|\psi_2\rangle$
$-3B + 4J = E_3$	$\|1_A 2_B\rangle = \|\psi_3\rangle$
$-B + 4J = E_4$	$\sqrt{\frac{1}{3}}\,\|0_A 2_B\rangle + \sqrt{\frac{2}{3}}\,\|1_A 1_B\rangle = \|\psi_4\rangle$
$B + 4J = E_5$	$\sqrt{\frac{2}{3}}\,\|0_A 1_B\rangle + \sqrt{\frac{1}{3}}\,\|1_A 0_B\rangle = \|\psi_5\rangle$
$3B + 4J = E_6$	$\|0_A 0_B\rangle = \|\psi_6\rangle$

Table 5.2: $S_A = 1/2$,$S_B = 1$

$|2_B\rangle \doteq \begin{pmatrix} 0 \\ 0 \\ 1 \end{pmatrix}$, are a set of basis vectors for the two and three dimensional Hilbert spaces respectively and they are the eigenstates of S^z operator both for A and B side. Like in the previous cases, for the measurement step of the engine cycle, we have a number of choices for the measurement operators and we explored those options in the previous sections for the case of two spin-$1/2$ particles. Now, for brevity, we will be considering one particular measurement setup and observe the effect of higher spin, such that this spin can also be a controlling parameter for the efficiency. We choose the following set of measurement operators,

$$
\begin{aligned}
M_1 &= |0_A^x\rangle\langle 0_A^x| \otimes |0_B\rangle\langle 0_B|, M_2 = |0_A^x\rangle\langle 0_A^x| \otimes |1_B\rangle\langle 1_B| \\
M_3 &= |0_A^x\rangle\langle 0_A^x| \otimes |2_B\rangle\langle 2_B|, M_4 = |1_A^x\rangle\langle 1_A^x| \otimes |0_B\rangle\langle 0_B| \\
M_5 &= |1_A^x\rangle\langle 1_A^x| \otimes |1_B\rangle\langle 1_B|, M_6 = |1_A^x\rangle\langle 1_A^x| \otimes |2_B\rangle\langle 2_B|,
\end{aligned}
$$

where, $|0_A^x\rangle = \sqrt{1/2}[|0\rangle + |1\rangle]$ and $|1_A^x\rangle = \sqrt{1/2}[|0\rangle - |1\rangle]$ are the eigenstates of the operator S^x for the spin-half particle A. In other words, we are doing measurement of the operator S^x on side A for the spin-$1/2$ and measurement of the operator S^z on the side B for spin-1. In the plots (see Fig. 5.7, 5.8, 5.9) we compared different scenarios for the same measurement settings on the two sides. By same measurement settings we mean that on the spin half side the measurement operators will be the projectors constructed from the eigenstates of the operator S^x and on the higher spin side, it will be the projectors of the eigenstates of S^z. For the above measurement operators, we calculate the quantities like work, heat (during measurement process and thermalization step) and evaluate the efficiency of the heat engine. The expression for the total work extracted for this case is,

$$
W_t = -W = \frac{(B_2-B_1)(-1+e^{2B_1})(3+e^{2B1}(4+3e^{2B1}-e^{12J}))}{3(1+e^{2B1})(1+e^{4B1}+e^{2(B_1+6J)})} \tag{5.30}
$$

From the expression above, one can see that only $B_2 > B_1$ will not guarantee the positivity of W_t for all J, unlike the previous case of two spin-$1/2$ particles. Specifically, the work extracted is negative when $4 + 3e^{2B1} - e^{12J} < 0$. This was not the case for two spin-$1/2$ particles, where expression of the extracted work was such that $B_2 > B_1$ always gives positive extracted work and $B_1 > B_2$ gives negative extracted work. But in the present case, for $B_2 > B_1$, extracted work can be negative and for $B_1 > B_2$, extracted work can be positive when, $4 + 3e^{2B1} - e^{12J} < 0$. As we will see further that this is special for the asymmetric cases only. We first plot the efficiency and compare it with the spin half scenario for $B_2 > B_1$, with same values of magnetic fields previously considered, i.e, $B_1 = 3$ and $B_2 = 4$. We note that (Fig. 5.7) the efficiency for the spin-1 scenario can be higher than that of spin half scenario for some range of non-zero values of J. For the uncoupled case, both the engines give same efficiencies, which is $1 - \frac{B_1}{B_2}$. Another point to note is that the efficiency can go to negative for the spin 1 scenario. As discussed earlier, the negative efficiency comes entirely from the negative extracted work, because Q_M is always positive also shown in the plots. Now, one can further

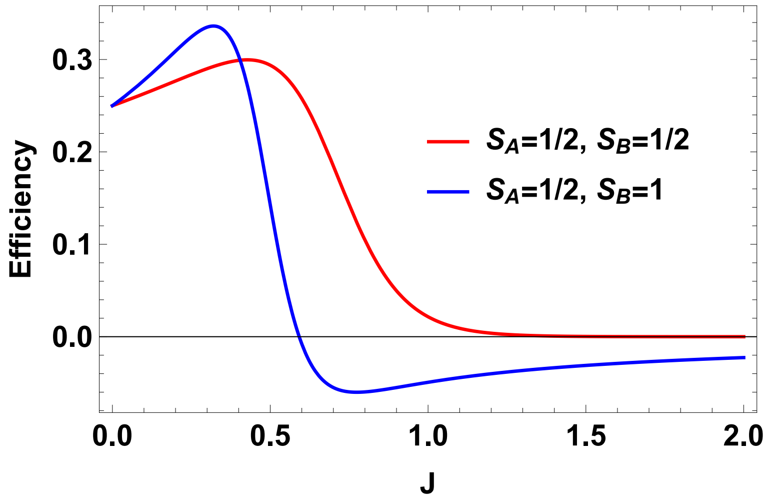

Figure 5.7: (Color online) Efficiency vs J plot for $S_A = 1/2$ and $S_B = 1$.

analyze the work strokes and see which work stroke is contributing more for negative work. Like before, the first adiabatic work stroke gives the positive work output whereas for second adiabatic work stroke, we get negative work. The total extracted work W_t can now be negative starting from a certain value of J as seen in Fig. 5.10 for $B_2 > B_1$, with $B_2 = 4$ and $B_1 = 3$, whereas Q_M is always positive, as shown in Fig. 5.9. Now, one can further analyze the work strokes and see which work

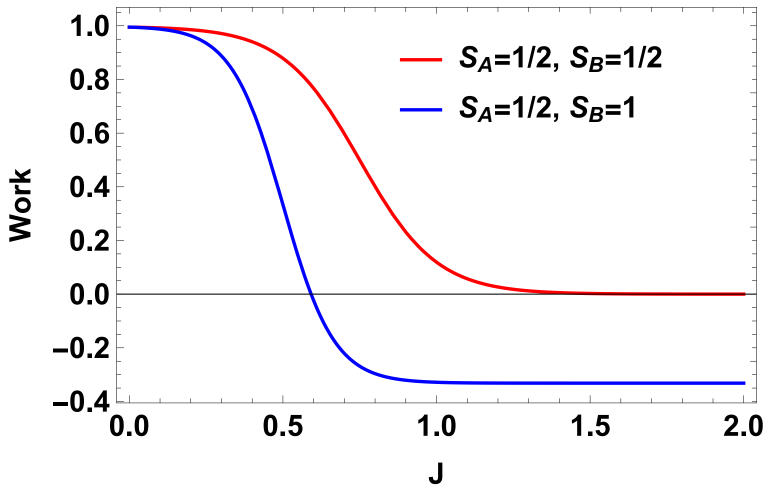

Figure 5.8: (Color online) Global work vs J plot for ($S_A = 1/2$, $S_B = 1/2$) and ($S_A = 1/2$, $S_B = 1$); $B_2 = 4$ and $B_1 = 3$.

stroke is contributing more for negative work. From the Fig. 5.10, one can note that, as before, the first adiabatic work stroke gives the positive work output, whereas, for second adiabatic work stroke, we get negative work. If we take $B_1 > B_2$, the situation is reversed. We have shown the case of $B_1 > B_2$, with $B_1 = 3$ and $B_2 = 4$, in Fig. 5.11. The plot is exactly opposite to the previous one with $B_2 = 4$ and $B_1 = 3$ (see Fig. 5.10) So, in the range of J where the efficiency is negative, the situation

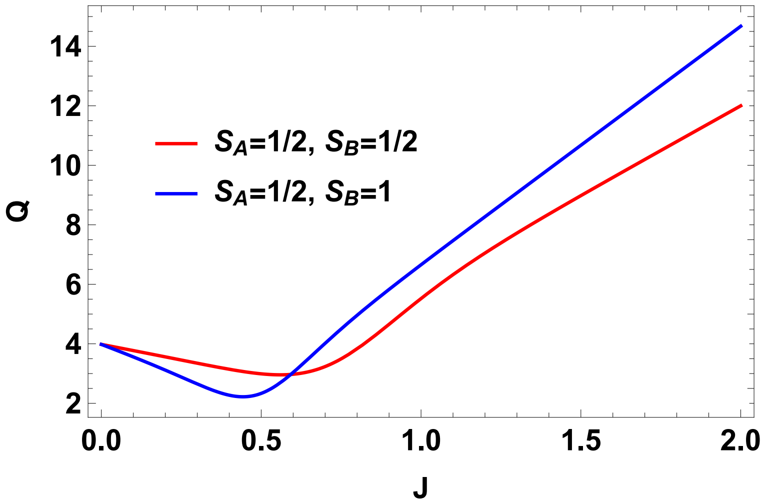

Figure 5.9: (Color online) Average energy change Q_M during the measurement step vs J plot for $(S_A = 1/2, S_B = 1/2)$ and $(S_A = 1/2, S_B = 1)$; $B_2 = 4$ and $B_1 = 3$.

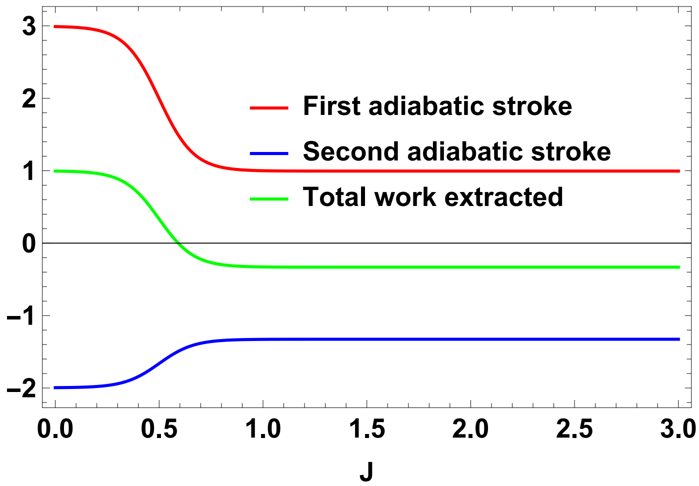

Figure 5.10: (Color online) $-W_1$, $-W_2$, W_t vs J plot for $B_2 > B_1$, with $B_2 = 4, B_1 = 3$. Here $S_A = 1/2, S_B = 1$.

appears as follows : the average energy Q_M is entering to the working medium, W_t work is being done and thereby heat Q_T goes into the heat bath of temperature T. In some sense one can associate a refrigerator action for this negative work scenario. In a conventional quantum Otto refrigerator, the system is first prepared in the thermal state with temperature corresponding to the cold bath. Then in the first and third adiabatic strokes a total work W is added to the working medium. In the second and fourth steps, Q_2 heat is taken from the cold bath and Q_1 heat is added to the hot heat bath and eventually cooling the cold bath more. The co-efficient of performance (COP) for the refrigerator is given as $\eta_{COP} = Q_2/W$. In our case Q_M is always positive and Q_T is always negative. That means

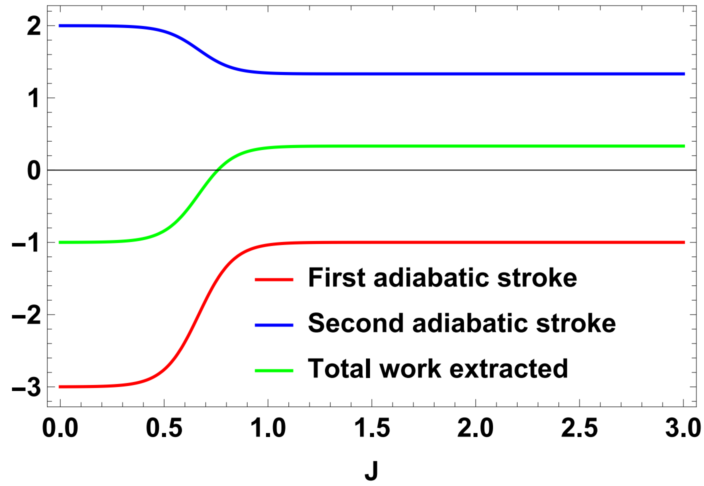

Figure 5.11: (Color online) $-W_1$, $-W_2$, W_t vs J plot for $B_2 < B_1$, with $B_2 = 3, B_1 = 4$. Here $S_A = 1/2$, $S_B = 1$.

we can consider a cold bath of effective temperature T_2, such that, after the second stroke, we have,

$$Q_M = Tr[((\rho^{eq}(T, B_2) - \rho^{eq}(T_2, B_2))H(B_2)], \tag{5.31}$$

where, $\rho^{eq}(T', B)$ is the thermal state at temperature T' with the Hamiltonian $H(B)$, given in Eq. (5.29), where $T' = (T, T_2)$. Solving the above equation we can associate an effective temperature T_2 with Q_M. So, now one can read the cycle as transferring heat from the cold bath of temperature T_2 to hot bath of temperature T and for this, W_t work has to be done. This means that the COP of this refrigerator action is $Q_M/(-W_t)$. So, in order to get a positive work output we have to judiciously choose the value of the coupling constant J, such that efficiency is not negative. Then we will get an advantage for higher efficiency over the uncoupled one. Let's now consider the next asymmetric scenarios and see whether similar trend, i.e, increase in efficiency and occurrence of negative efficiency is present or not. We start with the case where the spins on two sides are $S_A = 1/2$, $S_B = 3/2$. For spin $3/2$, we have the following spin operators,

$$S^x = \frac{1}{2}\begin{pmatrix} 0 & \sqrt{3} & 0 & 0 \\ \sqrt{3} & 0 & 2 & 0 \\ 0 & 2 & 0 & \sqrt{3} \\ 0 & 0 & \sqrt{3} & 0 \end{pmatrix}, S^y = \frac{1}{2}\begin{pmatrix} 0 & -i\sqrt{3} & 0 & 0 \\ i\sqrt{3} & 0 & -2i & 0 \\ 0 & 2i & 0 & -i\sqrt{3} \\ 0 & 0 & i\sqrt{3} & 0 \end{pmatrix} S^z = \frac{1}{2}\begin{pmatrix} 3 & 0 & 0 & 0 \\ 0 & 1 & 0 & 0 \\ 0 & 0 & -1 & 0 \\ 0 & 0 & 0 & -3 \end{pmatrix}$$

The eigenvalues and eigenstates of the Hamiltonian in Eq. (5.29) are given in the Appendix in Table 5.3. Now, we choose the same kind of of measurement operators like the previous case, i.e., on the spin-$1/2$ side we measure S_x and on the spin-3/2 side, S_z :

$$
\begin{aligned}
M_1 &= |0_A^x\rangle \langle 0_A^x| \otimes |0_B\rangle \langle 0_B| \,, M_2 = |0_A^x\rangle \langle 0_A^x| \otimes |1_B\rangle \langle 1_B| \\
M_3 &= |0_A^x\rangle \langle 0_A^x| \otimes |2_B\rangle \langle 2_B| \,, M_4 = |0_A^x\rangle \langle 0_A^x| \otimes |3_B\rangle \langle 3_B| \\
M_5 &= |1_A^x\rangle \langle 1_A^x| \otimes |0_B\rangle \langle 0_B| \,, M_6 = |1_A^x\rangle \langle 1_A^x| \otimes |1_B\rangle \langle 1_B| \\
M_7 &= |1_A^x\rangle \langle 1_A^x| \otimes |2_B\rangle \langle 2_B| \,, M_8 = |1_A^x\rangle \langle 1_A^x| \otimes |3_B\rangle \langle 3_B| \,,
\end{aligned}
$$

with $|0_A^x\rangle = \sqrt{1/2}(|0_A\rangle + |1_A\rangle)$, $|1_A^x\rangle = \sqrt{1/2}(|0_A\rangle - |1_A\rangle)$, and $|0_B\rangle$, $|1_B\rangle$, $|2_B\rangle$, $|3_B\rangle$ are the eigenstates of S_B^z corresponding to the eigenvalues 3/2,1/2,-1/2,-3/2 respectively. We also consider the scenario of $S_A = 1$, $S_B = 3/2$. For this case, the eigenvalues and eigenstates of the Hamiltonian in Eq. (5.29) is given in Table 5.4 of the Appendix. Again, we take the same measurement choices as before, i.e., measurement of S_x spin operator on the side A and S_z spin operator on the side B. We calculate W, Q_M and the engine efficiency for each case. Like in the previous asymmetric case, the condition, $B_2 > B_1$ does not guarantee the positivity of the extracted work W_t in both of present cases. Starting from a certain value of J, W_t can be negative for $B_2 > B_1$ and positive for $B_1 > B_2$. So, for asymmetric cases, $B_1 > B_2$ and $B_2 > B_1$, both the situations give rise to the extracted work to be negative staring from certain ranges of J. We plot the efficiency of the heat engine for the aforesaid three asymmetric cases together in Fig. 5.12 for $B_2 > B_1$ with $B_2 = 4$ and $B_1 = 3$. $B_1 > B_2$ case can be calculated in the similar way.

We observe that for asymmetric situation, the efficiency goes to negative after a certain value of J. Also, from Fig. 5.12, we can observe that as the difference of spins increases between the two sides, the efficiency goes to more negative value. So, from these observations, it is clear that if the two spins on both sides are not the same, then efficiency can be negative. Another interesting feature to notice from the plot is that, within the range of J where efficiency is positive, higher differences of the spin values give larger gain in efficiency over the uncoupled one. We have to take correct coupling strength J, to have a higher but positive work output from these measurement-based coupled higher spin coupled heat engines. As in the case of $S_A = 1/2$ and $S_B = 1$, we also plot the work done in two

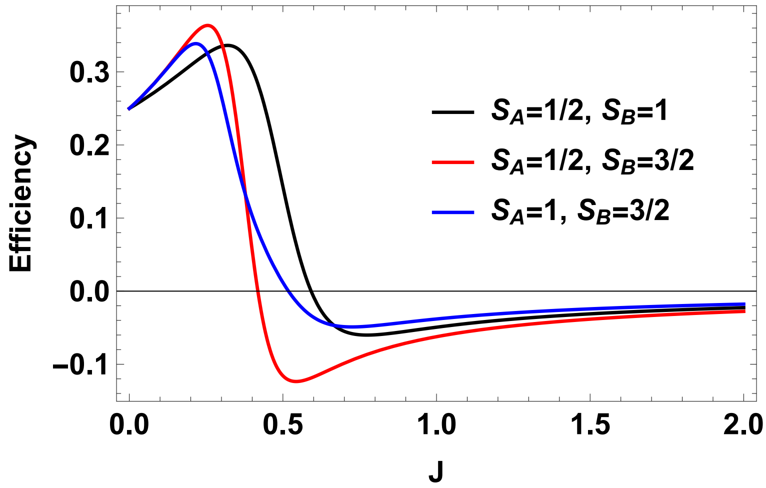

Figure 5.12: (Color online) Efficiency vs J plot for ($S_A = 1/2$, $S_B = 1$), ($S_A = 1/2$, $S_B = 3/2$) and ($S_A = 1$, $S_B = 3/2$) ; $B_2 = 4$ and $B_1 = 3$.

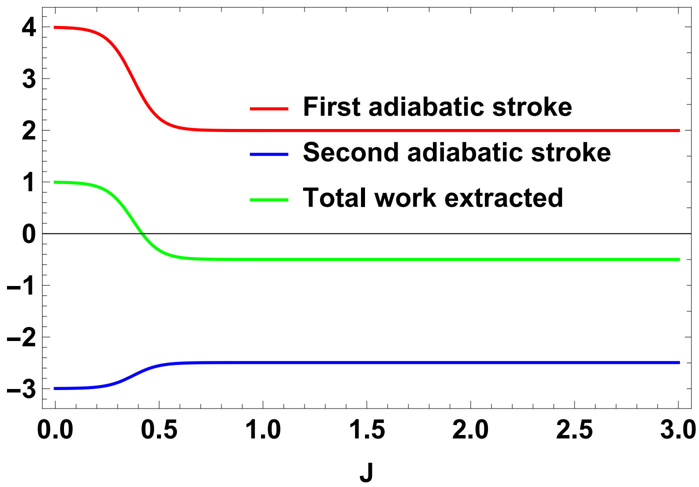

Figure 5.13: (Color online) $-W_1$, $-W_2$, W_t vs J plot for $B_2 > B_1$, with $B_2 = 4, B_1 = 3$. Here, $S_A = 1/2$, $S_B = 3/2$.

adiabatic strokes for these two asymmetric cases in Fig. 5.13 and Fig. 5.14 and note that the negative contribution in the extracted work is due to the second work stroke.

5.5.2 Symmetric case

In this section we consider the symmetric case. One particular characteristic to look at is whether the efficiency gets negative for symmetric situation also. We already had one symmetric situation, namely, the case of two spin-$1/2$ particles and there we had always positive efficiency. Let's investigate the case for higher spin symmetric situations. Three cases can arise for the symmetric scenario, if we restrict ourselves upto spin-$3/2$. Among these, two spin-$1/2$ case has already been discussed at the very beginning. Remaining two cases are the cases of two spin-1 and two spin-$3/2$ particles.

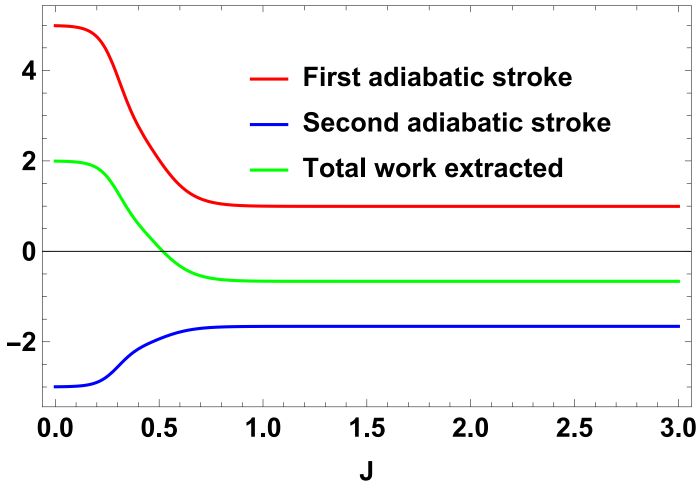

Figure 5.14: (Color online) $-W_1$, $-W_2$, W_t vs J plot for $B_2 > B_1$, with $B_2 = 4, B_1 = 3$. Here, $S_A = 1, S_B = 3/2$.

Eigenvalues and the eigenstates of the Hamiltonian Eq. (5.29) for these two cases are given in the Tables 5.5 and 5.6 respectively in the Appendix. We take the same measurement settings as before, i.e, measurement of S_x spin operator on the side A and S_z spin operator on the side B. We calculate W, Q_M, and the engine efficiency for all these symmetric cases. Interestingly, for the symmetric cases, for $B_2 > B_1$, we get the extracted work $W_t = -W$ to be positive for all J and for $B_1 > B_2$, W_t is negative for all J. This is exactly similar as in the case of two spin-$1/2$ particles (which is the simplest example of a symmetric case). For two spin-1 particles, the expression for W_t is given by,

$$W_t = -W = p/q, \ \text{ where,}$$
$$p = (B2 - B1)(e^{4B1} - 1)(2 + e^{2B1} + 2e^{4B1} + e^{2(B1+8J)}),$$
$$\text{and,} \quad q = 1 + e^{2B1} + e^{4B1} + e^{6B1} + e^{8B1} + e^{4(B1+6J)} + e^{2(B1+8J)}(1 + e^{2B1} + e^{4B1}).$$

From the above expression for W_t, it is evident that, whenever $B_2 > B_1$, we have the extracted work to be positive and for $B_1 > B_2$, the extracted work is negative. Similar is the situation for the other symmetric case, i.e., for two spin-$3/2$ particles. One can also analyze the contributions of two adiabatic work strokes and find that sum of these two strokes gives rise to the extracted work a positive quantity for $B_2 > B_1$. We plot the efficiency of the engine for all symmetric cases together in Fig. 5.15 for $B_2 > B_1$, with $B_2 = 4$ and $B_1 = 3$. Given the fact that Q_M is always positive, for symmetric case, we always get positive efficiency for $B_2 > B_1$. We also see that efficiency gets higher with the increase of spin value, though the efficiency decreases faster for higher spins.

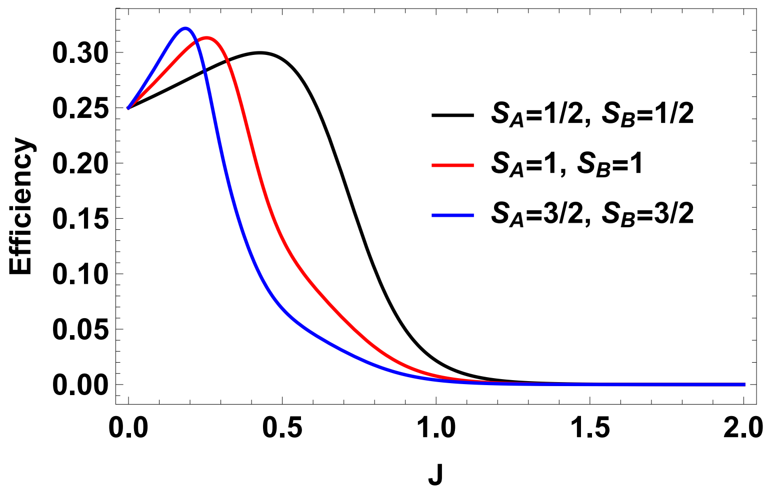

Figure 5.15: (Color online) Efficiency vs J plot for ($S_A = 1/2$, $S_B = 1/2$), ($S_A = 1$, $S_B = 1$) and ($S_A = 3/2$, $S_B = 3/2$)

So, from these observations we can conclude that for the asymmetric scenario, the work output is not always positive. But for the symmetric scenario this is not the case. For this latter scenario, we always get positive work output and hence positive efficiency for the heat engine. And also for higher spin scenario, the efficiency is always greater (as long as it is positive for the asymmetric case) than that of the two spin half case. So, along with the coupling J, spin also plays an important role for the increase in efficiency for the measurement driven single temperature coupled heat engine.

5.6 Local vs. Global work

In this section we will briefly touch upon the status of "local" and "global" works and how they are related. Till now we have been discussing the global aspect of the heat engine, i.e, global work output or global efficiency, etc. Local work can be evaluated by the sum of local average energy change during the measurement step and local heat exchange with the heat bath in the thermalization step for the two spins. Let's assume that before the measurement, total state of the system be ρ_{int} and after the measurement it becomes ρ_M. We denote, $\rho^A_{int} = Tr_B(\rho_{int})$ to be the reduced density matrix for the subsystem A and $\rho^B_{int} = Tr_A(\rho_{int})$ to be the reduced density matrix of subsystem B, and similarly for the reduced states after the measurement. In the same way we can calculate the reduced density matrix for the subsystems before and after the thermalization step. The local work outputs for the subsystems are defined as [114, 116], $w_i = -(q_1^i + q_2^i)$, where,

$$q_1^i = Tr[(\rho_M^i - \rho_{int}^i)H^i(B_2)], \;\; i = A, B; \tag{5.32}$$

$$q_2^i = Tr[(\rho_{int}^i - \rho_M^i)H^i(B_1)], \;\; i = A, B. \tag{5.33}$$

q_1^i represents the average energy exchange for the subsystem A or B ($i = A, B$) for the measurement step after the first adiabatic expansion and q_2^i is the conventional heat exchange with the heat bath in the last step, i.e., the thermalization step. $H^i(B_1)$ and $H^i(B_2)$ are the local Hamiltonians for the subsystems ($i = A, B$) for external magnetic field B_1 and B_2 respectively. After the first adiabatic expansion, the parameter of the Hamiltonian is changed from B_1 to B_2. In the next adiabatic stroke the magnetic field is changed back to the initial value B_1. So, the total local work done by the two subsystems is $w = w_A + w_B$. Nevertheless, the validity of these definitions in the scenario of measurement driven engine is under question as during the measurement stroke, the coupling between the working medium and the apparatus is in general not weak. Moreover after the non-selective measurement, the working medium is driven out of equilibrium, such that the state of the whole working medium is no longer a thermal state. In Figures 5.16, 5.17 and 5.18, we have plotted the local works and global works for three different spin combinations with same measurement settings considered before (S_x on side A and S_z on side B). The plots show very interesting behavior. Unlike

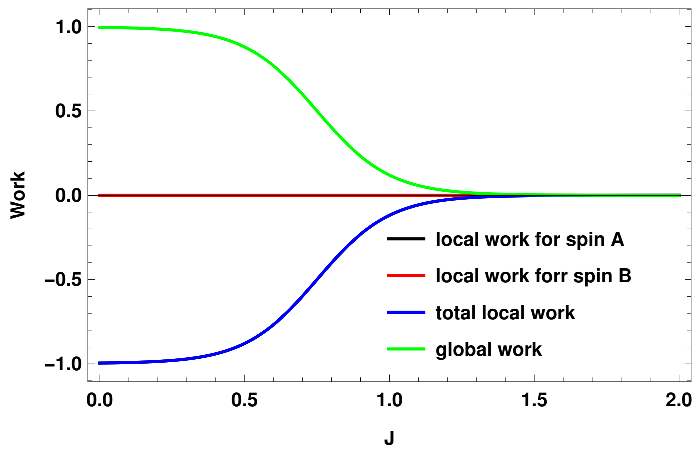

Figure 5.16: $B_2 > B_1$, with $B_2 = 4, B_1 = 3$. Here, $S_A = 1/2$, $S_B = 1/2$. Blue and black curve have merged together.

the coupled quantum otto cycle [114, 116] sum of local works for the subsystems is not always equal to the global work. The nature of the plots also change with the change of spin values. For two spin half case, sum of the local works start from a negative value and goes upto zero, whereas for

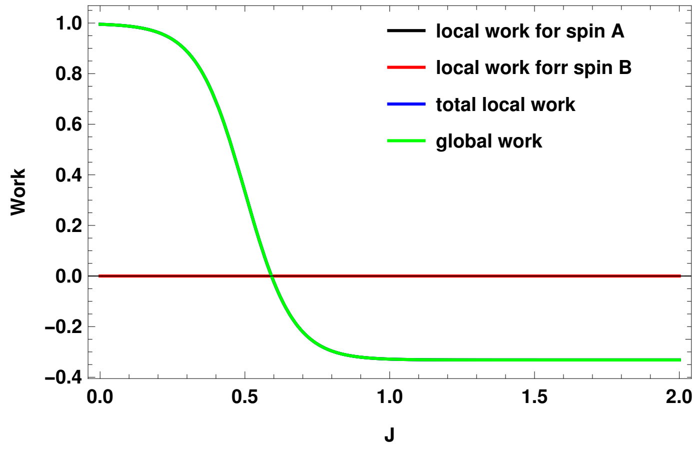

Figure 5.17: $B_2 > B_1$, with $B_2 = 4, B_1 = 3$. Here, $S_A = 1/2$, $S_B = 1$. Black, blue and green curve have merged together.

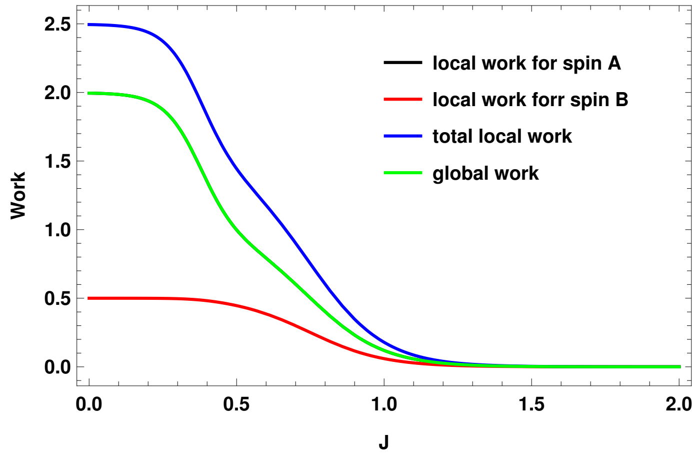

Figure 5.18: $B_2 > B_1$, with $B_2 = 4, B_1 = 3$. Here, $S_A = 1$, $S_B = 1$. Black and green curve have merged together.

other two scenarios it starts with a positive value. Interestingly, local work for one subsystem is zero for first two scenarios (Fig. 5.16 and 5.17). Moreover, except for the two spin half scenario, local work for one subsystem exactly matches with the global work (atleast for the cases considered here). As a result global work matches with the total local work for the second scenario (Fig. 5.17) (black, blue and green curve have merged together). In contrast to the conventional quantum otto cycle, the relationship between local and global works (assuming the above definition of local work) is complex. This also opens up the avenue for suitable definition of local work, taking into account the work cost for measurement, which demands a more detailed description of the engine cycle including the measuring apparatus. This may be a potential future area to explore.

5.7 Conclusion

In this chapter we investigated the effect of coupled working medium in the measurement based single temperature quantum heat engine without feedback. We considered here one dimensional Heisenberg model of two spins and calculated the efficiency of the heat engine. We showed that when the coupling constant J is non zero, i.e, the systems are correlated or entangled, the efficiency gets increased over the uncoupled scenario, i.e., $J = 0$ case. So, interaction enhances the efficiency of this type of heat engine also, as was seen for the coupled quantum Otto cycle [114, 116]. We also considered the higher dimensional scenario, where the two spins are not only spin-$1/2$ but also 1 or $3/2$. In these cases we observed a very interesting situation which is absent in the conventional coupled quantum Otto engine as well as in the case of uncoupled measurement driven heat engine. When the two spins of the two subsystems are the same, we always got the work output, and hence the efficiency to be positive, which means that we can extract work for this situation. But this is not true for the asymmetric situation. If the spins for the two subsystems are different, we can get negative efficiency after a certain nonzero value of the coupling constant, implying that we can not extract work, but have to invest work to run the cycle. It is very much similar to the case of a refrigerator in the absence of cold reservoir, which is replaced here by a measurement protocol. But as long as the efficiency is positive, it increases if we take higher spin system. So, both coupling and dimension of the Hilbert space decide the efficiency of the heat engine. Next, we considered the local work and global work for the engine cycle and their relations. For two cases we observed that the local work has the extensive property, i.e., sum of local works for two subsystems is equal to the global work. More specifically, for $S_A = 1/2, S_B = 1/2$ and $S_A = 1/2, S_B = 1$, total local work done by the two subsystems is exactly equal to the global work output for the engine. But this does not hold good when $S_A = 1, S_B = 1$. In this case, local work done by the systems is less than the global work output. Hence, extensive property does not hold good in this case. A general formalism connecting global and local work may be an interesting future investigation. Also, throughout the paper, we have focussed on the quasistatic regime for the engine. In the Ref. [200], the authors considered the scenario of imperfect thermalization stroke and analyzed the power of a single temperature measurement driven engine. So, the effect of a coupled working medium on the power of this engine might be a good candidate for subsequent study.

Appendix

We write down the tables for both symmetric and asymmetric situations listing all the eigenvalues and eigenstates for the Hamiltonian in Eq. (5.29). First and third tables are for asymmetric cases, whereas, second and fourth tables are for symmetric cases.

Eigenvalues	Eigenstates
$-2B-10J$	$-\sqrt{\frac{3}{2}}\|0_A3_B\rangle+\frac{1}{2}\|1_A2_B\rangle=\|\psi_1\rangle$
$2B-10J$	$-\frac{1}{2}\|0_A1_B\rangle+\sqrt{\frac{3}{2}}\|1_A0_B\rangle=\|\psi_2\rangle$
$-10J$	$-\sqrt{\frac{1}{2}}\|0_A2_B\rangle+\sqrt{\frac{1}{2}}\|1_A1_B\rangle=\|\psi_2\rangle$
$6J$	$\sqrt{\frac{1}{2}}\|0_A2_B\rangle+\sqrt{\frac{1}{2}}\|1_A1_B\rangle=\|\psi_4\rangle$
$-4B+6J$	$\|1_A3_B\rangle=\|\psi_5\rangle$
$-2B+6J$	$\frac{1}{2}\|0_A3_B\rangle+\sqrt{\frac{3}{2}}\|1_A2_B\rangle=\|\psi_6\rangle$
$2B+6J$	$\sqrt{\frac{3}{2}}\|0_A1_B\rangle+\frac{1}{2}\|1_A0_B\rangle=\|\psi_7\rangle$
$4B+6J$	$\|0_A0_B\rangle=\|\psi_8\rangle$

Table 5.3: $S_A=1/2$, $S_B=3/2$

Eigenvalues	Eigenstates
$-B-20J$	$\sqrt{\frac{1}{2}}\|0_A3_B\rangle-\sqrt{\frac{1}{3}}\|1_A2_B\rangle+\sqrt{\frac{1}{6}}\|2_A1_B\rangle$
$B-20J$	$\sqrt{\frac{1}{6}}\|0_A2_B\rangle-\sqrt{\frac{1}{3}}\|1_A1_B\rangle+\sqrt{\frac{1}{2}}\|2_A0_B\rangle$
$-3B-8J$	$-\sqrt{\frac{3}{5}}\|1_A3_B\rangle+\sqrt{\frac{2}{5}}\|2_A2_B\rangle$
$-B-8J$	$-\sqrt{\frac{2}{5}}\|0_A3_B\rangle-\sqrt{\frac{1}{15}}\|1_A2_B\rangle+\sqrt{\frac{8}{15}}\|2_A1_B\rangle$
$B-8J$	$-\sqrt{\frac{8}{15}}\|0_A2_B\rangle+\sqrt{\frac{1}{15}}\|1_A1_B\rangle+\sqrt{\frac{2}{5}}\|2_A0_B\rangle$
$3B-8J$	$-\frac{2}{5}\|0_A1_B\rangle+\sqrt{\frac{3}{5}}\|1_A0_B\rangle$
$-3B+12J$	$\sqrt{\frac{2}{5}}\|1_A3_B\rangle+\frac{3}{5}\|2_A2_B\rangle$
$3B+12J$	$\sqrt{\frac{3}{5}}\|0_A1_B\rangle+\sqrt{\frac{2}{5}}\|1_A0_B\rangle$
$-5B+12J$	$\|2_A3_B\rangle$
$-B+12J$	$\sqrt{\frac{1}{10}}\|0_A3_B\rangle+\sqrt{\frac{3}{5}}\|1_A2_B\rangle+\sqrt{\frac{3}{10}}\|2_A1_B\rangle$
$B+12J$	$\sqrt{\frac{3}{10}}\|0_A2_B\rangle+\sqrt{\frac{3}{5}}\|1_A1_B\rangle+\sqrt{\frac{1}{10}}\|2_A1_B\rangle$
$5B+12J$	$\|0_A0_B\rangle$

Table 5.4: $S_A=1$, $S_B=3/2$

Eigenvalues	Eigenstates
$-2B-8J$	$-\sqrt{\frac{1}{2}}\,\vert 1_A2_B\rangle + \frac{1}{2}\,\vert 2_A1_B\rangle$
$2B-8J$	$-\sqrt{\frac{1}{2}}\,\vert 0_A1_B\rangle + \sqrt{\frac{1}{2}}\,\vert 1_A0_B\rangle$
$-4B+8J$	$\vert 2_A2_B\rangle$
$-16J$	$\sqrt{\frac{1}{3}}\,\vert 0_A2_B\rangle - \sqrt{\frac{1}{3}}\,\vert 1_A1_B\rangle + \sqrt{\frac{1}{3}}\,\vert 2_A0_B\rangle$
$-8J$	$-\sqrt{\frac{1}{2}}\,\vert 0_A2_B\rangle + \sqrt{\frac{1}{2}}\,\vert 2_A0_B\rangle$
$8J$	$\sqrt{\frac{1}{6}}\,\vert 0_A2_B\rangle + \sqrt{\frac{2}{3}}\,\vert 1_A1_B\rangle + \sqrt{\frac{1}{6}}\,\vert 2_A0_B\rangle$
$4B+8J$	$\vert 0_A0_B\rangle$
$-2B+8J$	$\sqrt{\frac{1}{2}}\,\vert 1_A2_B\rangle + \sqrt{\frac{1}{2}}\,\vert 2_A1_B\rangle$
$2B+8J$	$\sqrt{\frac{1}{2}}\,\vert 0_A1_B\rangle + \sqrt{\frac{1}{2}}\,\vert 1_A0_B\rangle$

Table 5.5: $S_A = 1$, $S_B = 1$

Eigenvalues	Eigenstates
$-2B-22J$	$\sqrt{\frac{3}{10}}\,\vert 1_A3_B\rangle - \sqrt{\frac{2}{5}}\,\vert 2_A2_B\rangle + \sqrt{\frac{3}{10}}\,\vert 3_A1_B\rangle$
$2B-22J$	$\sqrt{\frac{3}{10}}\,\vert 0_A2_B\rangle - \sqrt{\frac{2}{5}}\,\vert 1_A1_B\rangle + \sqrt{\frac{3}{10}}\,\vert 2_A0_B\rangle$
$-4B-6J$	$-\sqrt{\frac{1}{2}}\,\vert 2_A3_B\rangle + \sqrt{\frac{1}{2}}\,\vert 3_A2_B\rangle$
$-2B-6J$	$-\sqrt{\frac{1}{2}}\,\vert 1_A3_B\rangle + \sqrt{\frac{1}{2}}\,\vert 3_A1_B\rangle$
$-6B+18J$	$\vert 3_A3_B\rangle$
$2B-6J$	$-\sqrt{\frac{1}{2}}\,\vert 0_A2_B\rangle + \sqrt{\frac{1}{2}}\,\vert 2_A0_B\rangle$
$4B-6J$	$-\sqrt{\frac{1}{2}}\,\vert 0_A1_B\rangle + \sqrt{\frac{1}{2}}\,\vert 1_A0_B\rangle$
$-30J$	$-\frac{1}{2}\,\vert 0_A3_B\rangle + \frac{1}{2}\,\vert 1_A2_B\rangle - \frac{1}{2}\,\vert 2_A1_B\rangle + \frac{1}{2}\,\vert 3_A0_B\rangle$
$-22J$	$\frac{3}{\sqrt{20}}\,\vert 0_A3_B\rangle - \frac{1}{\sqrt{20}}\,\vert 1_A2_B\rangle - \frac{1}{\sqrt{20}}\,\vert 2_A1_B\rangle + \frac{3}{\sqrt{20}}\,\vert 3_A0_B\rangle$
$-6J$	$-\frac{1}{2}\,\vert 0_A3_B\rangle - \frac{1}{2}\,\vert 1_A2_B\rangle + \frac{1}{2}\,\vert 2_A1_B\rangle + \frac{1}{2}\,\vert 3_A0_B\rangle$
$18J$	$\frac{3}{\sqrt{20}}\,\vert 0_A3_B\rangle + \frac{1}{\sqrt{20}}\,\vert 1_A2_B\rangle + \frac{1}{\sqrt{20}}\,\vert 2_A1_B\rangle + \frac{3}{\sqrt{20}}\,\vert 3_A0_B\rangle$
$6B+18J$	$\vert 0_A0_B\rangle$
$-4B+18J$	$\sqrt{\frac{1}{2}}\,\vert 2_A3_B\rangle + \sqrt{\frac{1}{2}}\,\vert 3_A2_B\rangle$
$-2B+18J$	$\sqrt{\frac{1}{5}}\,\vert 1_A3_B\rangle + \sqrt{\frac{3}{5}}\,\vert 2_A2_B\rangle + \sqrt{\frac{1}{5}}\,\vert 3_A1_B\rangle$
$2B+18J$	$\sqrt{\frac{1}{5}}\,\vert 0_A2_B\rangle + \sqrt{\frac{3}{5}}\,\vert 1_A1_B\rangle + \sqrt{\frac{1}{5}}\,\vert 2_A0_B\rangle$
$4B+18J$	$\sqrt{\frac{1}{2}}\,\vert 0_A1_B\rangle + \sqrt{\frac{1}{2}}\,\vert 1_A0_B\rangle$

Table 5.6: $S_A = 3/2$, $S_B = 3/2$

$|0_{A/B}\rangle \doteq \begin{pmatrix} 1 \\ 0 \end{pmatrix}$ and $|1_{A/B}\rangle \doteq \begin{pmatrix} 0 \\ 1 \end{pmatrix}$ are the eigenstates of $S^z_{A/B}$ for spin-$1/2$ particle. $|0_{A/B}\rangle \doteq \begin{pmatrix} 1 \\ 0 \\ 0 \end{pmatrix}$, $|1_{A/B}\rangle \doteq \begin{pmatrix} 0 \\ 1 \\ 0 \end{pmatrix}$ and $|2_{A/B}\rangle \doteq \begin{pmatrix} 0 \\ 0 \\ 1 \end{pmatrix}$ are the eigenstates of $S^z_{A/B}$ for spin-1 particle. $|0_{A/B}\rangle \doteq \begin{pmatrix} 1 \\ 0 \\ 0 \\ 0 \end{pmatrix}$, $|1_{A/B}\rangle \doteq \begin{pmatrix} 0 \\ 1 \\ 0 \\ 0 \end{pmatrix}$, $|2_{A/B}\rangle \doteq \begin{pmatrix} 0 \\ 0 \\ 1 \\ 0 \end{pmatrix}$ and $|3_{A/B}\rangle \doteq \begin{pmatrix} 0 \\ 0 \\ 0 \\ 1 \end{pmatrix}$ are the eigenstates of the operator $S^z_{A/B}$ for spin-$3/2$ particle.

CHAPTER 6

Summary and Outlook

This thesis has been dedicated to study the manifestation of entanglement in different forms, starting from the scenario of Bell nonlocality to Quantum Thermodynamics. Entanglement is one of the important features that distinguishes quantum physics from classical realm. From the mathematical structure of quantum mechanics it is easy to see how the entanglement comes into the picture. Physically it gives rise to nonlocal phenomena, which is very counter-intuitive and yet it is there. Quantum information theory takes an operational point of view to see entanglement as a resource with respect to Local Operations and Classical Communications (LOCC), in the sense that entanglement can not be generated from separable states with LOCC only. Entangled states can be used in numerous QIP processing tasks, which are otherwise impossible or less effective. On the other hand phenomena like Bell Nonlocality and Quantum Steering are due to the existence of entangled states. Entanglement is necessary but not sufficient to reveal these phenomena. Beside its importance in foundational scenario, it is important to understand the role of entanglement in the energetics of microscopic systems, due to the gradual miniaturization of current technologies. Mathematical structure of Entanglement gets more and more complex with the increase of number of parties and so does the nonlocality. Consequently, relation between them becomes intricate even for pure states.

We considered the problem of revelation of nonlocality of a certain class of multipartite entangled states, called generalized GHZ states. There are no known correlation Bell inequalities that are violated by these states (for a certain parameter range) in the minimal measurement scenario. We presented a set of new Bell inequalities in the scenario of n parties, two dichotomic measurements for two parties and only one for the rest. These inequalities are violated by all generalized GHZ states of n qubits. We also explicitly construct the facet Bell inequalities in this new scenario and find that they are the lifted version of Bell-CHSH inequality. These facet inequalities also show the violations for all generalized GHZ states. Both set of inequalities are checked numerically to show violation for any genuinely entangled three-qubit states. Moreover, the first set of Bell inequalities can distinguish between separable, bi-separable and genuinely entangled three-qubit states.

We introduced a new QIP protocol, called Co-operative QKD (CoQKD) using multipartite entangled state. CoQKD is a protocol, where two parties make a secret key under the supervision and intervention of other parties such that no cheating takes place. We find the suitable resource states for this protocol and introduce an implementable scheme for CoQKD in the same line of Ekert's protocol. We also investigate the suitability of the resource states in conference key scenario. Next, to investigate the role of entanglement in Quantum Thermodynamics we consider the direction of quantum heat engine. Specifically, we take the working medium of a measurement based quantum heat engine (without feedback) to be a coupled system of two spins. Then we show that coupling helps us to achieve greater efficiency than the uncoupled one. As coupling is directly related to entanglement, the advantageous role of entanglement is noteworthy in this case.

Lastly, to see the role of entanglement in other Thermodynamic protocols (in literature there are already many works) is potential area to investigate. Understanding the trade-off between our fundamental limitations in quantum systems and the advantages of quantum resources needs more careful studies. On the other hand to look at the other aspects of multipartite nonlocality, like genuine nonlocality or subsystem nonlocality and their connections with entanglement are the areas worth to look at. The area of hidden nonlocality in multipartite scenario has also a lot of unanswered questions.

Bibliography

[1] A. Einstein, B. Podolsky, and N. Rosen, *Phys. Rev.* **47**, 777 (1935).

[2] J. S. Bell, *Physics* **1**, 195 (1964).

[3] N. Brunner *et al.*, *Rev. Mod. Phys.*, **86**, 419 (2015).

[4] B. Hensen *et al.*, *Nature* **526**, 682 (2015); M. Giustina *et al.*, *Phys. Rev. Lett.* **115**, 250401 (2015); L. K. Shalm *et al.*, *Phys. Rev. Lett.* **115**, 250402 (2015).

[5] H. M. Wiseman, S. J. Jones, and A. C. Doherty, *Phys. Rev. Lett.* **98**, 140402 (2007).

[6] R. Uola *et al.*, *arXiv:* 1903.06663 (2019).

[7] R. Horodecki *et al.*, *Rev. Mod. Phys.* **81**, 865 (2009).

[8] M. A. Nielsen, and I. L. Chuang, *Quantum Computation and Quantum Information* (Cambridge University Press, Cambridge, 2000)

[9] G. Adesso, T. R. Bromley, and M. Clanciaruso, *J. Phys. A: Math. Theor.* **49**, 473001 (2016).

[10] K. Modi *et al.*, *Rev. Mod. Phys.* **84**, 1655 (2012).

[11] S. Virmani, and M. B. Plenio, *Quant. Inf. Comput.* **7**, 51 (2007).

[12] E. Chitambar, and G. Gour, *Rev. Mod. Phys.* **91**, 025001 (2019).

[13] C. H. Bennet, *Phys. Rev. Lett.* **70**, 1895 (1993).

[14] A. K. Ekert, *Phys. Rev. Lett.* **67**, 661 (1991).

[15] M. Hillery, V. Buzek, and A. Berthiaume *Phys. Rev. A* **59**, 1829 (1999).

[16] R. F. Werner, *Phys. Rev. A* **40**, 4277 (1989).

[17] J. Barret, *Phys. Rev. A* **65**, 042302 (2002).

[18] S. Popescu, *Phys. Rev. Lett.* **74**, 2622 (1995).

[19] N. Gisin, *Phys. Lett. A* **210**, 151 (1996).

[20] F. Hirsch *et al.*, *Phys. Rev. Lett.* **111**, 160402 (2013).

[21] J. Bowles *et al.*, *Phys. Rev. Lett.* **116**, 130401 (2016).

[22] C. Palazuelos, *Phys. Rev. Lett.* **109**, 190401 (2003).

[23] Y.-C. Liang, L. Masanes, and D. Rosset, *Phys. Rev. A* **86**, 052115 (2012).

[24] S. Vinjanampathy, and J. Anders, *Contemp. Phys* **57**, 1 (2015).

[25] J. V. Neumann, *Mathematical Foundations of Quantum Mechanics* (Princeton University Press; 1st edition) (1955).

[26] M. Schlosshauer, J. Kofler, and A. Zeilinger, *Studies in History and Philosophy of Science Part B* **44**, 222 (2013).

[27] M. Born, *Zeitschrift für Physik* **37**, 863 (1926).

[28] A. M. Gleason, *Journal of Mathematics and Mechanics* **6**, 885 (1957).

[29] P. Busch, *Phys. Rev. Lett* **91**, 120403 (2003).

[30] E. Schrödinger, *Naturwiss.* **23**, 807 (1935).

[31] E. Chitambar *et al.*, *Commun. Math. Phys.* **328**, 303 (2014).

[32] M. A. Nielsen, *Phys. Rev. Lett.* **83**, 436 (1999).

[33] G. Vidal, *Phys. Rev. Lett.* **83**, 1046 (1999).

[34] G. Vidal, D. Jonathan, and M. A. Nielsen, *Phys. Rev. A* **62.**, 012304 (2000).

[35] G. Vidal, *J. Mod. Opt.***47**, 355 (2000).

[36] W. K. Wootters, *Phys. Rev. Lett.* **80**, 2245 (1998).

[37] W. K. Wootters, *Quant. Inf. Comp.* **1**, 27 (2001).

[38] K. Audenaert, F. Verstraete and B. De Moor, *Phys. Rev. A* **64**, 052304 (2001).

[39] O. Gühne, and G. Toth, *Physics Reports* **474**, 1 (2009).

[40] A. Peres, *Phys. Rev. Lett.* **77**, 1413 (1996).

[41] M. Horodecki, P. Horodecki, and R. Horodecki, *Phys. Lett. A* **223**, 1 (1996).

[42] P. Horodecki, *Phys. Lett. A* **232**, 333 (1997).

[43] S. P. Boyd and L. Vandenberghe, *Convex Optimization*, **Cambridge University Press** (2004).

[44] B. M. Terhal, *Phys. Lett. A* **271**, 319 (2000).

[45] W. Dür, G. Vidal, and J. I. Cirac, *Phys. Rev. A* **62**, 062314 (2000).

[46] F. Verstraete *et al.*, *Phys. Rev. A* **65**, 052112 (2002).

[47] M. Walter, D. Gross, and J. Eisert, *arXiv:* 1612.02437v2 (2017).

[48] P. Fachhi *et al.*, *Phys. Rev. A* **77**, 060304 (2008).

[49] D. Goyeneche, and K. Życzkowski, *Phys. Rev. A* **90**, 022316 (2014).

[50] D. Goyeneche *et al.*, *Phys. Rev. A* **92**, 032316 (2015).

[51] M. Enríquez, I. Wintrowicz, and K. Życzkowski, *J. Phys.: Conf. Ser.* **698**, 012003 (2016).

[52] V. Coffman, J. Kundu, and W. K. Wooters, *Phys. Rev. A* **61**, 052306 (2000).

[53] A. Miyake, *Phys. Rev. A* **67**, 012108 (2003).

[54] A. Osterloh, and J. Siewert, *Phys. Rev. A* **72**, 012337 (2005).

[55] A. Osterloh, and J. Siewert, *, Int. J. Quantum Inf.* **4**, 531 (2005).

[56] M. Horodecki, P. Horodecki, and R. Horodecki, *Phys. Lett. A* **283**, 1 (2001).

[57] C. H. Bennet *et al.*, *Phys. Rev. Lett.* **70**, 1895 (1993).

[58] N. Linden, and S. Popescu, *Phys. Rev. A* **59**, 1 (1999).

[59] D. Cavalcanti, P. Skrzypczyk, and I. Šupić, *Phys. Rev. Lett.* **119**, 110501 (1993).

[60] S. Pirandola et al., *Nature Photonics*, **9**, 641 (2015).

[61] C. H. Bennett and S. J. Wiesner, *Phys. Rev. Lett.* **69**, 2881 (1993).

[62] C. H. Bennett, G. Brassard, *in Proceedings IEEE Int. Conf. on Computers, Systems and Signal Processing, Bangalore, India*, pp. 175-179.

[63] N. Gisin *et al.*, *Rev. Mod. Phys.* **74**, 145 (2002).

[64] A. S Hejamadi, A. Pathak, and S. Radhakrishna, *Quanta* **6**, 1 (2017).

[65] M. J. Hall, *Phys. Rev. Lett.* **105**, 250404 (2010).

[66] H. M. Wiseman, *Journal of Physics A: Mathematical and Theoretical* **47**, 424001 (2014).

[67] E. G. Cavalcanti, and H. M. Wiseman, *Found Phys* **42**, 1329 (2012).

[68] G. M. Ziegler, *Lectures notes on polytope*, **Springer** (1994).

[69] K. T. Goh *et al.*, *Phys. Rev. A* **97**, 022104 (2018).

[70] J. F. Clauser *et al.*, *Phys. Rev. Lett.* **23**, 880 (1969).

[71] B. S. Tsirelson, *Lett. Math. Phys.* **4**, 93 (1980); B. S. Tsirelson, *J. Sov. Math.* **36** , 557 (1987).

[72] N. Gisin, *Phys. Lett. A* **154**, 201 (1991).

[73] N. Gisin, and A. Peres, *Phys. Lett. A* **162**, 15 (1992).

[74] S. Popescu, and D. Rohrlich, *Phys. Lett. A* **166**, 293 (1992).

[75] S. K. Choudhary *et al.*, *Phys. Rev. A* **81, 042107** (2010).

[76] S. Yu *et al.*, *Phys. Rev. Lett.* **109**, 120402 (2012).

[77] M. Gachechiladze, and O. Gühne *Phys. Lett. A* **381**, 1281 (2017).

[78] R. Horodecki, M. Horodecki, P. Horodecki, *Phys. Lett. A* **200**, 340 (1995).

[79] D. Collins *et al.*, *Phys. Rev. Lett.* **88**, 040404 (2002).

[80] L. Masanes, *Quantum Inf. Comput.* **3**, 345 (2003).

[81] A. Acín *et al.*, *Phys. Rev. A* **65**, 052325 (2002).

[82] A. Salavrakos *et al.*, *Phys. Rev. Lett.* **119**, 040402 (2017).

[83] N. D. Mermin, *Phys. Rev. Lett.* **65**, 1838 (1990).

[84] M. Ardehali, *Phys. Rev. A* **46**, 5375 (1992); A. V. Belinskii and D. N. Klyshko, *Phys. Usp.* **36**, 653 (1993).

[85] G. Svetlichny, *Phys. Rev. D* **35**, 3066 (1987).

[86] J. D. Bancal *et al.*, *Phys. Rev. A* **88**, 014102 (2013).

[87] V. Scarani *et al.*, *Phys. Rev. A* **71**, 042325 (2005).

[88] H. J. Briegel and R. Raussendorf, *Phys. Rev. Lett.* **86**, 910 (2001).

[89] R. F. Werner and M. M. Wolf, *Phys. Rev. A* **64**, 032112 (2001); M. Żukowski and Č. Brukner, *Phys. Rev. Lett.* **88**, 210401 (2002).

[90] C. Śliwa, *Phys. Lett. A* **317**, 165 (2003).

[91] A. Sen *et al.*, *Phys. Rev. A* **68**, 062306 (2003).

[92] C. Schmid *et al*, *Phys. Rev. Lett.* **100**, 200407 (2008).

[93] N. Brunner, J. Sharam and T. Vértesi, *Phys. Rev. Lett.* **108**, 110501 (2012).

[94] J. Gemmer, M. Michel, and G. Mahler, *Quantum Thermodynamics* Springer, Second Edition.

[95] J. Goold *et al.*, *J. Phys. A: Math. Theor.* **49**, 143001 (2016).

[96] A. Ghosh, *Eur. Phys. J. Special Topics* **227**, 2043 (2019).

[97] C. E. Shannon, *Bell Syst. Tech. J.* **27**, 379 (1948).

[98] L. Henderson and V. Vedral, *J. Phys. A: Math. Gen.* **34**, 6899 (2001).

[99] V. Vedral, *Phys. Rev. Lett.* **90**, 050401 (2003).

[100] H. Ollivier and W. H. Zurek, *Phys. Rev. Lett.* **88**, 017901 (2001).

[101] C. Jarzynski, *Phys. Rev. X* **7**, 011008 (2017).

[102] S. Alipour *et al.*, *Sci. Rep.* **6**, 35568 (2016).

[103] M. N. Bera *et al.*, *Nat. Commun.* **8**, 2180 (2017).

[104] M. P. Müller, *Phys. Rev. X* **8**, 041051 (2018).

[105] M. H. Patrovi, *Phys. Rev. E* **77**, 021110 (2008).

[106] D. Jennigs, and T. Rudolph, *Phys. Rev. E* **81**, 061130 (2010).

[107] S. Jevtic, D. Jennings, and T. Rudolph, *Phys. Rev. Lett.* **108**, 110403 (2012).

[108] G. Vitagliano *et al.*, *Thermodynamics in the Quantum Regime, Chapter 30*, Springer International Publishing (2019).

[109] K. Micadei *et al.*, *Nat. Commun.* **10**, 2456 (2019).

[110] S. Carnot, *Reflections on the Motive Power of Fire and on Machines Fitted to Develop that Power*, Paris: Bachelier (1824).

[111] H. E. D. Scovil, and E. O. Schulz-DuBois, *Phys. Rev. Lett.* **2**, 263 (1959).

[112] R. Dillenschneider, and E. Lutz, *Eur. Phys. Lett.* **88**, 50003 (2009).

[113] X. L. Huang *et al.*, *Phys. Scr.* **88**, 065008 (2008)

[114] G. Thomas and R. Johal, *Phys. Rev. E* **83**, 031135 (2011).

[115] F. Altintas, A. Ü. C. Hardal, and Ö. E. Müstecaplıoğlu, *Phys. Rev. E* **90**, 032102 (2014).

[116] F. Altintas, and Ö. E. Müstecaplıoğlu, *Phys. Rev. E* **92**, 022142 (2015).

[117] X. L. Huang *et al.*, *Physica A* **491**, 604 (2018).

[118] G. A. Barrios *et al.*, *Phys. Rev. A* **96**, 052119 (2017).

[119] F. Altintas, *Physica A* **523**, 40 (2019).

[120] A. Hewgill, A. Ferraro and G. De Chiara, *Phys. Rev. A* **98**, 042102 (2018).

[121] A. E. Allahverdyan, R. Balian, and T. M. Nieuwenhuizen, *Eur. Phys. Lett.* **67**, 565 (2004).

[122] R. Alicki, and R. Fannes, *Phys. Rev. E* **87**, 042123 (2013).

[123] K. V. Hovhannisyan *et al.*, *Phys. Rev. Lett.* **111**, 240401 (2013).

[124] M. P. Llobet *et al.*, *Phys. Rev. X* **5**, 041011 (2015).

[125] G. Francica *et al.*, *npj Quantum information* **3**, 12 (2017).

[126] L. Szilard, *Z. Phys.* **53**, 840 (1929).

[127] H. S. Leff and A. F. Rex, *Maxwell's Demon 2* **IOP, Bristol**, (2003).

[128] S. W. Kim, T. Sagawa, S. DeLiberato, and M. Ueda, *Phys. Rev. Lett.* **106**, 070401 (2011).

[129] A. E. Allahverdyan and T. M. Nieuwenhuizen, *Phys. Rev. Lett.* **85**, 1799 (2000).

[130] W. H. Zurek, *Phys. Rev. A* **67**, 012320 (2003).

[131] L. del Rio, J. Aberg, R. Renner, O. Dahlsten, and V. Vedral, *Nature (London)*, **474**, 61 (2011).

[132] K. Funo, Y. Watanabe, and M. Ueda, *Phys. Rev. A* **88**, 052319 (2013).

[133] J. J. Park, Kang-H. Kim, T. Sagawa, and S. W. Kim *Phys. Rev. Lett.* **111**, 230402 (2013).

[134] J. Oppenheim *et al.*, *Phys. Rev. Lett.* **89**, 180402 (2002).

[135] M. Horodecki, P. Horodecki, and J. Oppenheim, *Phys. Rev. A* **67**, 062104 (2003).

[136] K. Maruyama, F. Morikoshi, and V. Vedral, *Phys. Rev. A* **71**, 012108 (2005).

[137] V. Viguié, K. Maruyama1, and V. Vedral, *New J. Phys.* **7**, 195 (2005).

[138] M. Brunelli, *Phys. Rev. A* **96**, 062311 (2017).

[139] R. Uzdin, A. Levy, and R. Kosloff, *Phys. Rev. X* **5**, 031004 (2015).

[140] D. Collins *et al.*, *Phys. Rev. Lett.* **88**, 170405 (2002).

[141] N. Gisin and H. Bechmann-Pasquinucci, *Phys. Lett. A* **246**, 1 (1998).

[142] V. Scarani and N. Gisin, *J. Phys. A* **34**, 6043 (2001).

[143] M. Żukowski, *et al.*, *Phys. Rev. Lett.* **88**, 210402 (2002).

[144] W. Laskowski *et al.*, *Phys. Rev. Lett.* **93**, 200401 (2004).

[145] A. Das, C. Datta, P. Agrawal, *Phys. Lett. A* **381**, 3928 (2017)

[146] M. Seevinck and J. Uffink, *Phys. Rev. A.* **65**, 012107 (2002).

[147] S. L. Braunstein, A. Mann, and M. Rezven, *Phys. Rev. Lett.* **68**, 3259 (1992).

[148] A. Acín *et al*, *Phys. Rev. Lett.* **87**, 040401 (2001).

[149] M. Froissard, *Nuovo Cimento B* **64**, 241 (1981).

[150] D. Collins and N. Gisin, *J. Phys. A: Math. Theor.* **37**, 1775 (2004).

[151] N. Brunner and N. Gisin, *Phys. Lett. A* **372**, 3162 (2008).

[152] A. Das, C. Datta, P. Agrawal, *arXiv :* **1809.05727** (2018).

[153] S. Pironio, *J. Math. Phys.* **46**, 062112 (2005).

[154] https://www.inf.ethz.ch/personal/fukudak/cdd_home/

[155] S. Ghose *et al*, *Phys. Rev. Lett.* **102**, 250404 (2009)

[156] A. Ajoy and P. Rungta, *Phys. Rev. A.* **81**, 052334 (2010).

[157] P. Agrawal and B. Pradhan, *J. Phys. A: Math. Theor.* 43, 235302 (2010).

[158] J- Q. Zhao *et al.*, *Phys. Lett. A* **382**, 1214 (2017).

[159] H. Chao, X. Peng, and G. G-Can, *Chin. Phys. Lett.* **20**, 183 (2003).

[160] A. Das *et al.*, *arXiv :* **1903.10163** (2019).

[161] V. Scarani, *Acta Physica Slovaca* **62**, 347 (2012).

[162] A. Cabello, *arxiv : quant-ph* **0009025** (2000).

[163] V. Scarani and N. Gisin, *Phys. Rev. A* **65**, 012311 (2001).

[164] K. Chen and H - K Lo, *Int. Symp. on Information Theory* **1607-11** (2005).

[165] M. Epping, H. Kampermann, C. Macchiavello, and D. Bruß, *New Journal of Physics*, **19**, 093012(2017).

[166] H. B. Callen, *Thermodynamics and an Introduction to Thermostatistics*, **Willey** (1985).

[167] R. Kosloff, *Entropy*, **15 (6)**, 2100 (2013).

[168] R. Alicki and R. Kosloff, *arxiv :* **1801.08314** (2018).

[169] H. E. D. Scovil and E. O. Schulz-DuBois, *Phys. Rev. Lett.* **2**, 263 (1959).

[170] T. D. Kieu, *Phys. Rev. Lett.* **93**, 140403 (2004).

[171] H. T. Quan, Y. X. Liu, C. P. Sun, and F. Nori, *Phys. Rev. E* **76**, 031105 (2007).

[172] R. Alicki, *J. Phys. A* **12**, L103 (1979).

[173] R. Kosloff, *J. Chem. Phys.* **80**, 1625 (1984).

[174] M. O. Scully, *Phys. Rev. Lett.* **88**, 050602 (2002).

[175] R. Kosloff and A. Levy, *Anual Rev. Phys. Chem* **65**, 365 (2014).

[176] E. Geva and R. Kosloff and, *J. Chem. Phys.* **96**, 3054 (1992).

[177] T. Feldmann and R. Kosloff, *Phys. Rev. E* **61**, 4774 (2000).

[178] A. E. Allahverdyan, K. V. Hovhannisyan, A. V. Melkikh and S. G. Gevorkian, *Phys. Rev. Lett.* **111**, 050601 (2013).

[179] M. Polettini, G. Verley and M. Esposito, *Phys. Rev. Lett.* **114**, 050601 (2002).

[180] M. Campisi and R. Fazio, *Nat. Commun.*, **7**, 11895 (2016)

[181] N. Shiraishi and H. Tajima, *Phys. Rev. E* **96**, 022138 (2017).

[182] V. Holubec and A. Ryabov, *Phys. Rev. Lett.* **121**, 120601 (2018).

[183] M. O. Scully, M. S. Zubairy, G. S. Agarwal, and H. Walther, *Science* **292**, 162 (2003).

[184] J. Roßnagel, O. Abah, F. Schmidt-Kaler, K. Singer, and E. Lutz, *Phys. Rev. Lett.* **112**, 030602 (2014).

[185] B. Gardas and S. Deffner, *Phys. Rev. E* **92**, 042126 (2015).

[186] M. Horodecki and J. Oppenheim, *Nat. Commun.* **4**, 2059 (2013).

[187] N. Ng, M. P. Woods, *arxiv :* **1805.09564** (2018).

[188] J. Yi, P. Talkner and Y. W. Kim, *Phys. Rev. E* **96**, 022108 (2017).

[189] R. Kosloff and Y. Rezek, *arxiv :* **1612.03582** (2016).

[190] S. Chand and A. Biswas, *Euro. Phys. Lett.* **118**, 6 (2017).

[191] S. Chand and A. Biswas, *Phys. Rev. E* **95**, 032111 (2017).

[192] A. Pozas-Kerstjens, E. G. Brown, K. V. Hovhannisyan, *New J. Phys.* **20**, 043034 (2018).

[193] C. Elouard, D. Herrera-Mart´í, B. Huard, and A. Aufféves, *Phys. Rev. Lett.* **118**, 260603 (2017).

[194] C. Elouard and A. N. Jordan, *Phys. Rev. Lett.* **120**, 260601 (2018).

[195] P. Faist, F. Dupuis, J. Oppenheim and R. Renner, *Nature Commun.* **6**, 7669 (2015).

[196] K. Abdelkhalek, Y. Nakata, D. Reeb, *arxiv :* **1609.06981** (2016).

[197] C. Elouard, D. Herrera-Mart´í, M. Clusel, and A. Auffeves, *npj Quantum Information* **3**, 9 (2017).

[198] M. H. Mohammady and J. Anders, *New J. Phys.* **19**, 113026 (2017).

[199] P. Faist and R. Renner, *Phys. Rev. X* **8**, 021011 (2018).

[200] X. Ding, J. Yi, Y. W. Kim, P. Talkner, *Phys. Rev. E* **98**, 042122 (2018).

[201] A. Das and S. Ghosh, *Entropy* **21 (11)**, 1131 (2019).

[202] M. Perarnau-Llobet, H. Wilming, A. Riera, R. Gallego, and J. Eisert, *Phys. Rev. Lett.* **120**, 120602 (2018).

[203] M. C. Arnesen, S. Bose, and V. Vedral, *Phys. Rev. Lett.* **87**, 017901 (2001).

[204] J. M. Renes, R. Blume-Kohout, A. J. Scott, C. M. Caves, *J. Math. Phys.* **45**, 2171 (2004).